Coupled cluster approaches with an approximate account of triexcitations and the optimized inner projection technique

I. General orthogonally spin-adapted formalism

Piotr Piecuch* and Josef Paldus**

Department of Applied Mathematics, University of Waterloo, Waterloo, Ontario, Canada N2L 3G1

Summary. A general orthogonally spin-adapted formalism for coupled cluster (CC) approaches, with an approximate account of triexcited configurations, and for optimized inner projection (OIP) technique is described. Modifying the linear part of the CC equations for pair clusters (CCD) we obtain the orthogonally spin-adapted, non-iterative version of the CCDT-1 method of Bartlett et al. [J. Chem. Phys. 80, 4371 (1984), 81, 5906 (1984), 82, 5761 (1985)]. Similar modification of an approximate coupled pair theory corrected for connected quadruply excited clusters (ACPQ) yields a new approach called ACPTQ. Both the CCDT-1 and ACPTQ methods can be formulated in terms of effective interaction matrix elements between the orthogonally spin-adapted biexcited singlet configurations. The same matrix elements also appear in the orthogonally spin-adapted form of the CCD + T(CCD) perturbative estimate of triply excited contributions due to Raghavachari [J. Chem. Phys. 82, 4607 (1985)] and Urban et al. [J. Chem. Phys. 83, 4041 (1985)], and in the OIP method when applied to the Pariser–Parr–Pople (PPP) model Hamiltonians. We use the diagrammatic approach based on the graphical methods of spin algebras to derive the explicit form of these interaction matrix elements. Finally, the relationship between different diagrammatic spin-adaptation procedures and their relative advantages are discussed in detail.

Key words: Many-electron correlation problem – Spin-adaptation – Coupled cluster approach – Optimized inner projection – Graphical methods of spin algebras

1. Introduction

The need to account for higher than biexcited configurations in various approaches to the molecular many-electron correlation problem was recognized

---

* *Permanent address:* Institute of Chemistry, University of Wroclaw, F. Joliot-Curie 14, PL-50-383 Wroclaw, Poland
** Also affiliated with the Department of Chemistry, and Guelph-Waterloo Center for Graduate Work in Chemistry, Waterloo Campus, University of Waterloo, Waterloo, Ontario, Canada. Killam Research Fellow 1987–89

more than two decades ago. By that time, the problem of size extensivity was
well understood [1] (although this term was introduced only much later [2], see
also [3]) since it was absolutely essential for a successful treatment of extended
systems, such as the jellium model [4] of solid state physics or the infinite nuclear
matter of nuclear physics [5], and the connected cluster structure of the exact
wave function was clearly formulated by Hubbard [6]. These facts were soon
exploited in the nuclear correlation problem by Coester and Kümmel [7], who
first employed the exponential ansatz for the wave operator. A systematic,
general procedure yielding explicit equations for the connected cluster compo-
nents was, however, developed almost a decade later in the context of the
many-electron correlation problem by Čížek [8]. Various subsequent develop-
ments of the coupled cluster (CC) approach, that are amply documented in
numerous reviews [9–19] and monographs [20–23], resulted in one of the most
efficient and reliable methodologies for the description of correlation effects in
non-degenerate closed-shell ground states of molecular systems.

The first *ab initio* comparison of the coupled cluster (CC) and configuration
interaction (CI) wave functions at various levels of approximation [24] was carried
out for a simple minimum basis set model of the BH_3 molecule (which was chosen
because it was known to provide the largest triexcited contribution to the energy
from amongst the systems examined to that time). This study showed that, in
contrast to tetraexcited clusters that are normally well approximated by their
disconnected $\frac{1}{2}T_2^2$ component, just the opposite holds for triexcited clusters, whose
major contribution comes from the *connected* T_3 component. Unfortunately, an
explicit inclusion of T_3, which was generally implemented only recently [25, 26],
is computationally very demanding, thus leaving room for various approximate
approaches. Among these, the most useful ones are a simple perturbative estimate,
referred to as CCSD + T(CCSD) [27] or CCD + ST(CCD) [28], and the so-called
CCSDT-1 approximation introduced by Lee et al. [29] and Urban et al. [27]. This
latter method was recently examined from a perturbation theoretical viewpoint
[30] and its relationship with the optimized inner projection (OIP) method [31–34]
was also outlined. The application of the CCDT-1 and OIP techniques to the first
two members of the cyclic polyene series [30, 33, 34] showed certain promise and
indicated the desirability of finding out more precisely the limits of applicability
of these approaches by examining the larger cyclic polyene models over the entire
range of the coupling constant, thus complementing our earlier study [35, 36] of
the CC approach with doubles (CCD) and an approximate coupled pair theory
with quadruples (ACPQ) [37].

In order to facilitate these investigations we first undertook the derivation of
a standard orthogonally spin-adapted form of the three different approximate
CC models involving connected triexcitations, namely, a non-iterative version of
the CCDT-1 method, a perturbative CCD + T(CCD) model and the ACPQ
method corrected for T_3 referred to as ACPTQ, along the lines followed earlier
for other CC approaches [38–40]. An orthogonally spin-adapted form is essen-
tial for a simple formulation of the ACPQ approximation [37] as well as for the
exploitation of CC wavefunctions in the polarization propagator calculations of
excitation energies and transition moments [41, 42], since it employs the *pp-hh*
coupled biexcited configurations [38–40, 43–45] providing a simple and direct
relationship with the CISD formalism [16, 46]. Moreover, it yields sparser
matrices for the nonlinear CC coefficients [47] and enables one to cast the CC
formalism into the self-consistent electron pair form as shown by Chiles and
Dykstra [48]. The same formulation is also applied to the OIP formalism,

providing a direct derivation of compact expressions (with eliminated excitation operator matrix elements and corresponding summations when compared with [34]). The methods thus derived are then systematically applied to cyclic polyene model systems [49] and the results will be reported in two subsequent papers of this series.

In order to make this paper self-contained, a brief review of general CC methodology is provided in Sect. 2. The basic CC approximations of triexcited clusters are then reviewed in Sect. 3, while the OIP technique, particularly as it applies to the Pariser–Parr–Pople (PPP) model Hamiltonians [50], is described in Sect. 4. The derivation of effective interaction matrix elements that are relevant to either procedure is carried out in Sect. 5, and finally Sect. 6 discusses and interrelates different spin-adaptation procedures.

2. Orthogonally spin-adapted coupled cluster formalism

We first introduce the notation employed and briefly discuss the orthogonally spin-adapted coupled cluster approaches that will form a basis of further developments studied in this series.

Consider a closed shell system described by a spin independent Hamiltonian H, which we write in the normal product form H_N [8, 51, 52],

$$H = H_N + \langle \Phi_0 | H | \Phi_0 \rangle, \tag{1}$$

where

$$H_N = F_N + V_N, \tag{2}$$

$$F_N = \sum_{mn} \langle m | f | n \rangle N[E_{mn}], \tag{3}$$

$$V_N = \tfrac{1}{2} \sum_{mnpq} \langle mn | v | pq \rangle N[E_{mp} E_{nq}]. \tag{4}$$

Here E_{mn} are the orbital unitary group generators [53],

$$E_{mn} = \sum_{\sigma} X_{m\sigma}^{\dagger} X_{n\sigma}, \tag{5}$$

where $X_{m\sigma}^{\dagger}(X_{m\sigma})$ designate the usual fermion creation (annihilation) operators associated with a certain orthonormal spin-orbital basis $|m\sigma\rangle = |m\rangle|\sigma\rangle$, $\sigma = \pm\tfrac{1}{2}$. The normal product $N[\cdots]$ is defined with respect to a conveniently chosen independent particle model (IPM) reference state Φ_0 that is built from a certain set of doubly occupied orbitals. Here and elsewhere in this series, the orbitals occupied in Φ_0 (hole states) are labeled by a, b, c, d or k' $(k = 1, 2, \ldots)$, and the unoccupied ones (particle states) by r, s, u, w or k'' $(k = 1, 2, \ldots)$. The indices m, n, p, q run over all (both occupied and unoccupied) orbitals. The matrix elements $\langle m | f | n \rangle$ of the one-electron operator F, Eq. (3), are defined in terms of the usual one- and two-electron integrals as follows:

$$\langle m | f | n \rangle = \langle m | z | n \rangle + \sum_{1'} (2\langle m 1' | v | n 1' \rangle - \langle m 1' | v | 1' n \rangle). \tag{6}$$

Note that in the restricted Hartree–Fock (RHF) independent particle model

$$\langle m | f | n \rangle = \varepsilon_m^{\text{RHF}} \delta_{mn}, \tag{7}$$

where $\varepsilon_m^{\text{RHF}}$ are the RHF orbital energies.

In the closed-shell CC approach, the exact ground eigenstate Ψ_0 of the Hamiltonian H, Eq. (1), is represented in the cluster expansion form

$$\Psi_0 = e^T \Phi_0, \qquad \langle \Phi_0 | \Psi_0 \rangle = \langle \Phi_0 | \Phi_0 \rangle = 1, \tag{8}$$

with the cluster operator T given by the sum of its j-particle components T_j,

$$T = \sum_j T_j. \tag{9}$$

The operator T_j acting on Φ_0 creates all possible connected j-times excited cluster components of the exact wave function Ψ_0,

$$T_j \Phi_0 = \sum_K t_K^{(j)} \Phi_K^{(j)}, \tag{10}$$

the summation running over an appropriate set of spin-orbital (orbital, or orbital and spin) labels, $\Phi_K^{(j)}$ designating the pertinent j-times excited configurations and $t_K^{(j)}$ the corresponding cluster amplitudes.

Substituting the exponential ansatz, Eq. (8), into the time-independent Schrödinger equation

$$H\Psi_0 = E\Psi_0, \tag{11}$$

we obtain

$$(H_N e^T)_C \Phi_0 = \Delta E \Phi_0, \tag{12}$$

where

$$\Delta E = E - \langle \Phi_0 | H | \Phi_0 \rangle \tag{13}$$

represents the correlation energy when Φ_0 is the RHF reference and the subscript C indicates the connected part of a given expression [8, 51, 52]. An explicit form of the left-hand side of Eq. (12) in terms of f, v and $t^{(j)}$ matrix elements is conveniently obtained by considering all connected and distinct resulting diagrams which can be constructed from one H_N (F_N or V_N) diagram and up to four T_j diagrams [8, 51, 52].

Formula (12) represents the fundamental equation of the CC approach; projecting this equation onto the excited configurations $\Phi_K^{(j)}$ we obtain an energy independent system of nonlinear algebraic equations for the unknown cluster amplitudes $t_K^{(j)}$,

$$\langle \Phi_K^{(j)} | (H_N e^T)_C | \Phi_0 \rangle = 0 \quad (j = 1, 2, \ldots, N). \tag{14}$$

A similar projection onto Φ_0 yields the CC energy

$$\Delta E = \langle \Phi_0 | (H_N e^T)_C | \Phi_0 \rangle. \tag{15}$$

In practice, CC equations (14) must be simplified by truncating the expansion (9) at a low-order excitation level $j = j_{\max} \ll N$. In contrast with the limited CI approach, this can be done without losing the size extensivity of the resulting approximate energy, since only connected diagrams appear in Eq. (14) [8, 52] (it can be shown that the unlinked terms exactly cancel, cf. e.g. [54, 55]).

Since the pair clusters T_2 represent the most important contribution to T, the basic truncation scheme is

$$T \cong T_2, \tag{16}$$

resulting in the CCD [11] or CPMET (coupled-pair many-electron theory)

[8, 52, 54] approach that normally accounts for a large part ($>80\%$) of correlation effects. Inclusion of monoexcited clusters T_1 (CCSD approach) can be easily accomplished in either spin-orbital or nonorthogonally [56, 57] and orthogonally [39, 40, 42] spin-adapted formulations. With an appropriate choice of Φ_0 (Brueckner or maximum overlap orbitals), the monoexcited clusters vanish exactly. Even with the HF reference, their contribution does not exceed a few percent of the correlation energy (they contribute in higher orders of the MBPT than the T_2 clusters [52, 55]). Their inclusion becomes essential when non-HF orbitals are employed (e.g., when localized orbitals are used [58]).

Numerous applications of the CC approach indicate that the CCD or CCSD methods provide an accurate approximation of the correlation energy, assuming that the ground state considered is not quasidegenerate (for a review see, e.g. [13, 14]). The remaining small percentage of the correlation energy is mostly due to the triexcited T_3 clusters [24]. The full account of the T_3 clusters (CCSDT) is, however, very demanding because of the large number of cluster amplitudes involved, even at the orthogonally spin-adapted level [39]. Indeed, while the *ab initio* implementation of CCD was carried out in 1978 [2, 59, 60], the general purpose computer codes for the full CCSDT were not available until recently [25, 26]. Fortunately, in nondegenerate situations, T_3 clusters can be efficiently accounted for in an approximate way (cf., the next section). Numerical calculations show that full CCSDT results are in excellent agreement with full CI results (even when nonequilibrium geometries are involved [25]), being very close to the results of CISDTQ (configuration interaction with all singles, doubles, triples and quadruples) [26]. This is connected with the fact that the CCSDT method includes all possible single, double and triple excitations in the CI expansion, as well as the most important quadruple excitations, i.e. the disconnected term $\frac{1}{2}T_2^2$, which is accounted for through the exponential ansatz (8) already at the CCD level (the CCSDT model adds all the other disconnected tetraexcited terms: $T_1 T_3$, $\frac{1}{2}T_1^2 T_2$, and $\frac{1}{24}T_1^4$, but they are usually less important). The only quadruply excited cluster contribution, which does not appear in the CCSDT model, is the connected T_4 component. While $\frac{1}{2}T_2^2$ already appears in the second-order MBPT wave function (and the fourth order MBPT energy), the lowest orders in which T_4 contributes to the wave function and energy are rather high (third and fifth, respectively) [52, 55]. Thus, normally, T_4 is negligible (see, e.g. [13, 14, 52] and references therein). This is often symbolically expressed as

$$T_4 \ll \tfrac{1}{2}T_2^2. \tag{17}$$

However, once the quasidegeneracy becomes appreciable, for example, in metallic-like or extended systems [35, 36], assumption (17) is violated and the T_4 contribution becomes essential [35, 61–64] so that CCD (CCSD) or even the full CCSDT approach may suffer a singular behavior. To overcome this difficulty, we have to account for the T_4 clusters in CC equations. Clearly, a direct inclusion of T_4 in the standard CC formalism is computationally hardly feasible in the foreseeable future (cf., however, the XCC or CCSDTQ-1 or CCSDT + Q(CCSDT) formalisms [65]). We can, however, account for T_4 clusters in an approximate manner (approximate coupled-pair theory with quadruples or ACPQ, for short) whenever the unrestricted HF (UHF) solution can provide a reasonable approximation of T_4 clusters [35a, 36, 37]. We shall return to this approach later. The other possibility is to extend the CC formalism to a general multireference case, but such a generalization is not straightforward and still far from being routine [66–78] (see also [13, 14]).

It follows from the above discussion that CCD represents a basic approximate CC scheme, whose orthogonally spin-adapted formulation we now briefly recall. Adopting a particle-particle-hole-hole (pp-hh) coupling scheme, which leads to desirable symmetry properties of the resulting states [38, 39, 43–45] (see also, e.g., [42, 48, 75]), we define the required singlet spin-adapted biexcited configurations as follows [40]:

$$\left|\begin{matrix} r & s \\ a & b \end{matrix}\right\rangle_{S_i} = N_{ab}^{rs}[S_i]^{-1/2} \sum_{\substack{\sigma_a\sigma_b \\ \sigma_r\sigma_s}} \sum_\sigma \langle\tfrac{1}{2}\sigma_a,\tfrac{1}{2}\sigma_b|S_i\sigma\rangle\langle\tfrac{1}{2}\sigma_r,\tfrac{1}{2}\sigma_s|S_i\sigma\rangle \left|\begin{matrix} r\sigma_r & s\sigma_s \\ a\sigma_a & b\sigma_b \end{matrix}\right\rangle, \quad (18)$$

where $\langle j_1 m_1, j_2 m_2|jm\rangle$ are SU(2) Clebsch–Gordan coefficients and $[S_i] = 2S_i + 1$. The biexcited spin-orbital configurations $\left|\begin{matrix} r\sigma_r & s\sigma_s \\ a\sigma_a & b\sigma_b \end{matrix}\right\rangle$ are defined in the usual way,

$$\left|\begin{matrix} r\sigma_r & s\sigma_s \\ a\sigma_a & b\sigma_b \end{matrix}\right\rangle = X_{r\sigma_r}^\dagger X_{a\sigma_a} X_{s\sigma_s}^\dagger X_{b\sigma_b}|\Phi_0\rangle. \quad (19)$$

The factor N_{ab}^{rs},

$$N_{ab}^{rs} = [(1 + \delta_{ab})(1 + \delta_{rs})]^{-1/2}, \quad (20)$$

assures normalization in the case where the hole and/or particle labels are the same [44]. The intermediate spin quantum number, S_i, assumes only two values: $S_i = 0$ (intermediate singlet case) and $S_i = 1$ (intermediate triplet case). The orthogonally spin-adapted doubly excited configurations $\left|\begin{matrix} r & s \\ a & b \end{matrix}\right\rangle_{S_i}$, Eq. (18), are practically identical with configurations of [38, 39] and [43–45]; they only differ by the phase factor $(-1)^{S_i + 1}$. Therefore, they have the same symmetry properties with respect to interchanges of particle and/or hole orbital labels [38, 44],

$$\left|\begin{matrix} r & s \\ a & b \end{matrix}\right\rangle_{S_i} = (-1)^{S_i}\left|\begin{matrix} r & s \\ b & a \end{matrix}\right\rangle_{S_i} = (-1)^{S_i}\left|\begin{matrix} s & r \\ a & b \end{matrix}\right\rangle_{S_i} = \left|\begin{matrix} s & r \\ b & a \end{matrix}\right\rangle_{S_i}. \quad (21)$$

Since we consider the case of a spin-independent Hamiltonian and the reference state Φ_0 is a closed-shell determinant, orthogonally spin-adapted biexcited singlet configurations, Eq. (18), can be used to write expansion of type (10) for the doubly excited connected component $T_2\Phi_0$ of the exact wave function Ψ_0,

$$T_2|\Phi_0\rangle = \sum_{\substack{a \leqslant b \\ r \leqslant s}} \sum_{S_i} \langle rs|t_2|ab\rangle_{S_i} \left|\begin{matrix} r & s \\ a & b \end{matrix}\right\rangle_{S_i} \quad (22a)$$

$$= \tfrac{1}{4}\sum_{abrs}\sum_{S_i}(N_{ab}^{rs})^{-2}\langle rs|t_2|ab\rangle_{S_i}\left|\begin{matrix} r & s \\ a & b \end{matrix}\right\rangle_{S_i}. \quad (22b)$$

As in the case of spin-adapted doubly excited states, the normalized spin-adapted cluster amplitudes $\langle rs|t_2|ab\rangle_{S_i}$ occurring in Eqs. (22), and the analogous ones defined in [38] and [39], differ only by the phase factor $(-1)^{S_i + 1}$. Consequently, coefficients $\langle rs|t_2|ab\rangle_{S_i}$ have the same symmetry properties as the corresponding pp-hh coupled states, namely,

$$\langle rs|t_2|ab\rangle_{S_i} = (-1)^{S_i}\langle rs|t_2|ba\rangle_{S_i} = (-1)^{S_i}\langle sr|t_2|ab\rangle_{S_i} = \langle sr|t_2|ba\rangle_{S_i}. \quad (23)$$

Equation (23) guarantees that the number of independent cluster coefficients in expansion (22b) is the same as the number of biexcited singlet configurations. As in our previous papers [38–40, 45], it is also convenient to introduce unnormalized matrix elements

$$\langle rs|\tau_2|ab\rangle_{S_i} = (N_{ab}^{rs})^{-1}\langle rs|t_2|ab\rangle_{S_i}, \tag{24}$$

which will play the role of scalar factors associated with orbital diagrams representing T_2's, whereas all the spin-coupling coefficients will be represented by appropriate spin diagrams [38], as we shall briefly describe later. In this way, all summations over the orbital labels in the final orthogonally spin-adapted CCD equations will be unrestricted and, simultaneously, the normalization factors, Eq. (20), will not appear (cf., Eq. (22b)).

In order to determine the unknown cluster amplitudes $\langle rs|t_2|ab\rangle_{S_i}$ or $\langle rs|\tau_2|ab\rangle_{S_i}$, we have to write energy independent equations of type (14). They result by projecting Eq. (12) with T given by Eqs. (16) and (22) onto one-dimensional subspaces defined by orthogonally spin-adapted doubly excited configurations, Eq. (18). In this way, we get the system of equations,

$$\left\langle \begin{matrix} r & s \\ a & b \end{matrix} \right|_{S_i} (H_N e^{T_2})_C \left| \Phi_0 \right\rangle = 0, \tag{25}$$

which, together with the expansion (22b), represents the set of basic relations for the orthogonally spin-adapted formulation of the CCD method.

Expanding the left-hand side of Eq. (25), we find [38]

$$\sum_{k=0}^{2} \Lambda^{(k)}(rs, ab; S_i) = 0, \tag{26}$$

where

$$\Lambda^{(k)}(rs, ab; S_i) = \frac{1}{k!}(N_{ab}^{rs})^{-1} \left\langle \begin{matrix} r & s \\ a & b \end{matrix} \right|_{S_i} (H_N T_2^k)_C \left| \Phi_0 \right\rangle, \quad k = 0, 1, 2. \tag{27}$$

Explicit expressions in terms of f-, v- and spin-adapted t_2-matrix elements for the absolute, linear and bilinear components $\Lambda^{(k)}$, $k = 0, 1$ and 2, respectively, are most conveniently derived by applying the diagrammatic approach based on graphical methods of spin algebras. According to this scheme, which was elaborated in [38] (see also [39, 40, 45]), we first construct the pertinent Goldstone–Hugenholtz orbital diagrams in the Brandow representation (so-called Goldstone–Brandow diagrams) using the Goldstone form for F_N and V_N vertices (the latter are referred to as bare two-electron interaction vertices) and the Brandow form for the T_j vertices (T_2, when the CCD equations are considered). The Hugenholtz vertices have to be represented in Brandow form in order to determine the orbital phase factors [8b, 38, 52, 79] as well as to construct the corresponding spin diagrams, which are then evaluated by exploiting elegant and powerful graphical methods of spin algebras [80, 81] (see also [22, 23, 44]). The desired final expressions are obtained by combining the resulting spin coupling coefficients with the orbital factors associated with orbital diagrams (cf., also [82]). The basic diagrams that are needed to derive the orthogonally spin-adapted CCD equations in an explicit form are presented in Fig. 1. Figure 1a,b shows the orbital Goldstone-type diagrams corresponding to one- and two-body operators F_N, Eq. (3), and V_N, Eq. (4), respectively, whereas Brandow-type orbital diagrams together with the 3-jm-type spin diagrams that represent biexcited connected cluster component T_2 in an orthogonally spin-adapted form,
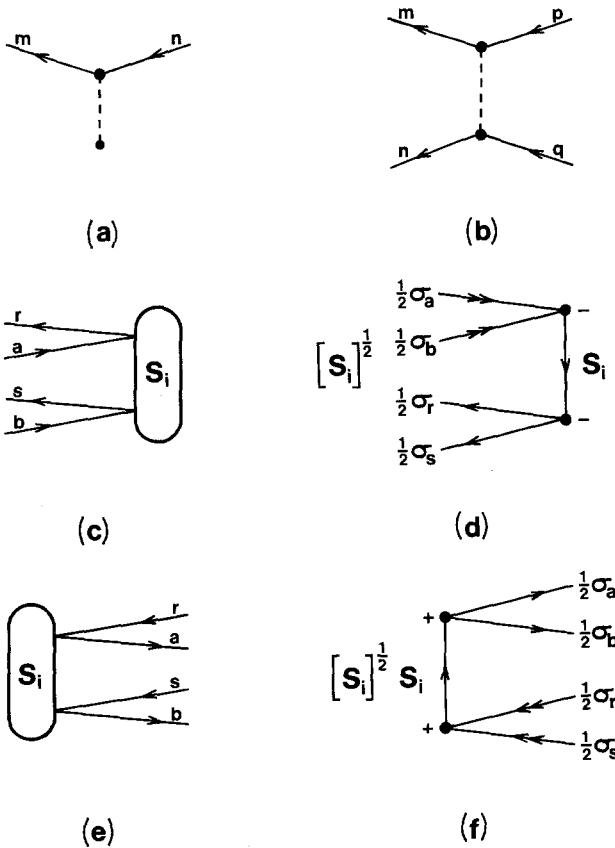
Fig. 1a–f. Basic diagrams used throughout the present paper, in particular to derive the orthogonally spin-adapted CCD equations: **a** and **b** are Goldstone-type diagrams corresponding, respectively, to arbitrary spin independent one-and two-body operators in the normal product form (in particular F_N, Eq. (3), and V_N, Eq. (4)); **c** is a Brandow-type orbital diagram representing either biexcited connected cluster component T_2 or unnormalized orthogonally spin-adapted doubly excited ket state $(N_{ab}^{rs})^{-1} \left| \begin{smallmatrix} r & s \\ a & b \end{smallmatrix} \right\rangle_{S_i}$, while **e** is a Brandow-type orbital diagram representing unnormalized biexcited bra state $(N_{ab}^{rs})^{-1} {}_{S_i}\!\left\langle \begin{smallmatrix} r & s \\ a & b \end{smallmatrix} \right|$; **d**, **f** are the 3-jm-type spin diagrams associated with orbital diagrams **c**, **e**, respectively. Pairs of diagrams **c**, **d** and **e**, **f** may also serve as a graphical representation of the normalized doubly excited singlet spin-adapted configurations $\left| \begin{smallmatrix} r & s \\ a & b \end{smallmatrix} \right\rangle_{S_i}$ and ${}_{S_i}\!\left\langle \begin{smallmatrix} r & s \\ a & b \end{smallmatrix} \right|$, respectively, provided that the normalization factor N_{ab}^{rs} is incorporated into the spin diagrams **d**, **f**; see text for details

Eq. (22b), are given in Fig. 1c,d. Diagrams in Fig. 1c,d can also serve as a graphical representation for the normalized orthogonally spin-adapted doubly excited configurations, Eq. (18), provided that thé orbital and the intermediate spin labels are fixed and the normalization factors N_{ab}^{rs}, Eq. (20), are incorporated into the spin graph (Fig. 1d) [44]; otherwise they represent unnormalized biexcited ket states $(N_{ab}^{rs})^{-1} \left| \begin{smallmatrix} r & s \\ a & b \end{smallmatrix} \right\rangle_{S_i}$ [40]. For the projection onto the corre-

sponding unnormalized bra states $(N_{ab}^{rs})^{-1} \left\langle {}_{S_i} \begin{array}{cc} r & s \\ a & b \end{array} \right|$ (see Eq. (27)), we also need the spin graph (Fig. 1f) which is dual to that of Fig. 1d (cf., [38, 39, 44, 45]). Again, the normalization factor N_{ab}^{rs} must be incorporated into the spin diagram (Fig. 1f) when the projection onto normalized biexcited bra states is considered [44], for example, in Eq. (25). For the sake of completeness, we also give in Fig. 1e the orbital Brandow diagram representing (normalized or unnormalized) doubly excited singlet spin-adapted bra state. Obviously, the diagrams in Fig. 1e,c are mutually conjugate and carry fixed orbital and intermediate spin labels. It should be noticed that the hole lines in spin graphs (Fig. 1d,f) are interchanged in comparison with the analogous diagrams given in [38] and [45]. This is a consequence of the phase convention used in the present series (see the text following Eqs. (20) and (22); see also [40]).

The resulting explicit expressions for the quantities $\Lambda^{(k)}$ ($k = 0, 1, 2$), Eq. (27), can be written as follows [38–40]:

$$\Lambda^{(0)}(rs, ab; S_i) = [S_i]^{1/2}\langle rs \| ab \rangle_{S_i}, \tag{28}$$

$$\Lambda^{(1)}(rs, ab; S_i) = \mathscr{S}_{rs}(S_i) \sum_{\tilde{r}} \langle r|f|\tilde{r}\rangle [\tilde{r}s, ab]_{S_i} - \mathscr{S}_{ab}(S_i) \sum_{\tilde{a}} \langle \tilde{a}|f|a\rangle [rs, \tilde{a}b]_{S_i}$$

$$+ \sum_{\tilde{r}\tilde{s}} \langle rs \| \tilde{r}\tilde{s}\rangle [\tilde{r}\tilde{s}, ab]_{S_i} + \sum_{\tilde{a}\tilde{b}} \langle \tilde{a}\tilde{b} \| ab \rangle [rs, \tilde{a}\tilde{b}]_{S_i}$$

$$- \mathscr{S}_{ab}(S_i)\mathscr{S}_{rs}(S_i) \sum_{\tilde{a}\tilde{r}} \sum_{\tilde{S}_i} (\delta_{S_i\tilde{S}_i}\langle \tilde{a}r \| a\tilde{r}\rangle - \tfrac{1}{2}[S_i, \tilde{S}_i]^{1/2}\langle \tilde{a}r \| \tilde{r}a \rangle)[\tilde{r}s, \tilde{a}b]_{S_i}, \tag{29}$$

and

$$\Lambda^{(2)}(rs, ab; S_i) = \Lambda^{(2)}_{1,2}(rs, ab; S_i) + \Lambda^{(2)}_3(rs, ab; S_i)$$

$$+ \Lambda^{(2)}_4(rs, ab; S_i) + \Lambda^{(2)}_5(rs, ab; S_i), \tag{30}$$

where

$$\Lambda^{(2)}_{1,2}(rs, ab; S_i) = \tfrac{1}{4}[S_i]^{1/2}\mathscr{S}_{rs}(S_i) \sum_{\tilde{S}_i^1 \tilde{S}_i^2} [\tilde{S}_i^1, \tilde{S}_i^2]^{1/2}$$

$$\times \sum_{\tilde{a}\tilde{b}\tilde{r}\tilde{s}} \{\langle \tilde{a}\tilde{b} \| \tilde{r}\tilde{s}\rangle - F(S_i + \tilde{S}_i^1 + \tilde{S}_i^2)\langle \tilde{a}\tilde{b} \| \tilde{s}\tilde{r}\rangle\}[r\tilde{r}, a\tilde{a}]_{\tilde{S}_i^1}[s\tilde{s}, b\tilde{b}]_{\tilde{S}_i^2}, \tag{31a}$$

$$\Lambda^{(2)}_3(rs, ab; S_i) = -\tfrac{1}{2}\mathscr{S}_{rs}(S_i) \sum_{\tilde{S}_i} [\tilde{S}_i]^{1/2} \sum_{\tilde{a}\tilde{b}\tilde{r}\tilde{s}} \langle \tilde{a}\tilde{b} \| \tilde{r}\tilde{s}\rangle [r\tilde{r}, ab]_{S_i}[s\tilde{s}, \tilde{a}\tilde{b}]_{\tilde{S}_i}, \tag{31b}$$

$$\Lambda^{(2)}_4(rs, ab; S_i) = -\tfrac{1}{2}\mathscr{S}_{ab}(S_i) \sum_{\tilde{S}_i} [\tilde{S}_i]^{1/2} \sum_{\tilde{a}\tilde{b}\tilde{r}\tilde{s}} \langle \tilde{a}\tilde{b} \| \tilde{r}\tilde{s}\rangle [rs, a\tilde{a}]_{S_i}[\tilde{r}\tilde{s}, b\tilde{b}]_{\tilde{S}_i}, \tag{31c}$$

$$\Lambda^{(2)}_5(rs, ab; S_i) = \tfrac{1}{2}[S_i]^{-1/2} \sum_{\tilde{a}\tilde{b}\tilde{r}\tilde{s}} \langle \tilde{a}\tilde{b} \| \tilde{r}\tilde{s}\rangle [\tilde{r}\tilde{s}, ab]_{S_i}[rs, \tilde{a}\tilde{b}]_{S_i}. \tag{31d}$$

The algebraic coefficient F appearing in Eq. (31a),

$$F(S_i + \tilde{S}_i^1 + \tilde{S}_i^2) = 4C(S_i, \tilde{S}_i^1, \tilde{S}_i^2) = 4 \begin{Bmatrix} S_i & \tfrac{1}{2} & \tfrac{1}{2} \\ \tfrac{1}{2} & \tilde{S}_i^1 & \tfrac{1}{2} \\ \tfrac{1}{2} & \tfrac{1}{2} & \tilde{S}_i^2 \end{Bmatrix}, \tag{32}$$

assumes the following values [37]:

$$-F(0) = F(1) = 1, \qquad F(2) = \tfrac{1}{3}, \qquad F(3) = \tfrac{5}{9}. \tag{33}$$

The symbol C, Eq. (32), is a 9-j symbol introduced in [39]. The operator $\mathscr{S}_{mn}(S_i)$ is a two-index symmetrizer ($S_i = 0$) or antisymmetrizer ($S_i = 1$), i.e.,

$$\mathscr{S}_{mn}(S_i) = 1 + (-1)^{S_i}(mn), \tag{34}$$

where (mn) designates a transposition of indices m and n. The multiple symbol $[X_1, X_2, \ldots, X_j]$ is defined as

$$[X_1, X_2, \ldots, X_j] = \prod_{i=1}^{j} [X_i]. \tag{35}$$

For simplicity we dropped the interaction operator v in all two-electron integrals, i.e.

$$\langle mn \| pq \rangle = \langle mn | v | pq \rangle. \tag{36}$$

Consequently [cf. Eq. (28)], the (anti)symmetrized v-matrix elements become

$$\langle mn | v | pq \rangle_S = \mathscr{S}_{mn}(S) \langle mn | v | pq \rangle = \mathscr{S}_{pq}(S) \langle mn | v | pq \rangle$$
$$= \langle mn | v | pq \rangle + (-1)^S \langle mn | v | qp \rangle \equiv \langle mn \| pq \rangle_S. \tag{37}$$

In order to write rather complex expressions for $\Lambda^{(k)}$ ($k = 0, 1, 2$) in a condensed form, we also introduced the shorthand notation for the unnormalized cluster amplitudes, Eq. (24), namely [35a],

$$[rs, ab]_{S_i} = \langle rs | \tau_2 | ab \rangle_{S_i}. \tag{38}$$

   The resulting Goldstone–Brandow orbital diagrams, which represent successive terms appearing on the right-hand sides of Eqs. (28), (29) and (31), are shown in Figs. 2–4, respectively. As usual [8, 38–40, 52], vertices representing a bra state $(N_{ab}^{rs})^{-1} {}_{S_i}\!\left\langle \begin{smallmatrix} r & s \\ a & b \end{smallmatrix} \right|$, onto which we project, are not drawn. Instead, external lines carry the fixed orbital labels characterizing the configuration ${}_{S_i}\!\left\langle \begin{smallmatrix} r & s \\ a & b \end{smallmatrix} \right|$. We do not present the associated spin diagrams, because they are very simple and can be easily obtained from the orbital diagrams by interconnecting corresponding lines of spin graphs representing cluster components, Fig. 1d, and projections onto the biexcited states, Fig. 1f (for more detail reader is referred to [38]; [39] and [45] are also recommended). Summation over the intermediate spin quantum numbers $\tilde{S}_i$, labeling Brandow T_2 vertices, is always understood to be
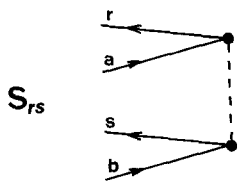
$$\mathbf{S}_{rs}$$

Fig. 2. Goldstone–Brandow orbital diagrams $[\mathscr{S}_{rs} = 1 + (rs)]$ representing $\Lambda^{(0)}$, Eq. (28)
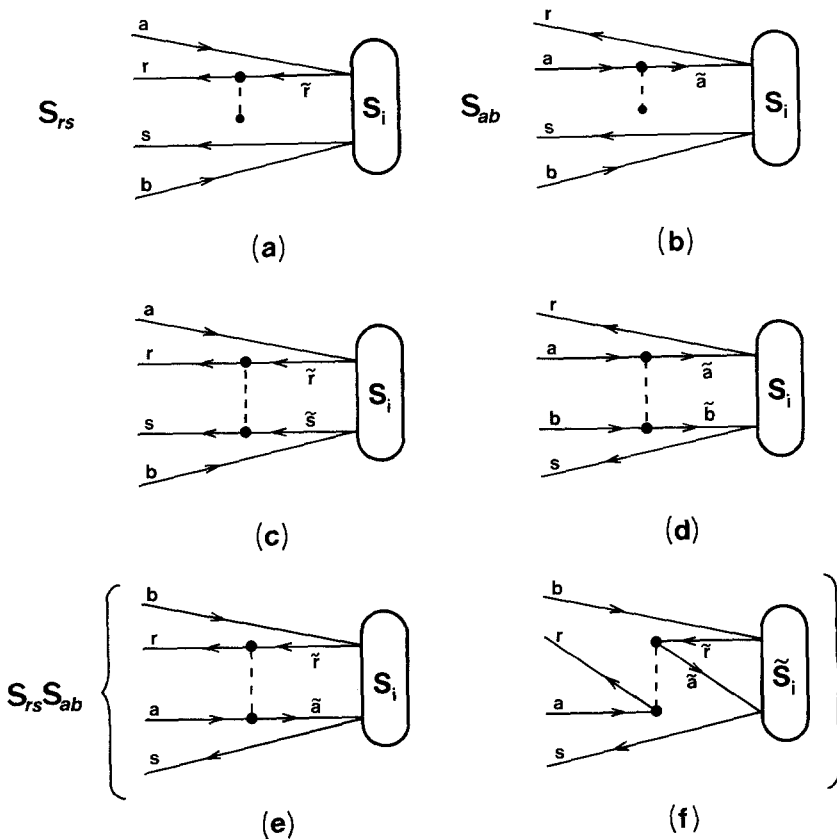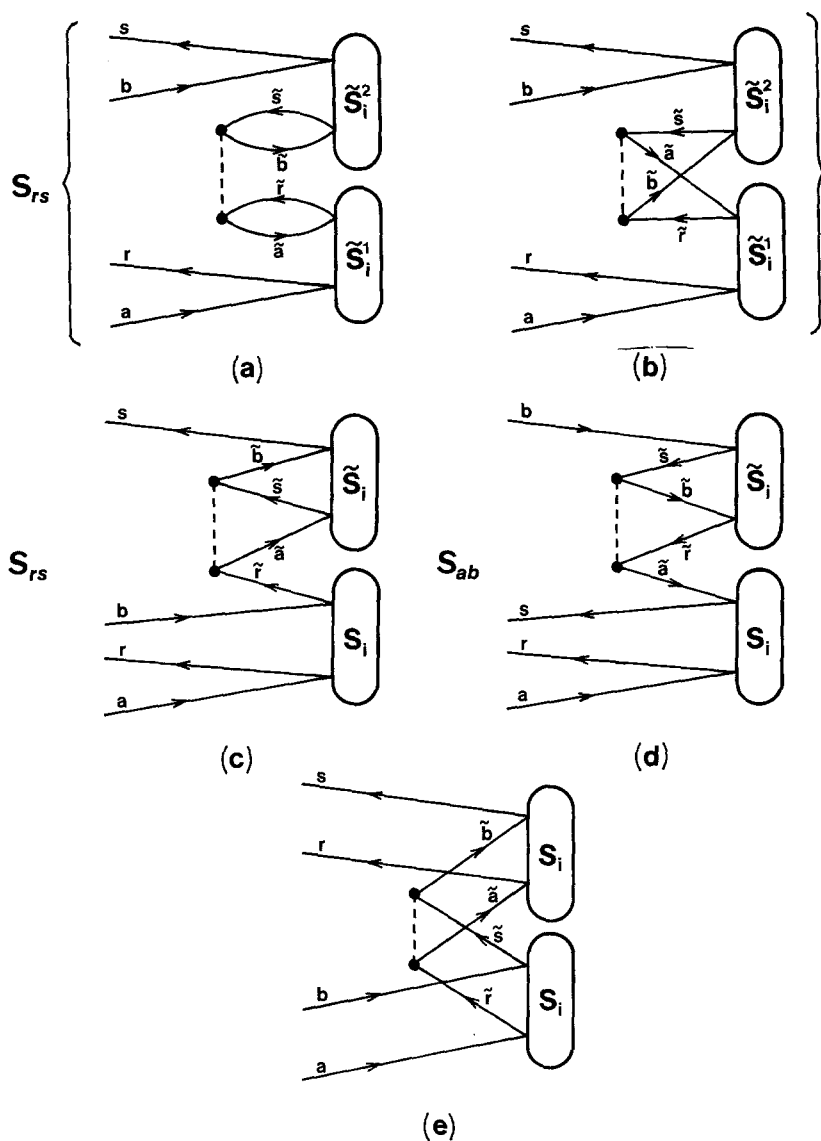
Fig. 3a–f. Goldstone–Brandow orbital diagrams corresponding to successive terms on the right-hand side of Eq. (29)

carried out. In some cases, however, spin diagrams restrict the summation over $\tilde{S}_i$'s to only one term labeled by the value $\tilde{S}_i = S_i$ characterizing the biexcited bra state onto which we project. In the orbital diagrams corresponding to these cases we replaced the free label $\tilde{S}_i$ by the fixed label S_i. The operators $\mathscr{S}_{ab}$ and $\mathscr{S}_{rs}$ acting on orbital diagrams in Figs. 2–4 denote two-index symmetrizers

$$\mathscr{S}_{mn} \equiv \mathscr{S}_{mn}(0) = 1 + (mn); \qquad (mn) = (ab) \text{ or } (rs). \qquad (39)$$

Thus, for example, Fig. 4c represents two diagrams: one, which is given in Fig. 4c and corresponds to canonical labeling of external lines [38] and another one, which results by interchanging indices r and s in Fig. 4c and corresponds to non-canonical labeling of the open paths. This concise notation was introduced in our recent paper [40], where we also pointed out a one-to-one correspondence between the symmetrizers $\mathscr{S}_{ab}(\mathscr{S}_{rs})$ in orbital diagrams and the (anti)symmetrizers $\mathscr{S}_{ab}(S_i)$ ($\mathscr{S}_{rs}(S_i)$) in algebraic expressions. Consequently, the number of (anti)symmetrizers is reduced to a minimum, since they are only present when the open paths in the orbital diagrams can be labeled in several distinct ways [40].

Fig. 4a–e. Goldstone–Brandow orbital diagrams associated with the individual contributions $\Lambda_i^{(2)}$ $(i = 1, \ldots, 5)$ to the nonlinear part of the CCD equations $\Lambda^{(2)}$, Eq. (30). $\Lambda_{1,2}^{(2)}$, Eq. (31a), is sum of the contributions $\Lambda_1^{(2)}$ and $\Lambda_2^{(2)}$ corresponding to diagrams a and b, respectively. The remaining three diagrams, c–e, correspond to contributions $\Lambda_i^{(2)}$ $(i = 3–5)$ given by Eqs. (31b)–(31d), respectively; cf. text for details

Once Eqs. (26) and (28)–(31) are solved for the unknown spin-adapted cluster coefficients $[rs, ab]_{S_i}$, the energy ΔE is evaluated from the formula [38–40]

$$\Delta E = \langle \Phi_0 | (H_N T_2)_C | \Phi_0 \rangle = \frac{1}{2} \sum_{abrs} \langle ab \| rs \rangle \sum_{S_i} [S_i]^{1/2} [rs, ab]_{S_i}, \qquad (40)$$

which results by assuming approximation (16) in the general expression (15).

The orbital diagram corresponding to Eq. (40) is not reproduced here, since it can be found elsewhere [38, 39].

The nonlinear part of the CCD equations, $\Lambda^{(2)}$, is broken into the contributions corresponding to five diagrams given in Fig. 4. Contributions associated with diagrams of Fig. 4a,b are collected in one term $\Lambda_{1,2}^{(2)}$, Eq. (31a), since they are exchange versions of one another. Neglecting the nonlinear part of the CCD equations completely, i.e. setting $\Lambda^{(2)} = 0$, we obtain the corresponding linear approximation, L-CCD, which is equivalent to an infinite order perturbation theory with intermediate doubly excited states (DMBPT(∞)) [11, 52]. As long as no quasidegeneracy is present, the L-CCD approach yields very good results. It breaks down, however, and becomes singular when the lowest-lying canonical biexcitation becomes degenerate with the reference configuration Φ_0 [46]. In many cases, the nonlinear terms of the full CCD method are capable of correcting this behavior [62–64, 83]. However, as already mentioned, when condition (17) is violated (for example, when linear metallic-like systems are considered) even the full CCD approach becomes singular [35]. Yet, when we retain only nonlinear diagrams that are separable over the hole line(s), i.e. those in Fig. 4d,e (so that we set

$$\Lambda_{1,2}^{(2)} = \Lambda_{3}^{(2)} = 0 \tag{41}$$

in Eq. (30)), the resulting approximate coupled-pair (ACP-D45 or ACP, for short [47, 62]) or approximate CCD (ACCD [84]) approach provides correlation energies that are not only very close to those obtained with the full CCD method in all standard cases, both at the semiempirical [35, 36, 62] and *ab initio* [47, 62, 64, 84] levels, but also represents an excellent approximation in highly degenerate situations [35, 36, 47, 62, 64] where the L-CCD [35, 36, 62, 64] or even the full CCD [35] approach is plagued with singularities. This remarkable behavior of the ACP approach can be partially explained by the mutual cancellation of the contributions arising from the first three diagrams of Fig. 4; indeed, careful numerical inspection indicates that the ACP-D123 approximation, in which nonlinear contributions $\Lambda_{4}^{(2)}$ and $\Lambda_{5}^{(2)}$ are neglected, yields correlation energies that are very close to the L-CCD results [35a, 47, 62]. The fact that the ACP approach provides good results even in highly degenerate cases, when the basic assumption of the CCD method, Eq. (17), and the CCD method itself, break down [35, 36], indicates that the approximation (41) simulates an incorporation of the higher-excited connected cluster components, such as T_4. The evidence for this was given in [37]. By examining the general cluster structure of the UHF solution, it was shown that correcting the CCD equations for the effect of connected tetraexcited clusters by including the term

$$\Lambda^{(4)}(rs, ab; S_i) = (N_{ab}^{rs})^{-1} \left\langle \begin{array}{cc} r & s \\ & \\ a & b \end{array} \middle|_{S_i} (H_N T_4)_C \middle| \Phi_0 \right\rangle, \tag{42}$$

effectively eliminates the contribution from the first three nonlinear diagrams in Fig. 4. The resulting approximate procedure, referred to as the ACPQ approach [37], is identical with the ACP-D45 approximation, except for the numerical factor of 9 associated with the fifth nonlinear diagram contribution (Fig. 4e) when projected onto the triplet coupled ($S_i = 1$) state. Thus, the explicit ACPQ equations take the form

$$\Lambda^{(0)}(rs, ab; S_i) + \Lambda^{(1)}(rs, ab; S_i) + \tilde{\Lambda}^{(2)}(rs, ab; S_i) = 0, \tag{43}$$

where $\Lambda^{(0)}$ and $\Lambda^{(1)}$ are given by Eqs. (28) and (29), respectively, and

$$\tilde{\Lambda}^{(2)}(rs, ab; S_i) = \Lambda_4^{(2)}(rs, ab; S_i) + [S_i]^2 \Lambda_5^{(2)}(rs, ab; S_i), \qquad (44)$$

with $\Lambda_4^{(2)}$ and $\Lambda_5^{(2)}$ given by Eqs. (31c) and (31d), respectively. It should be pointed out that the above simple relationship between the ACPQ and ACP-D45 approaches (a factor of 9 for the fifth nonlinear diagram in triplet coupled equations) can *only* be achieved when we employ the orthogonally spin-adapted formulation of the CC theory, as briefly outlined in the present section.

We must emphasize that the ACPQ approach will provide good results only when the UHF wave function reasonably approximates the T_4 clusters. This does not imply, however, that this approach will yield essentially the same results as the UHF based CCSD, since the latter approach will be plagued with a singular behavior (noncontinuous first derivatives of the potential energy surface) when the triplet (nonsinglet) instability [85] sets in, while the ACPQ approach is completely free of this problem. Numerical calculations, both at the semiempirical and *ab· initio* levels, for both orbital and configurational-type [35b] quasidegeneracies, show that the ACPQ approach yields amazingly good correlation energies and invariably provides a slight improvement over the ACP results [35a, 36, 64]. Therefore, in the present series of papers, the ACPQ approach is employed as an approximate CC scheme accounting for the connected tetraexcited cluster components. Computationally efficient methods for the approximate incorporation of the connected triply excited clusters in both ACPQ and CCD approaches are explored in the next section.

3. Approximate account of the connected triply excited clusters in CCD and ACPQ equations: CCDT-1, CCD + T(CCD) and ACPTQ schemes

Numerous MBPT and CC studies indicate that connected triply excited clusters play an important role in various problems of physical and chemical interest, particularly when high degree of accuracy is required (for some examples, see [14, 18, 19, 25, 27, 29, 39, 83a] and references therein). In contrast with T_4 clusters, T_3 clusters can be appreciable in both quasidegenerate and nondegenerate situations, and are normally much more important than their disconnected counterparts $T_1 T_2$ and $\frac{1}{6}T_1^3$ (the latter two terms are accounted for in the full CCSD approach), as first pointed out in [24]. Since the full inclusion of T_3 clusters is very demanding [25, 26], there is a need for development and implementation of approximate schemes.

We shall concentrate on an approximate account of T_3 clusters in the CCD and ACPQ approaches. Although an incorporation of the monoexcited clusters is straightforward, we assume that $T_1 = 0$, since in the following papers of this series we shall deal with systems, for which the HF orbitals are completely determined by the symmetry and thus represent simultaneously Brueckner orbitals. We shall employ the orthogonally spin-adapted formulation of the CC theory outlined in the preceding section.

Consider the CCDT approximation, i.e.

$$T \cong T_2 + T_3. \qquad (45)$$

In order to write the corresponding CCDT equations that determine T_2 and T_3 cluster components, we have to project Eq. (12), with T given by Eq. (45), onto the space spanned by doubly and triply excited configurations. Projection onto

doubles gives

$$\left\langle \begin{array}{cc} r & s \\ a & b \end{array} \right|_{S_i} (H_N e^{T_2 + T_3})_C \left| \Phi_0 \right\rangle = \left\langle \begin{array}{cc} r & s \\ a & b \end{array} \right|_{S_i} [H_N(1 + T_2 + \tfrac{1}{2}T_2^2 + T_3)]_C \left| \Phi_0 \right\rangle = 0.$$

(46)

However, the number of similar equations projected onto triexcited configurations rapidly increases with electron number and the size of the basis. Even when we simplify these equations by neglecting higher-order terms, as was done in the extended CPMET (ECPMET) approach [24, 39], the problem is still untractable for larger bases. A possible remedy is to reduce the number of equations to be solved. We thus consider only Eq. (46) and estimate the correction due to triexcitations,

$$\Lambda^{(3)}(rs, ab; S_i) = \left\langle \begin{array}{cc} r & s \\ a & b \end{array} \right|_{S_i} (H_N T_3)_C \left| \Phi_0 \right\rangle,$$

(47)

through some approximation for $T_3 | \Phi_0 \rangle$. Let us consider this possibility in greater detail. We shall employ RHF orbitals, so that

$$\Lambda^{(3)}(rs, ab; S_i) = \left\langle \begin{array}{cc} r & s \\ a & b \end{array} \right|_{S_i} (V_N T_3)_C \left| \Phi_0 \right\rangle.$$

(48)

Since we cannot estimate the T_3 amplitudes from the UHF wave function, as explained in [37], another method of approximating the component $T_3 | \Phi_0 \rangle$ must be found. We start by writing the MBPT expansion for $T_3 | \Phi_0 \rangle$, namely [52],

$$T_3 | \Phi_0 \rangle = \sum_{n=2}^{\infty} \sum_{C_3} \{(P_0 V_N)^n | \Phi_0 \rangle\}_{C_3}.$$

(49)

The sum over C_r indicates that we include all the connected resulting MBPT diagrams with $2r$ external lines, P_0 is the reduced resolvent for the unperturbed Hamiltonian operator $K_0 = F_N$,
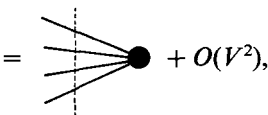
$$P_0 = \sum_j P_0^{(j)},$$

(50)

with

$$P_0^{(j)} = \frac{Q^{(j)}}{\kappa_0^{(0)} - K_0},$$

(51)

and $\kappa_0^{(0)}$ is the eigenvalue of K_0 corresponding to its ground eigenstate $\Phi_0^{(0)} \equiv \Phi_0$, so that $\kappa_0^{(0)} = 0$. Finally, $Q^{(j)}$ is a projector onto the subspace spanned by the j-times excited determinants.

Let us approximate the connected triexcited cluster component of the exact wave function Ψ, given by expansion (49), by considering only diagrams of the type shown in Fig. 5, where a small solid circle represents the non-oriented Hugenholtz V_N vertex and a large open circle the non-oriented Hugenholtz T_2 vertex. A vertical dashed line indicates the MBPT denominator. This approximation is correct up to second order in the wave function (fourth order in the energy), since

$$T_2 | \Phi_0 \rangle = \sum_{n=1}^{\infty} \sum_{C_2} \{(P_0 V_N)^n | \Phi_0 \rangle\}_{C_2}$$
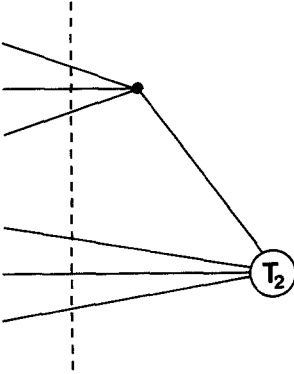

$$= \quad + O(V^2),$$

(52)

Fig. 5. Hugenholtz diagrams contributing to the triexcited connected cluster component of the exact wave function, $T_3|\Phi_0\rangle$, considered in the approximate account of triple excitations in the CCD and ACPQ methods. For the sake of simplicity, we use nonoriented fermion lines, so that the above arrowless diagram represents in fact two oriented diagrams

and, consequently,

$$+ O(V^3) = T_3^{(2)}|\Phi_0\rangle + O(V^3), \qquad (53)$$

where $T_3^{(2)}$ is the second-order contribution to T_3. Diagrams of the type shown in Fig. 5 represent an infinite class of the MBPT diagrams contributing to $T_3|\Phi_0\rangle$, although this class does not contain all the possible diagrams contributing to $T_3|\Phi_0\rangle$. For example, diagrams of the type shown in Fig. 6 which contribute to the third order, are not included.

Rewriting Eq. (48) in a diagrammatic form and replacing the T_3 vertex by diagrams of the type shown in Fig. 5, we get

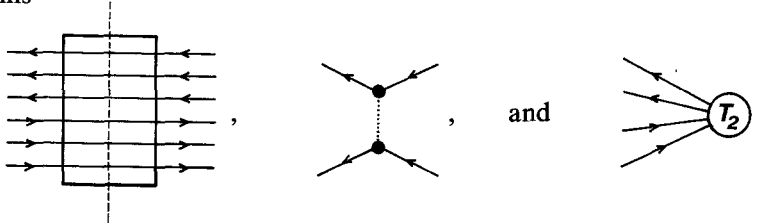$$\Lambda^{(3)}(rs, ab; S_i) \cong$$

$$(54)$$

where, according to our notation, C_0 indicates the set of vacuum resulting diagrams (connected resulting diagrams that have no external lines [52]). To obtain Eq. (54), we have introduced the orientation of lines into the arrowless skeleton of Fig. 5 and replaced Hugenholtz V_N vertices by Goldstone ones (see Fig. 1b). We can easily verify that the subscript C in Eq. (54) is superfluous and that the two diagrams enclosed in parentheses represent all the possible resulting diagrams that we can form from one $P_0^{(3)}$, one V_N and one T_2 diagrams, i.e. from
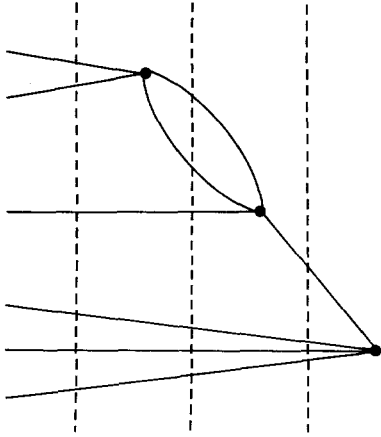
Fig. 6. Hugenholtz diagrams contributing to the connected cluster component $T_3|\Phi_0\rangle$ and not included in the infinite class of MBPT wave function diagrams represented by Fig. 5. Again, arrowless fermion lines are used (cf., caption to Fig. 5), so that the above diagram represents in fact three oriented Hugenholtz diagrams contributing to the third-order MBPT wave function

diagrams

respectively. Thus, Eq. (54) becomes

$$\Lambda^{(3)}(rs, ab; S_i) \cong$$

$$= {}_{S_i}\left\langle \begin{matrix} r & s \\ a & b \end{matrix} \middle| V_N P_0^{(3)} V_N T_2 \middle| \Phi_0 \right\rangle$$

$$= \sum_{\tilde{a} \leqslant \tilde{b}} \sum_{\tilde{r} \leqslant \tilde{s}} \sum_{\tilde{S}_i} {}_{S_i}\left\langle \begin{matrix} r & s \\ a & b \end{matrix} \middle| V_N P_0^{(3)} V_N \middle| \begin{matrix} \tilde{r} & \tilde{s} \\ \tilde{a} & \tilde{b} \end{matrix} \right\rangle_{\tilde{S}_i} \langle \tilde{r}\tilde{s}|t_2|\tilde{a}\tilde{b}\rangle_{\tilde{S}_i}, \qquad (55)$$

where we have used Eq. (22a) in the last step.

It follows that, in the RHF case, the correction accounting for the triples, Eq. (47), can be approximated by the linear form in the t_2 cluster amplitudes, Eq. (55). Assuming some fixed but arbitrary ordering of the orthogonally spin-adapted biexcited states $\left| \begin{matrix} r & s \\ a & b \end{matrix} \right\rangle_{S_i}$, and designating them and the corresponding cluster amplitudes $\langle rs|t_2|ab\rangle_{S_i}$ by Φ_i and t_i ($i = 1, \ldots, M$), respectively, we can

write this correction as

$$\Lambda^{(3)}(i) \cong \sum_j W_{ij}^{(3)} t_j, \tag{56}$$

where

$$W_{ij}^{(3)} = \langle \Phi_i | V_N \frac{Q^{(3)}}{-F_N} V_N | \Phi_j \rangle. \tag{57}$$

With the same notation, the CCD and ACPQ equations, (26) and (43), take the form

$$a_i + \sum_j b_{ij} t_j + \sum_{j \le k} c_{ijk} t_j t_k = 0 \quad (i = 1, \ldots, M), \tag{58}$$

where the constant and linear terms

$$a_i = \langle \Phi_i | H_N | \Phi_0 \rangle = \langle \Phi_i | V_N | \Phi_0 \rangle, \tag{59}$$

$$b_{ij} = \langle \Phi_i | H_N | \Phi_j \rangle, \tag{60}$$

are identical with the corresponding CI matrix elements. The connected triple excitations can thus be incorporated into the CCD and ACPQ approaches through a slight modification of their linear part, namely

$$a_i + \sum_j \tilde{b}_{ij} t_j + \sum_{j \le k} c_{ijk} t_j t_k = 0 \quad (i = 1, \ldots, M), \tag{61}$$

where

$$\tilde{b}_{ij} = b_{ij} + W_{ij}^{(3)}, \tag{62}$$

with $W_{ij}^{(3)}$ given by Eq. (57). In a similar way we can account for the effect of triples in the orthogonally spin-adapted CCSD [40] (or ACPQ with singles) approach, provided that we neglect $T_1 T_3$ term (contributing for the first time in the fourth-order MBPT wave function, assuming the HF reference) in equations projected onto doubles. In addition to the matrix elements between doubles, Eq. (57), we also need analogous matrix elements between singles and doubles. We note that the system of Eqs. (61) has the same structure as the corresponding CCD or ACPQ systems, Eq. (58), so that it can be solved in the same way as CCD equations [13, 14, 18, 47].

An equivalent procedure at the spin-orbital level was proposed by Lee et al. [29] and is referred to as the CCSDT-1 [29] or CCSDT-la [27] method (for CCSDT-n models, see [18, 25, 27, 86]). It is easily seen that CCSDT-1 accounts for diagrams of the same type as shown in Fig. 5 and neglects disconnected $T_1 T_3$ clusters. When these latter terms are taken into account, a more complete model referred to as CCSDT-1b [27, 87] results. However, for the vanishing monoexcitations ($T_1 = 0$) considered in the present series, both CCSDT-la and CCSDT-1b models are identical and the resulting approximation can be simply termed CCDT-1. Thus, the orthogonally spin-adapted CCD theory corrected for connected triples, defined by Eqs. (61) and (62), where c_{ijk} are given by Eqs. (30) and (31), will be designated as the CCDT-1 approach. Our formulation of the CC(S)DT-1 method differs somewhat from that given by Lee et al. [29], since we first incorporate triples by correcting the linear part of the CC(S)D equations. Once this is done, the resulting system of nonlinear equations is solved iteratively. In the Bartlett group implementation [29], the CCSD equations are corrected for the triples in every iteration. Provided that the iterative scheme converges, the result of both implementations is the same. Clearly, in large scale

ab initio computations, when we cannot store even the linear b_{ij} coefficients, the iterative method of solving the CC(S)DT-1 equations is inevitable. However, the noniterative formulation, as presented above, will prove useful in calculations for small or model problems.

Numerical applications confirm the high accuracy of the CCSDT-1 model and its ability to reproduce a large portion of the triple excitation contribution to both the correlation energy and molecular properties in several chemically interesting systems [25–27, 29, 88–91] (for a comprehensive review and recent references, see [19]; cf. also review articles [14, 18]). However, a neglect of higher-order contributions to T_3 may result in a poor performance of the CCSDT-1 approach. This happens particularly for nonequilibrium geometries [91(b)] when T_3 effects become very prominent.

Equations (61) and (62), with coefficients c_{ijk} given by Eqs. (44), (31c) and (31d), represent the ACPQ equations corrected for the effect of connected triples. We thus refer to the resulting approach as the ACPTQ (approximate coupled-pair theory with connected triples and quadruples) approximation. We expect that this method will yield rather accurate correlation energies even in quasidegenerate situations (similar to the ACPQ model), although convergence problems connected with the perturbative way of including the triples certainly will arise.

There is yet another simple approach, which is almost as good as the CCSDT-1 method for many applications. It was suggested by Urban et al. [27] and, independently, by Raghavachari [28] and, like the CCSDT-1 scheme, requires the calculation of matrix elements $W_{ij}^{(3)}$, Eq. (57). In the formulation presented by Urban et al. this approach is referred to as the CCSD + T(CCSD) model, while Raghavachari labeled his version CCD + ST(CCD). In the CCSD + T(CCSD) scheme, converged CCSD t_2-cluster coefficients t_i^{CCSD} ($i = 1, \ldots, M$) are used to evaluate the triple excitation contribution to the correlation energy, ΔE^T, according to the formula

$$\Delta E^T = \sum_{i,j} (t_i^{CCSD})^* W_{ij}^{(3)} t_j^{CCSD}. \tag{63}$$

This contribution is then simply added to the result of the CCSD calculations. In CCD + ST(CCD) method, the converged solution of the CCD equations (58) is employed and contributions of both singles and triples, ΔE^S and ΔE^T, respectively, are evaluated. The corresponding expressions are

$$\Delta E^S = \sum_{i,j} (t_i^{CCD})^* W_{ij}^{(1)} t_j^{CCD}, \tag{64}$$

where

$$W_{ij}^{(1)} = \langle \Phi_i | V_N \frac{Q^{(1)}}{-F_N} V_N | \Phi_j \rangle, \tag{65}$$

and

$$\Delta E^T = \sum_{i,j} (t_i^{CCD})^* W_{ij}^{(3)} t_j^{CCD}. \tag{66}$$

Since the amplitudes $t_i^{CC(S)D}$ are correct to the first order, both the CCSD + T(CCSD) and CCD + ST(CCD) approaches provide the correlation energy correct through the fourth order (one can easily verify this by replacing t_i^{CCSD} in Eq. (63) and t_i^{CCD} in Eqs. (64) and (66) by the first-order wave function expansion coefficients $t_i^{(1)}$; the resulting expressions give standard formulas for the contribution of singles and triples to the correlation energy in the fourth order). In addition, just as the CCSDT-1 scheme, they include significant fifth and

higher-order contributions. In many cases, the CCSD + T(CCSD) and CCD + ST(CCD) methods yield very accurate results, as the correlation energy calculations [27, 89, 90], calculations of the excitation [28, 89] and dissociation [28, 92] energies, the reaction energy calculations [90], and the molecular structure studies [89, 91] indicate (see also [18, 19]). There are, however, situations where CCSD + T(CCSD) and CCD + ST(CCD) are likely to fail. These are: (i) the strongly correlated limit, where V_N becomes the dominant part of the Hamiltonian, and (ii) highly degenerate situations, when the CC(S)D approach suffers a singular behavior and solution of the CC(S)D equations is no longer available (cf. the previous section). Clearly, in the first case, perturbative inclusion of triples (and singles) is no longer correct and additivity of the triexcited contribution, which is assumed in both the CCSD + T(CCSD) and CCD + ST(CCD) models, breaks down [61]. Both cases will be studied in Part II of this series.

The main reason for introducing the simple non-iterative CCSD + T(CCSD) model [90] was to eliminate the iterative way of inclusion of triples in the original formulation of the CCSDT-1 method [29]. As already mentioned, our formulation of the CCSDT-1 model is noniterative, since in our case matrices of coefficients a_i, b_{ij} and c_{ijk} can be kept in the fast core and thus we can use standard Newton–Raphson method combined with the non-iterative Gauss elimination algorithm to solve the linear systems. Consequently, there is no essential difference in the computational effort that is required in the CCSD + T(CCSD) and CCD + ST(CCD) approaches, and in our formulation of the CCSDT-1 scheme. When $T_1 = 0$ (the case considered here), the CCSD + T(CCSD) and CCD + ST(CCD) methods become identical. In this case we shall refer to this approach as the CCD + T(CCD) approximation. It is defined by Eq. (58), where the coefficients c_{ijk} are given by Eqs. (30) and (31), together with Eqs. (40) and (66).

The three CC models presented in this section, namely CCDT-1, ACPTQ and CCD + T(CCD), require calculation of the effective interaction matrix elements $W_{ij}^{(3)}$, Eq. (57), between orthogonally spin-adapted biexcited singlet configurations $\left| \begin{array}{cc} r & s \\ a & b \end{array} \right\rangle_{S_i}$, Eq. (18). Before deriving the explicit form of these elements, we note that the same matrix elements are also required in the OIP method, belonging to a completely different category of quantum mechanical approaches. We consider this approach in the next section.

4. Optimized inner projection technique for PPP model Hamiltonians

It is well known that the determination of lower bounds is much more difficult than the calculation of upper bounds using a standard variation principle. Even today, the lower bound determination remains to be limited to simple or model Hamiltonians and, at the *ab initio* level, to three-electron systems (see, e.g., [93] and references therein). Nonetheless, the study of lower bounds represents one of the basic and challenging problems that focusses the attention of many scientists. The sixties and early seventies were particularly productive. Weinstein's intermediate problem method [94], further developed by Aronszajn [95], was adapted to quantum mechanics by Bazley [96] and Bazley and Fox [97], and later combined by Löwdin with his concept of a bracketing function [98–100]. Subsequently, Löwdin's method of inner projection [99, 101] became a subject of numerous studies and applications [102, 103] (see also review [100] and references therein).

More recently, classical Löwdin's formulation of the inner projection technique was slightly modified and the optimized inner projection (OIP) scheme (referred to also as the renormalized inner projection method) was introduced [31]. It was applied with remarkable success to evaluation of lower energy bounds for simple one-particle systems (anharmonic oscillator and hydrogen atom in magnetic field) [31, 32] as well as for more complex PPP model of cyclic polyenes [33, 34]. In the latter case the results are much less convincing [34] and a further investigation of the applicability of the OIP technique is needed. We shall first present the main ideas of the OIP approach as formulated by Čížek and Vrscay [31]. Then, we shall concentrate on the OIP method for the PPP model Hamiltonians, particularly as applied to cyclic polyenes.

In order to apply the OIP technique, we first write the Hamiltonian $\mathcal{H}$ of our system as a sum of an unperturbed Hamiltonian $\mathcal{H}^{(0)}$ and a perturbation $\mathcal{V}$. It is assumed that the solutions of an unperturbed eigenvalue problem,

$$\mathcal{H}^{(0)}\phi_k^{(0)} = \mathcal{E}_k^{(0)}\phi_k^{(0)}, \qquad \mathcal{E}_0^{(0)} < \mathcal{E}_1^{(0)} < \mathcal{E}_2^{(0)} < \cdots, \tag{67}$$

are available, and $\mathcal{V}$ is a positive definite operator, i.e.,

$$\mathcal{V} > 0. \tag{68}$$

As in perturbation theory, we consider the perturbed eigenvalue problem,

$$\mathcal{H}\psi_k = \mathcal{E}_k\psi_k, \tag{69}$$

where $\mathcal{E}_k \to \mathcal{E}_k^{(0)}$ and $\psi_k \to \phi_k^{(0)}$ as $\mathcal{V} \to 0$. We do not pretend, however, to solve it. Our objective is to evaluate lower bounds to the eigenenergies $\mathcal{E}_k$ and this is achieved by finding the eigenvalues $\mathcal{E}_k'$ of an intermediate Hamiltonian

$$\mathcal{H}' = \mathcal{H}^{(0)} + \mathcal{V}', \tag{70}$$

where $\mathcal{V}'$ satsifies the inequality

$$\mathcal{V}' < \mathcal{V}, \tag{71}$$

which in turn implies that

$$\mathcal{E}_k' < \mathcal{E}_k. \tag{72}$$

In the OIP method, $\mathcal{V}'$ satisfying Eq. (71) is defined by partitioning the solution space for $\mathcal{H}^{(0)}$ and considering the $(M + 1)$-dimensional manifold $\mathcal{M}_g^{(0)}$ spanned by $\phi_0^{(0)}$ and M excited eigenstates of $\mathcal{H}^{(0)}$,

$$\mathcal{M}_g^{(0)} = \langle g_0, g_1, \ldots, g_M \rangle, \tag{73}$$

where

$$g_0 = \phi_0^{(0)}, \qquad g_i = \phi_{k_i}^{(0)} \quad (i = 1, \ldots, M). \tag{74}$$

Then, the new manifold

$$\mathcal{M}_f^{(0)} = \langle f_0, f_1, \ldots, f_M \rangle, \tag{75}$$

spanned by the functions

$$f_i = \mathcal{V}^{1/2}g_i \quad (i = 0, 1, \ldots, M), \tag{76}$$

where $\mathcal{V}^{1/2}$ denotes the positive square root of $\mathcal{V}$ (note that, in contrast to the functions g_i, the f_i are not necessarily mutually orthogonal), is introduced and $\mathcal{V}'$ is simply defined as an inner projection of $\mathcal{V}$ onto the manifold $\mathcal{M}_f^{(0)}$,

$$\mathcal{V}' = \mathcal{V}^{1/2}Q_f\mathcal{V}^{1/2}, \tag{77}$$

where Q_f is the projection operator associated with the subspace $\mathscr{M}_f^{(0)}$. In this way, condition (71) is automatically satisfied, since

$$0 \leqslant Q_f \leqslant 1. \tag{78}$$

The OIP lower energy bounds are the eigenvalues of the Hamiltonian (70), where $\mathscr{V}'$ is given by Eq. (77). Therefore, they are found by solving the equation

$$f'(\mathscr{E}) = \mathscr{E}, \tag{79}$$

where $f'(\mathscr{E})$ is the bracketing function [98–100] for the Hamiltonian $\mathscr{H}'$. The particular choice of the subspaces $\mathscr{M}_f^{(0)}$ and $\mathscr{M}_g^{(0)}$ [see Eqs. (73)–(76)] enables us to write the following expression for $f'(\mathscr{E})$ [31]:

$$f'(\mathscr{E}) = \mathscr{E}_0^{(0)} + \sum_{i,j=0}^{M} \mathscr{V}_{0i}(A(\mathscr{E})^{-1})_{ij}\mathscr{V}_{j0}, \tag{80}$$

where

$$\mathscr{V}_{ij} = \langle g_i | \mathscr{V} | g_j \rangle, \quad 0 \leqslant i, j \leqslant M, \tag{81}$$

and $A(\mathscr{E})$ is the $(M + 1)$ by $(M + 1)$ parameter dependent matrix, whose entries are given by

$$A(\mathscr{E})_{ij} = \mathscr{V}_{ij} - \sum_{k=1}^{\infty} \frac{\mathscr{V}_{ik}\mathscr{V}_{kj}}{\mathscr{E} - \mathscr{E}_k^{(0)}}, \quad 0 \leqslant i, j \leqslant M. \tag{82}$$

It must be noticed that the summation over k in Eq. (82) is not restricted to functions g_i, Eq. (74), which span the manifold $\mathscr{M}_g^{(0)}$, but is infinite and runs over all excited eigenstates of the Hamiltonian $\mathscr{H}^{(0)}$. Therefore, not only matrix elements $\mathscr{V}_{ij}$, Eq. (81), have to be evaluated, but, in principle, we need to know all the matrix elements of $\mathscr{V}$ between the eigenfunctions of $\mathscr{H}^{(0)}$ which span $\mathscr{M}_g^{(0)}$ and all the eigenstates of $\mathscr{H}^{(0)}$, i.e.,

$$\mathscr{V}_{ik} = \mathscr{V}_{ki}^* = \langle g_i | \mathscr{V} | \phi_k^{(0)} \rangle, \quad 0 \leqslant i \leqslant M, \, k = 0, 1, \ldots. \tag{83}$$

Fortunately, in well-behaved cases, including the PPP model of unsaturated hydrocarbons considered below, the matrix elements $\mathscr{V}_{ik}$ vanish for $|i - k|$ sufficiently large. Consequently, the summation over k in Eq. (82) becomes finite and, as we shall see, can be relatively easily performed.

Once the bracketing function $f'(\mathscr{E})$, Eq. (80), is known, several numerical schemes can be employed to solve Eq. (79). A very simple iterative procedure, with the individual iterates oscillating about one of the roots $\mathscr{E}_k'$, was suggested in a paper by Čížek and Vrscay [31]. It is based on the iteration sequence $\mathscr{E}_{k,m+1} = f'(\mathscr{E}_{k,m})$ $(m = 0, 1, \ldots)$, where the initial guess $\mathscr{E}_{k,0}$ is the upper bound to $\mathscr{E}_k$. The sequence $\mathscr{E}_{k,m}$ $(m = 0, 1, \ldots)$ converges to the lower bound $\mathscr{E}_k'$, provided that $|df'(\mathscr{E})/d\mathscr{E}| < 1$ for every $\mathscr{E} \in (\mathscr{E}_k' - \Delta\mathscr{E}_k, \mathscr{E}_k' + \Delta\mathscr{E}_k)$, where $\Delta\mathscr{E}_k = |\mathscr{E}_{k,0} - \mathscr{E}_k'|$. In view of the properties of bracketing functions [98–100], this implies that the initial guess $\mathscr{E}_{k,0}$ lies on the same branch of $f'(\mathscr{E})$ as does $\mathscr{E}_k'$ and is sufficiently close to $\mathscr{E}_k'$. Čížek and Vrscay [31] suggest the kth variational energy $\mathscr{E}_k^{\text{var}}$ calculated in a basis $\{g_0, g_1, \ldots, g_M\}$ as an optimal choice for $\mathscr{E}_{k,0}$. This choice makes the whole method self-contained and transparent. It can cause, however, serious difficulties in practical applications. Higher-order procedures for finding the solutions of Eq. (79), e.g., Newton's method or more advanced root searching techniques, may serve as a possible remedy for these difficulties (cf. Part III of this series).

Equations (79)–(83) represent the basic set of formulas characterizing the OIP approach. In order to apply them, we have to know how to split a given Hamiltonian into the uperturbed part and the positive definite perturbation. In the case of simple one-particle systems, like anharmonic oscillator or hydrogen atom in a magnetic field, this can be achieved with the help of simple renormalization procedures [31, 32]. However, when real many-electron systems are considered at the *ab initio* level, the positive definiteness of the perturbation is affected by the presence of the effective one-electron part in the Hamiltonian [cf. Eqs. (1)–(4)] and, consequently, a decomposition of the Hamiltonian into $\mathscr{H}^{(0)}$ and a positive definite $\mathscr{V}$ may not be possible.

At a semiempirical level, the situation is somewhat better. Consider, for example, the PPP model of neutral planar conjugated hydrocarbons [50]. It assumes that the π-electrons constitute a separable electronic group and move in an unpolarizable field of nuclei, inner-shells and σ-electrons. In the second quantized form, the PPP Hamiltonian can be expressed as

$$H_\pi = \sum_{\mu\nu} z_{\mu\nu} E_{\mu\nu} + \tfrac{1}{2} \sum_{\mu\nu} \gamma_{\mu\nu} (E_{\mu\mu} E_{\nu\nu} - \delta_{\mu\nu} E_{\mu\nu}), \tag{84}$$

where the orbital unitary group generators $E_{\mu\nu}$ are given by Eq. (5) and the creation and annihilation operators are defined on a hypothetical minimum basis of symmetrically orthonormalized [104, 105] $2p_z$ carbon atomic spin-orbitals $|\mu\sigma\rangle = |\mu\rangle|\sigma\rangle$, $\sigma = \pm\frac{1}{2}$, localized on carbon nuclei. Like all semiempirical Hamiltonians, H_π is defined directly by specifying the one- and two-electron matrix elements,

$$z_{\mu\nu} = \langle \mu | z | \nu \rangle, \tag{85}$$

and

$$\gamma_{\mu\nu} = \langle \mu\nu \| \mu\nu \rangle, \tag{86}$$

respectively, rather than by selecting the spin-orbital basis set $\{|\mu\sigma\rangle\}$ as is done for *ab initio* model Hamiltonians. The absence of other than one- and two-center Coulomb-type two-electron integrals, Eq. (86), in the Hamiltonian H_π is due to the assumption of zero differential overlap [50]. The diagonal one-electron matrix elements $z_{\mu\mu}$ are determined with the help of the Goepert–Mayer and Sklar approximation [50]. Consequently,

$$z_{\mu\mu} = \alpha_\mu - \sum_{\nu(\neq\mu)} \gamma_{\mu\nu}, \tag{87}$$

where α_μ is a so-called Coulomb integral. For the off-diagonal matrix elements $z_{\mu\nu}$, $\mu \neq \nu$, the tight-binding approximation is invoked, so that

$$z_{\mu\nu} = \begin{cases} \beta_{\mu\nu}, & \text{if } \mu \text{ and } \nu \text{ are nearest neighbors,} \\ 0, & \text{otherwise,} \end{cases} \tag{88}$$

where $\beta_{\mu\nu}$ is a so-called resonance integral. For the neutral conjugated hydrocarbons considered here, we can further assume that all the one-center integrals are equivalent, namely that

$$\alpha_\mu = \alpha_0, \qquad \gamma_{\mu\mu} = \gamma_{00}. \tag{89}$$

Consequently, the PPP Hamiltonian H_π, Eq. (84), is fully determined by the integrals α_0, $\beta_{\mu\nu}$ (μ, ν nearest neighbors), γ_{00} and $\gamma_{\mu\nu}$ ($\mu \neq \nu$), considered as empirical parameters. The problem of parametrization choice can be found elsewhere [50] and will be addressed in Part II of this series.

In order to split the PPP model Hamiltonian into the unperturbed part $\mathscr{H}^{(0)}$ and the positive definite perturbation $\mathscr{V}$, and thus fulfil the basic requirement of the OIP technique, we have to consider the total Hamiltonian, hereafter denoted as $\mathscr{H}$, including the internuclear repulsion term $\sum_{\mu < \nu} \gamma_{\mu\nu}$ [50], rather than the purely electronic Hamiltonian H_π given by Eqs. (84) and (87)–(89). It can be shown (see, e.g., [53]) that

$$\mathscr{H} \equiv H_\pi + \sum_{\mu < \nu} \gamma_{\mu\nu}, \tag{90}$$

can be decomposed as follows:

$$\mathscr{H} = \mathscr{H}^{(0)} + \mathscr{V}, \tag{91}$$

where

$$\mathscr{H}^{(0)} = \sum_\mu \alpha_\mu n_\mu + \sum_{\mu\nu}{}' \beta_{\mu\nu} E_{\mu\nu} = N\alpha_0 + \sum_{\mu\nu}{}' \beta_{\mu\nu} E_{\mu\nu}, \tag{92}$$

and

$$\mathscr{V} = \tfrac{1}{2} \sum_{\mu\nu} \gamma_{\mu\nu} (n_\mu - 1)(n_\nu - 1). \tag{93}$$

The prime on the second summation symbol in Eq. (92) indicates that it extends over nearest neighbors only. Further, $n_\mu = E_{\mu\mu}$ is the μth site occupation number operator. The positive definiteness of the operator $\mathscr{V}$, Eq. (93), results immediately from the fact that for any physically reasonable parametrization of the PPP model, $\gamma_{\mu\nu} > 0$. Thus, the OIP method can be directly applied.

It is seen that the unperturbed part $\mathscr{H}^{(0)}$ is the Hückel Hamiltonian. Therefore, the ground eigenstate $\phi_0^{(0)}$ of the Hamiltonian $\mathscr{H}^{(0)}$ represents the Hückel solution for the system considered, i.e. the IPM single determinantal state Φ_0, which is built from doubly occupied energetically lowest Hückel orbitals. Excited eigenstates $\phi_k^{(0)}$ are then obtained by single, double, triple, etc. excitations from the reference determinant Φ_0. Since we consider a closed-shell case, only singlet excited configurations need to be constructed, all other eigenstates $\phi_k^{(0)}$ that are not singlets may be ignored. Obviously, eigenvalues $\mathscr{E}_k^{(0)}$ of the Hamiltonian $\mathscr{H}^{(0)}$ are the appropriate sums of the Hückel orbital energies, namely those associated with the orbitals occupied in $\phi_k^{(0)}$.

Following the OIP scheme, it remains to partition the solution space for the unperturbed Hamiltonian $\mathscr{H}^{(0)}$, Eq. (92), into the manifold $\mathscr{M}_g^{(0)}$, which is spanned by $\phi_0^{(0)}$ and some of the excited eigenstates of $\mathscr{H}^{(0)}$ [cf. Eqs. (73) and (74)], and its orthogonal complement $\mathscr{M}_g^{(0)\perp}$. Clearly, this can be done in a completely arbitrary manner. Since, however, we consider the application of the OIP technique to the quantum chemical model Hamiltonian $\mathscr{H}$, Eq. (90), it is best to choose the relevant manifold $\mathscr{M}_g^{(0)}$ as a linear span of the Hückel solution Φ_0 and all possible singlet spin-adapted mono- and biexcited configurations relative to Φ_0. In this way, the summation over k in the definition of matrix $A(\mathscr{E})$, Eq. (82), will extend over at most quadruply excited configurations relative to Φ_0, because the perturbation $\mathscr{V}$, Eq. (93), includes at most two-electron interactions.

In some cases, for example, when quasidegeneracy becomes appreciable or stricter OIP lower energy bounds are required, it may be necessary to consider a larger manifold $\mathscr{M}_g^{(0)}$ that includes triply and quadruply excited configurations as

well (cf. Sect. 2). However, such an extension is hardly feasible, even for relatively small systems, in view of a large number of triple and quadruple excitations, even at the orthogonally spin-adapted level. We thus only consider the problem of evaluation of the OIP matrix elements $A(\mathscr{E})_{ij}$, Eq. (82), for the case when the manifold $\mathscr{M}_g^{(0)}$ is spanned by Φ_0 and all possible singlet spin-adapted mono- and biexcitations.

We could now consider the general case of neutral conjugated hydrocarbons by transforming the second quantized expression for the perturbation $\mathscr{V}$, Eq. (93), from an atomic to Hückel molecular orbital (HMO) basis and by exploiting either the diagrammatic methods of the MBPT [8, 51, 52] combined with the graphical methods of spin algebras [38, 44, 106, 107] or algebraic techniques [53, 108, 109] in order to calculate the pertinent matrix elements. Our intention, however, is to use the OIP formalism to determine lower energy bounds for the PPP model of cyclic polyenes with nondegenerate ground state, $C_N H_N$, $N = 2n = 4v + 2$, $v = 1, 2, \ldots$ [49]; this will be reported in Part III of the present series. To keep this presentation at a very transparent level, we focus our attention on the evaluation of the OIP matrix $A(\mathscr{E})$ for the case of cyclic polyenes, where the high symmetry greatly simplifies the considerations. These considerations, however, should give us an idea how the general case of neutral conjugated hydrocarbons might be treated, if necessary.

The cyclic polyene model will be described in greater detail in Part II of the present series. Let us now only mention that in this case the atomic orbitals $|\mu\rangle$, $\mu = 0, 1, \ldots, N - 1$, are localized on the vertices of the regular N-gon. Consequently, general relations between one- and two-body parts of the electronic Hamiltonian H_π, Eq. (84), Z and V, respectively, and the Hückel Hamiltonian $\mathscr{H}^{(0)}$ and the perturbation $\mathscr{V}$, Eqs. (92) and (93), respectively, i.e.

$$\mathscr{H}^{(0)} = Z + \sum_{\mu \neq v} \gamma_{\mu v} n_\mu, \tag{94}$$

$$\mathscr{V} = V + \sum_{\mu < v} \gamma_{\mu v} - \sum_{\mu \neq v} \gamma_{\mu v} n_\mu, \tag{95}$$

can be simplified by the symmetry property,

$$\gamma_{\mu v} = \gamma_{\mu + \kappa, v + \kappa} = \gamma_{0, \mu - v}, \tag{96}$$

where the indices are understood to be taken modulo N. We obtain

$$\mathscr{H}^{(0)} = Z + 2 \sum_{\mu < v} \gamma_{\mu v} = Z_N + \langle \Phi_0 | Z | \Phi_0 \rangle + 2 \sum_{\mu < v} \gamma_{\mu v}, \tag{97}$$

$$\mathscr{V} = V - \sum_{\mu < v} \gamma_{\mu v} = V_N + G_N + \langle \Phi_0 | V | \Phi_0 \rangle - \sum_{\mu < v} \gamma_{\mu v}, \tag{98}$$

where

$$Z_N = \sum_{\mu v} z_{\mu v} N[E_{\mu v}], \tag{99}$$

and

$$G_N = \sum_{\mu v} g_{\mu v} N[E_{\mu v}]. \tag{100}$$

Here $g_{\mu v} = \langle \mu | g | v \rangle$, where $g = f - z$, and the normal product operation $N[\cdots]$ is defined with respect to the Hückel solution Φ_0. In view of the high spatial

symmetry of cyclic polyenes (C_N or D_{Nh}), the Hückel molecular orbitals are completely determined by symmetry and they become simultaneously both the HF and Brueckner orbitals labeled by an appropriate quasimomentum (see, e.g., [35a] and Part II). Consequently, the Hückel solution Φ_0 is identical with the RHF ground state and all the monoexcited configurations relative to Φ_0 may be ignored, since they necessarily belong to a different symmetry species than Φ_0 itself. Moreover, because of the relation (97), the one-electron operator z is diagonal in the molecular orbital basis $\{|m\rangle\}$. Therefore, all three one-body operators, f, z and g become diagonal in the basis $\{|m\rangle\}$ and Hückel orbital energies ε_m^{HMO} differ from eigenvalues $\langle m|z|m\rangle$ only by a constant factor [cf., Eq. (97)].

A further consequence of the high spatial symmetry of cyclic polyenes is a so-called zero quasimomentum rule, which has to be satisfied by molecular integrals $\langle mn\|pq\rangle$, and all doubly, triply, etc. excited configurations (see, e.g., [35a]). In addition, the PPP cyclic polyene model possesses the hole-particle and so-called alternancy symmetries [35a, 50]. These symmetries enable drastic simplifications of the formalism. We do not exploit them here, however, since in this paper we wish to concentrate on those formal aspects of the OIP and CC theories that appear at a very general orthogonally spin-adapted level. They will be exploited in Parts II and III of this series.

As already mentioned, we can ignore all singly excited configurations. We thus assume that the manifold $\mathscr{M}_g^{(0)}$ is spanned by Φ_0 and all possible orthogonally spin-adapted doubly excited configurations $\left|\begin{smallmatrix} r & s \\ a & b \end{smallmatrix}\right\rangle_{S_i}$, Eq. (18), which we designate by Φ_i ($i = 1, \ldots, M$) as in Sect. 3. Then, Eq. (74) takes the form:

$$g_i = \Phi_i \quad (i = 0, 1, \ldots, M), \tag{101}$$

and the sum on the right-hand side of Eq. (82) can be decomposed into the three parts corresponding to summations over doubly, triply and quadruply excited configurations. Making use of the fact that [see Eq. (97)]

$$\mathscr{E}_0^{(0)} = \langle \Phi_0|\mathscr{H}^{(0)}|\Phi_0\rangle = \langle \Phi_0|Z|\Phi_0\rangle + 2 \sum_{\mu < \nu} \gamma_{\mu\nu} = \mathscr{H}^{(0)} - Z_N, \tag{102}$$

and introducing a new parameter ε defined as

$$\varepsilon = \mathscr{E} - \mathscr{E}_0^{(0)}, \tag{103}$$

we now write Eq. (82) as

$$A(\varepsilon)_{ij} = \mathscr{V}_{ij} - [W_{ij}^{(2)}(\varepsilon) + W_{ij}^{(3)}(\varepsilon) + W_{ij}^{(4)}(\varepsilon)] \quad (i, j = 0, 1, \ldots, M), \tag{104}$$

where

$$\mathscr{V}_{ij} = \langle \Phi_i|\mathscr{V}|\Phi_j\rangle, \tag{105}$$

$$W_{ij}^{(k)}(\varepsilon) = \langle \Phi_i|\mathscr{V} \frac{Q^{(k)}}{\varepsilon - Z_N} \mathscr{V}|\Phi_j\rangle \quad (k = 2, 3, 4). \tag{106}$$

Clearly, evaluation of $W_{ij}^{(2)}(\varepsilon)$ requires only the knowledge of the matrix elements $\mathscr{V}_{ij}$, Eq. (105), which have to be calculated anyway as indicated by

Eq. (104). Applying relation (98), one can find the following expressions,

$$\mathscr{V}_{00} = \langle \Phi_0 | V | \Phi_0 \rangle - \sum_{\mu < \nu} \gamma_{\mu\nu}, \tag{107}$$

$$\mathscr{V}_{0j} = \mathscr{V}_{j0}^* = \langle \Phi_0 | V_N | \Phi_j \rangle \quad (j = 1, \ldots, M), \tag{108}$$

$$\mathscr{V}_{ij} = \langle \Phi_i | V_N | \Phi_j \rangle + \delta_{ij}[\langle r|g|r \rangle + \langle s|g|s \rangle - \langle a|g|a \rangle - \langle b|g|b \rangle + \mathscr{V}_{00}]$$
$$(i, j = 1, \ldots, M), \tag{109}$$

where r, s and a, b are, respectively, the particle and hole orbital labels characterizing the orthogonally spin-adapted biexcited state $\Phi_i = \begin{vmatrix} r & s \\ a & b \end{vmatrix}_{S_i}$. Equations (107) and (108) immediately follow from Eq. (98). To get Eq. (109), we have to evaluate matrix elements $_{S_i}\left\langle \begin{matrix} r & s \\ a & b \end{matrix} \middle| G_N \middle| \begin{matrix} \tilde{r} & \tilde{s} \\ \tilde{a} & \tilde{b} \end{matrix} \right\rangle_{\bar{S}_i}$. The result is [43, 44]

$$_{S_i}\left\langle \begin{matrix} r & s \\ a & b \end{matrix} \middle| G_N \middle| \begin{matrix} \tilde{r} & \tilde{s} \\ \tilde{a} & \tilde{b} \end{matrix} \right\rangle_{\bar{S}_i} = N_{ab}^{rs} N_{\tilde{a}\tilde{b}}^{\tilde{r}\tilde{s}} \delta_{S_i \bar{S}_i}[A_{ab}^{\tilde{a}\tilde{b}}(S_i)\mathscr{S}_{rs}(S_i)\mathscr{S}_{\tilde{r}\tilde{s}}(S_i)\langle r|g|\tilde{r} \rangle \langle s|\tilde{s} \rangle$$
$$- A_{rs}^{\tilde{r}\tilde{s}}(S_i)\mathscr{S}_{ab}(S_i)\mathscr{S}_{\tilde{a}\tilde{b}}(S_i)\langle \tilde{a}|g|a \rangle \langle b|\tilde{b} \rangle], \tag{110}$$

where we have introduced the new quantity

$$A_{mn}^{\tilde{m}\tilde{n}}(S) = \mathscr{S}_{mn}(S)\langle m|\tilde{m} \rangle \langle n|\tilde{n} \rangle, \tag{111}$$

which will be particularly useful in the next section. If we also employ the fact that g is diagonal in the basis $\{|m\rangle\}$, we get

$$_{S_i}\left\langle \begin{matrix} r & s \\ a & b \end{matrix} \middle| G_N \middle| \begin{matrix} \tilde{r} & \tilde{s} \\ \tilde{a} & \tilde{b} \end{matrix} \right\rangle_{\bar{S}_i} = N_{ab}^{rs} N_{\tilde{a}\tilde{b}}^{\tilde{r}\tilde{s}} \delta_{S_i \bar{S}_i} A_{ab}^{\tilde{a}\tilde{b}}(S_i) A_{rs}^{\tilde{r}\tilde{s}}(S_i)[\mathscr{S}_{rs}\langle r|g|r \rangle - \mathscr{S}_{ab}\langle a|g|a \rangle], \tag{112}$$

which is the desired expression, since [43, 44]

$$N_{ab}^{rs} N_{\tilde{a}\tilde{b}}^{\tilde{r}\tilde{s}} \delta_{S_i \bar{S}_i} A_{ab}^{\tilde{a}\tilde{b}}(S_i) A_{rs}^{\tilde{r}\tilde{s}}(S_i) = _{S_i}\left\langle \begin{matrix} r & s \\ a & b \end{matrix} \middle| \begin{matrix} \tilde{r} & \tilde{s} \\ \tilde{a} & \tilde{b} \end{matrix} \right\rangle_{\bar{S}_i} \tag{113}$$

represents the overlap integral $\langle \Phi_i | \Phi_j \rangle = \delta_{ij}$. We thus see the both $\mathscr{V}_{ij}$ and $W_{ij}^{(2)}(\varepsilon)$ can be simply evaluated using the two-body part of the D-CI matrix. Explicit expressions for

$$\left\langle \Phi_0 \middle| V_N \middle| \begin{matrix} \tilde{r} & \tilde{s} \\ \tilde{a} & \tilde{b} \end{matrix} \right\rangle_{\bar{S}_i} \quad \text{and} \quad _{S_i}\left\langle \begin{matrix} r & s \\ a & b \end{matrix} \middle| V_N \middle| \begin{matrix} \tilde{r} & \tilde{s} \\ \tilde{a} & \tilde{b} \end{matrix} \right\rangle_{\bar{S}_i}$$

can be found elsewhere [43, 44]. A simple diagrammatic rederivation of these expressions as well as of formula (110), that is based on the graphical methods of spin algebras, and employs Goldstone form for V_N vertices, Fig. 1b, and Hugenholtz (Brandow) vertices, representing orthogonally spin-adapted doubly excited states, Fig. 1c,e, is briefly outlined in the Appendix.

Let us now concentrate our attention on the third and fourth terms on the right-hand side of Eq. (104), i.e. $W_{ij}^{(3)}(\varepsilon)$ and $W_{ij}^{(4)}(\varepsilon)$. Obviously,

$$W_{ij}^{(3)}(\varepsilon) = W_{ij}^{(4)}(\varepsilon) = 0 \quad \text{for } i = 0 \text{ or } j = 0. \tag{114}$$

Since in matrix elements of $\mathscr{V}$ between doubly and triply and doubly and quadruply excited states we can replace $\mathscr{V}$ by V_N (see Eq. (98) and note that for

cyclic polyenes all matrix elements $\langle r|g|a \rangle$ vanish), expressions for $W_{ij}^{(k)}(\varepsilon)$, $k = 3, 4$, $i, j = 1, \ldots, M$, become

$$W_{ij}^{(3)}(\varepsilon) = \langle \Phi_i | V_N \frac{Q^{(3)}}{\varepsilon - Z_N} V_N | \Phi_j \rangle, \tag{115}$$

$$W_{ij}^{(4)}(\varepsilon) = \langle \Phi_i | V_N \frac{Q^{(4)}}{\varepsilon - Z_N} V_N | \Phi_j \rangle. \tag{116}$$

We could, of course, compute these quantities in the same way as the component $W_{ij}^{(2)}(\varepsilon)$, namely by generating first the matrix elements of the operator V_N between doubly and triply and doubly and quadruply excited configurations. Although this could, in principle, easily be done using similar algorithms to those of the CI matrix generation, it is more efficient to derive explicit expressions for $W_{ij}^{(3)}(\varepsilon)$ and $W_{ij}^{(4)}(\varepsilon)$ in terms of two-electron integrals $\langle mn \| pq \rangle$. In this way, we obtain expressions of the same complexity as the second-order MBPT (see Sect. 5).

We conclude this section by explaining briefly how to find the OIP lower bounds to the energy for cyclic polyene systems as described by the Hamiltonian $\mathscr{H}$, Eq. (90). To be consistent with Eq. (103), we slightly modify the original definition of the bracketing function $f'(\mathscr{E})$, Eq. (80), and consider the new bracketing function $f(\varepsilon)$ defined as follows:

$$f(\varepsilon) \equiv f'(\mathscr{E}) - \mathscr{E}_0^{(0)} = \sum_{i,j=0}^{M} \mathscr{V}_{0i}(A(\varepsilon)^{-1})_{ij} V_{j0}, \tag{117}$$

where $A(\varepsilon)$ is given by Eq. (104). In this way, the fundamental equation of the OIP approach, i.e. Eq. (79), becomes

$$f(\varepsilon) = \varepsilon. \tag{118}$$

By solving this equation, we get the OIP lower bounds to the eigenvalues of the operator $(\mathscr{H} - \mathscr{E}_0^{(0)})$. Since we are interested in the determination of the lower bounds to the ground state correlation energy and since $\mathscr{E}$ corresponds to the eigenvalues of the total Hamiltonian $\mathscr{H}$, Eq. (90), we define

$$\Delta\mathscr{E} = \mathscr{E} - E_{\text{RHF}} - \sum_{\mu < \nu} \gamma_{\mu\nu}, \tag{119}$$

where

$$E_{\text{RHF}} = \langle \Phi_0 | H_\pi | \Phi_0 \rangle = \langle \Phi_0 | Z | \Phi_0 \rangle + \langle \Phi_0 | V | \Phi_0 \rangle, \tag{120}$$

is the ground state RHF energy. From Eqs. (119), (120), as well as (102), (103) and (107), we immediately obtain

$$\Delta\mathscr{E} = \varepsilon - \mathscr{V}_{00}. \tag{121}$$

Thus, subtracting $\mathscr{V}_{00}$, Eq. (107), from the lowest root of Eq. (118), we obtain the OIP lower bound to the correlation energy in the ground state of cyclic polyenes as described by the PPP model Hamiltonians H_π and $\mathscr{H}$.

To summarize, Eqs. (104)–(109), (114)–(118), and (121) respresent the set of working equations characterizing the OIP approach. The problems connected with their practical implementation, particularly when higher cyclic polyenes (with $N \geqslant 14$) are examined, are the subject of Part III of this series. Formally, the main difficulty is to evaluate the effective interaction matrix elements $W_{ij}^{(3)}(\varepsilon)$ and $W_{ij}^{(4)}(\varepsilon)$, Eqs. (115) and (116), respectively, between the orthogonally spin-

adapted biexcited singlet configurations $\left| \begin{smallmatrix} r & s \\ a & b \end{smallmatrix} \right\rangle_{S_i}$. In Sect. 3 we have shown that very similar matrix elements $[W_{ij}^{(3)},$ Eq. (57)] are needed in the approximate account of triple excitations in the CC theory. In the next two sections we thus concentrate our attention on the derivation of general expressions for $W_{ij}^{(3)}$, $W_{ij}^{(3)}(\varepsilon)$ and $W_{ij}^{(4)}(\varepsilon)$ using different diagrammatic procedures for spin-adaptation. We are not only interested in the final result, but we also wish to find out which spin-adaptation procedure yields the most transparent and computationally appealing formulas.

5. Diagrammatic evaluation of the effective interaction matrix elements

We now turn our attention to the derivation of general expressions for the effective interaction matrix elements $W_{ij}^{(3)}$, $W_{ij}^{(3)}(\varepsilon)$ and $W_{ij}^{(4)}(\varepsilon)$, given by Eqs. (57), (115) and (116), respectively, in terms of two-electron molecular integrals $\langle mn \| pq \rangle$. Since the matrix elements $W_{ij}^{(3)}(\varepsilon)$ and $W_{ij}^{(4)}(\varepsilon)$ of the OIP formalism and the matrix elements $W_{ij}^{(3)}$, that occur in CCDT-1, ACPTQ and CCD + T(CCD) equations, only differ in the denominators (in the latter case they are given by the RHF orbital energy differences while in the former case they are given by appropriate differences of Hückel orbital energies), it is convenient to define generalized effective interaction matrix elements as

$$W_{ij}^{(k)X}(\varepsilon) = {}_{S_i}\!\left\langle \begin{smallmatrix} r & s \\ a & b \end{smallmatrix} \right| V_N \frac{Q^{(k)}}{\varepsilon - \Omega_N^X} V_N \left| \begin{smallmatrix} \tilde{r} & \tilde{s} \\ \tilde{a} & \tilde{b} \end{smallmatrix} \right\rangle_{S_i}, \qquad (122)$$

where $k = 3$ or 4, $X = \text{RHF}$ or HMO, $\Omega^{\text{RHF}} = F$, and $\Omega^{\text{HMO}} = Z$ or $\mathcal{H}^{(0)}$, Eq. (92) (recall that for the PPP model of cyclic polyenes z is diagonal in the HMO basis and Hückel orbital energies $\varepsilon_m^{\text{HMO}}$ differ from $\langle m|z|m \rangle$ only by a constant). Clearly

$$W_{ij}^{(3)\,\text{RHF}}(0) = W_{ij}^{(3)}, \qquad (123)$$

$$W_{ij}^{(3)\,\text{HMO}}(\varepsilon) = W_{ij}^{(3)}(\varepsilon), \qquad (124)$$

$$W_{ij}^{(4)\,\text{HMO}}(\varepsilon) = W_{ij}^{(4)}(\varepsilon). \qquad (125)$$

Equation (122) is very similar to standard perturbation theory expressions and can be efficiently evaluated by applying time-independent diagrammatic techniques of MBPT [8, 51, 52], together with graphical methods of spin algebras [80, 81], to achieve spin-adaptation [38, 39, 44, 106, 107]. In this section we follow the diagrammatic spin-adaptation procedure of [38], as outlined in Sect. 2. As in [44], we employ bare (Goldstone) two-electron interaction vertices (cf. Appendix), while orthogonally spin-adapted biexcited configurations are represented by Hugenholtz vertices. In the procedure of [106] and [107], even two-electron interaction vertices are represented in a Hugenholtz form (and are referred to as spin-adapted interaction vertices [40]). We shall compare expressions derived in this section with those obtained with the procedure of [106] and [107] in the next section.

In order to apply the diagrammatic procedure of [38] to the right-hand side of Eq. (122), we must first draw all possible nonequivalent nonoriented vacuum Hugenholtz skeletons that can be formed from two nonoriented Hugenholtz V_N vertices and two similar vertices representing bra and ket doubly excited configu-

rations (cf. Figs. 1 and 2 of [34]). In the tetraexcited ($k = 4$) case, $W_{ij}^{(4)X}(\varepsilon)$, all lines from both vertices representing biexcitations must go across the interval separating the interaction vertices (cf. Fig. 1 of [34]), while in the triexcited ($k = 3$) case, $W_{ij}^{(3)X}(\varepsilon)$, only three lines from each biexcitation (and each two-electron interaction) vertex will go across, one being incident to the nearest interaction vertex (cf. Fig. 2 of [34]). This is a consequence of the presence of the reduced resolvent-type operator $Q^{(k)}/(\varepsilon - \Omega_N^X)$ ($k = 3, 4$) in Eq. (122) (see, e.g., [51, 52]). Once all the arrowless Hugenholtz diagrams are drawn, it is easy to introduce orientation and labeling of lines in all nonequivalent ways (recall that bra and ket vertices must also carry labels S_i and $\tilde{S}_i$, respectively). All the unlabeled resulting Hugenholtz diagrams corresponding to Eq. (122), both nonoriented and oriented, can be found in Figs. 1–5 of [34], where a special-purpose diagrammatic spin-adaptation procedure, that is not based on the graphical methods of spin algebras, was employed. Note that these diagrams can be brought into a one-to-one correspondence with the diagrams for the second-order effective Hamiltonian matrix elements [110] or with the fourth-order MBPT diagrams by regarding all four vertices as equivalent [34].

Following the procedure of [38], it thus remains to draw all nonequivalent Goldstone–Hugenholtz diagrams by replacing Hugenholtz V_N vertices with Goldstone ones, Fig. 1b, and by performing an "exchange" operation on each bare interaction vertex, starting with any Goldstone–Hugenholtz representative (see, e.g., [38, 51, 52]). These resulting Goldstone–Hugenholtz diagrams are shown in Figs. 7–9. Diagrams in Fig. 7 correspond to $W_{ij}^{(4)X}(\varepsilon)$, whereas those in Figs. 8 and 9 correspond to $W_{ij}^{(3)X}(\varepsilon)$. Distinct Goldstone–Hugenholtz diagrams that are associated with a given Hugenholtz diagram are grouped together. Since we wish to compare our results with the expressions of [34], diagrams in Figs. 7–9 are ordered in the same way as diagrams in Figs. 3a–i, 4a–h and 5a–h of [34]. Thus, Fig. 7x, $x = a$–i, and Figs. 8x and 9x, $x = a$–h, of this paper correspond to Figs. 3x, 4x, 5x of [34], respectively. For example, Fig. 8c shows two distinct Goldstone–Hugenholtz diagrams that are associated with Hugenholtz diagram 4c of [34]. In the case of Hugenholtz diagram 5b of [34], four distinct Goldstone–Hugenholtz representatives, given in Fig. 9b, can be constructed, etc. The reason for splitting up the triexcited diagrams, $W_{ij}^{(3)X}(\varepsilon)$, into the two sets (Figs. 8 and 9) is given in [34]. Recall that these two sets are structurally related when the Hugenholtz representation is employed, namely, they may be transformed one into the other by interchanging the role of one biexcitation vertex with its nearest interaction vertex [34]. In other words, in the Hugenholtz representation, they correspond to different time versions of one set of diagrams [51, 52].

In Figs. 7–9, a Brandow representation is assumed, i.e., each Hugenholtz vertex representing bra or ket orthogonally spin-adapted configuration is replaced by its Brandow version. However, Brandow vertices representing $\left. \left\langle \begin{matrix} r & s \\ a & b \end{matrix} \right|_{S_i} \right.$ and $\left| \begin{matrix} \tilde{r} & \tilde{s} \\ \tilde{a} & \tilde{b} \end{matrix} \right\rangle_{\tilde{S}_i}$, Fig. 1e and c, respectively, are not drawn explicitly. Instead, as in the diagrams corresponding to the orthogonally spin-adapted CCD equations, Figs. 2–4, all external lines are labeled by the fixed orbital indices characterizing bra and ket states $\left\langle \begin{matrix} r & s \\ a & b \end{matrix} \right|_{S_i}$ and $\left| \begin{matrix} \tilde{r} & \tilde{s} \\ \tilde{a} & \tilde{b} \end{matrix} \right\rangle_{\tilde{S}_i}$, respectively, and distinct labeling schemes carried by external lines are indicated by the symmetrizers $\mathscr{S}_{ab}$, $\mathscr{S}_{rs}$, $\mathscr{S}_{\tilde{a}\tilde{b}}$ and $\mathscr{S}_{\tilde{r}\tilde{s}}$. In this way, Goldstone–Brandow diagrams of Figs. 7–9

are much more transparent than they would be if all the vertices were explicitly drawn. Following the notation of Sect. 2, the remaining internal particle and hole lines (between interaction vertices) are labeled by summation indices k' and k'', respectively, $k = 1, 2, \ldots$.

To obtain an algebraic expression that is associated with each Goldstone–Brandow orbital diagram of Figs. 7–9, we have to multiply the corresponding orbital and spin factors and sum over all free orbital labels [38] (intermediate spin quantum numbers are fixed labels in this case). However, the sign rule given in Eq. (37) of [38] requires a slight modification when applied to diagrams of Figs. 7–9, where neither bra nor ket state vertices are shown explicitly. Thus, to obtain the number of closed loops (l) and the number of internal hole lines (h), that determine the sign factor $(-1)^{l+h}$ [8, 51, 52], we have to join all the external lines of our orbital diagrams with those of diagrams representing bra and ket states, Fig. 1e and c, respectively, while regarding them as internal lines.

As mentioned in Sect. 2, the appropriate spin coupling coefficients are evaluated by applying graphical methods of angular momentum theory [22, 80, 81]. Thus, we have to draw the spin diagrams associated with orbital diagrams of Figs. 7–9. They are very simple and can be immediately obtained by interconnecting the appropriate lines of spin diagrams representing bra and ket states, Fig. 1f and d, respectively, since in bare-interaction approach of [38], two-electron interaction vertices do not enter the resulting spin diagrams. Consequently, there is no need to present them here.

We can easily verify that a one-to-one correspondence between the symmetrizers $\mathscr{S}_{ab}$, $\mathscr{S}_{rs}$, $\mathscr{S}_{\bar{a}\bar{b}}$ and $\mathscr{S}_{\bar{r}\bar{s}}$ in the orbital diagrams and the (anti)symmetrizers $\mathscr{S}_{ab}(S_i)$, $\mathscr{S}_{rs}(S_i)$, $\mathscr{S}_{\bar{a}\bar{b}}(\tilde{S}_i)$ and $\mathscr{S}_{\bar{r}\bar{s}}(\tilde{S}_i)$, respectively, in the associated algebraic expressions, which was emphasized in the context of the CCSD theory in [40] (cf. Sect. 2), also holds for the Goldstone–Brandow diagrams of Figs. 7–9. Consequently, the easiest method to obtain algebraic expressions that are associated with orbital diagrams of Figs. 7–9 is as follows: evaluate and combine orbital and spin factors corresponding to a given orbital diagram, in which the symmetrizers are ignored, and then assign the operator $\mathscr{S}_{ab}(S_i)$ to $\mathscr{S}_{ab}$, $\mathscr{S}_{rs}(S_i)$ to $\mathscr{S}_{rs}$, $\mathscr{S}_{\bar{a}\bar{b}}(\tilde{S}_i)$ to $\mathscr{S}_{\bar{a}\bar{b}}$, and $\mathscr{S}_{\bar{r}\bar{s}}(\tilde{S}_i)$ to $\mathscr{S}_{\bar{r}\bar{s}}$. In this way, the following compact expressions for the effective interaction matrix elements $W_{ij}^{(k)X}(\varepsilon)$ ($k = 3, 4$), Eq. (122), can be derived

$$W_{ij}^{(k)X}(\varepsilon) = \sum_x R_{ij}^{(k)}(x), \tag{126}$$

where

$$R_{ij}^{(4)}(x) = N_{ab}^{rs} N_{\bar{a}\bar{b}}^{\bar{r}\bar{s}} \sum_{\{\bar{r}\bar{r}\}} \mathscr{P}_4(x)\{v_4(x)[\varepsilon - \varDelta_4(x)]^{-1}\} \quad (x = a-i), \tag{127}$$

while

$$R_{ij}^{(3)}(x) = R_{ij}^{(3)\prime}(x) + R_{ij}^{(3)\prime\prime}(x) \quad (x = a-h), \tag{128}$$

and

$$R_{ij}^{(3)\prime(\prime\prime)}(x) = N_{ab}^{rs} N_{\bar{a}\bar{b}}^{\bar{r}\bar{s}} \sum_{\{\bar{r}\bar{r}\}} \mathscr{P}_3^{\prime(\prime\prime)}(x)\{v_3^{\prime(\prime\prime)}(x)[\varepsilon - \varDelta_3^{\prime(\prime\prime)}(x)]^{-1}\}. \tag{129}$$

Clearly, x designates the resulting Goldstone–Brandow orbital diagrams of Figs. 7–9. Thus, $R_{ij}^{(4)}(x)$, $x = a-i$, $R_{ij}^{(3)\prime}(x)$ and $R_{ij}^{(3)\prime\prime}(x)$, $x = a-h$, are the algebraic expressions associated with Figs. 7x, $x = a-i$, 8x and 9x, $x = a-h$, respectively.
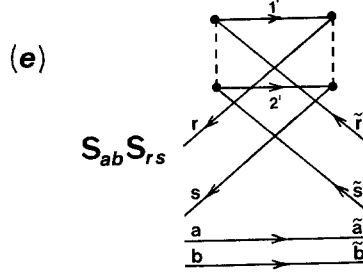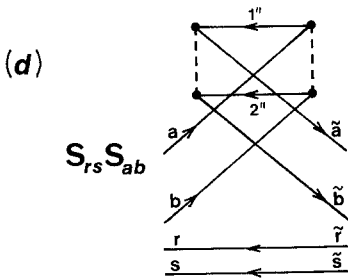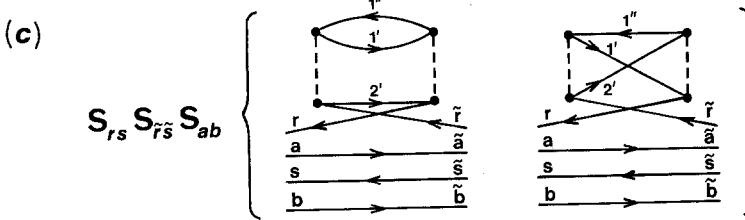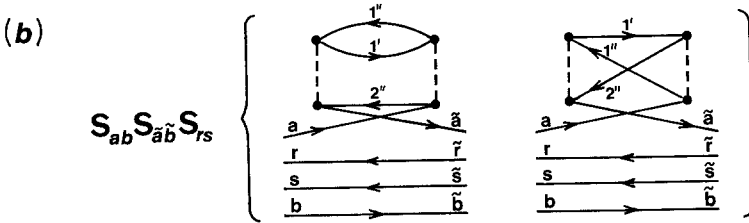
Fig. 7a–e

(f)

$S_{rs}S_{\tilde{r}\tilde{s}}S_{ab}S_{\tilde{a}\tilde{b}}$

(g)

$S_{rs}S_{\tilde{r}\tilde{s}}S_{ab}S_{\tilde{a}\tilde{b}}$

(h)

$S_{ab}S_{\tilde{a}\tilde{b}}S_{rs}S_{\tilde{r}\tilde{s}}$
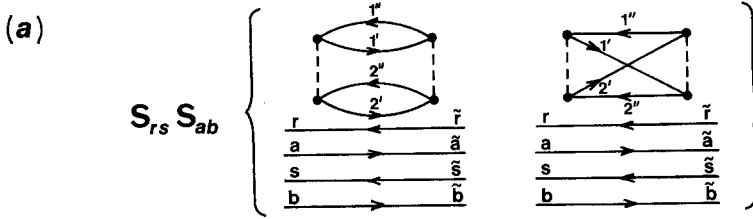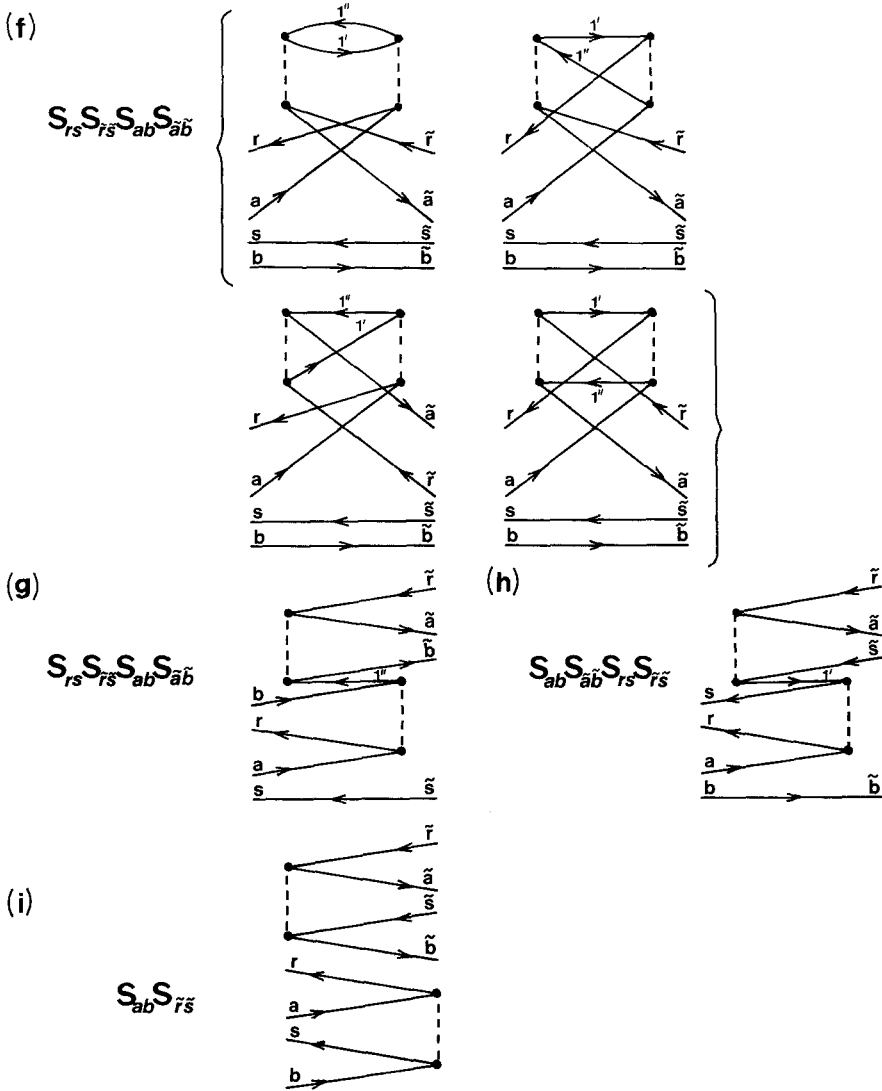
(i)

$S_{ab}S_{\tilde{r}\tilde{s}}$

Fig. 7a–i. Goldstone–Brandow orbital diagrams representing the effective interaction matrix elements $W_{ij}^{(4)X}(\varepsilon)$. (x) $(x = a-i)$ designates a group of one $(x = d, e, g-i)$, two $(x = a-c)$ or four $(x = f)$ Goldstone–Brandow representatives that can be associated with each oriented unlabeled Hugenholtz diagram, Fig. $3x$ of [34] (see text for details)
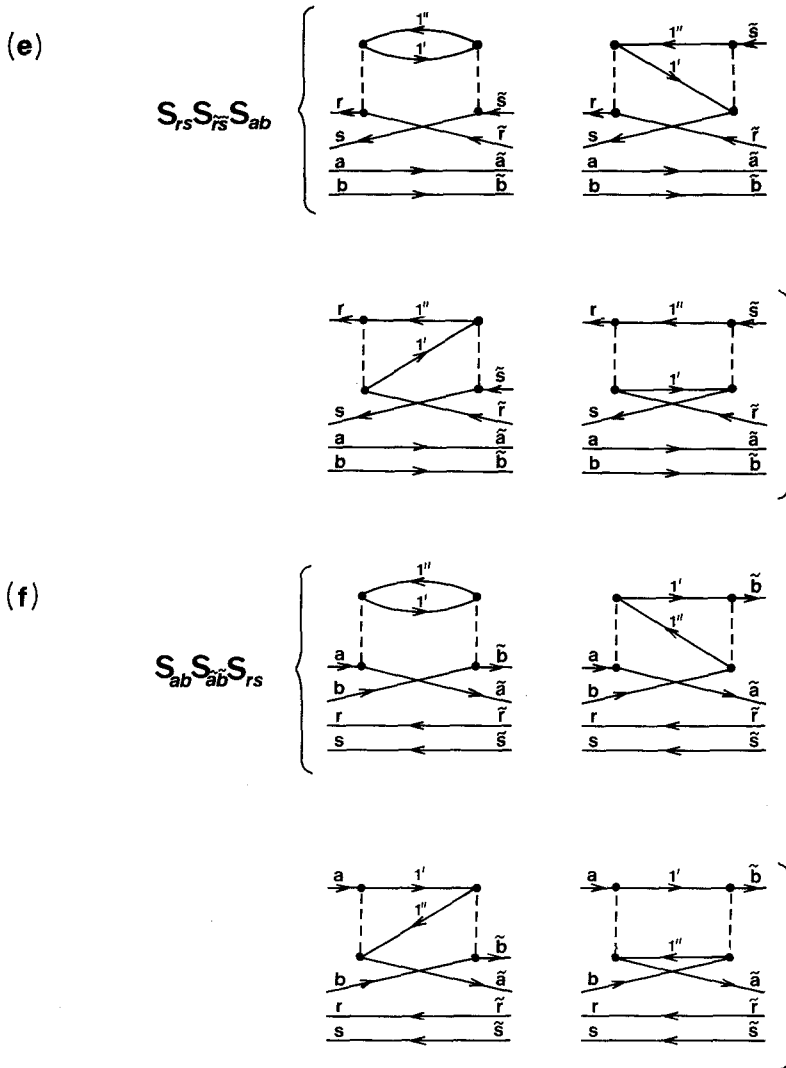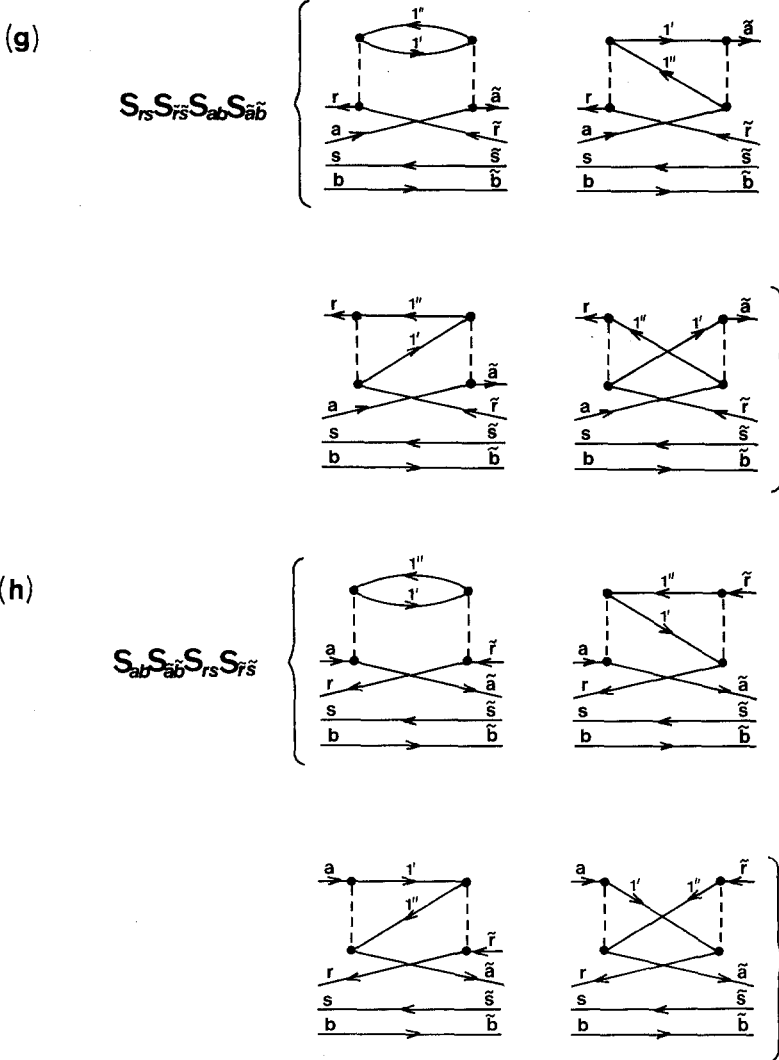
Fig. 8a–d

(e)

$S_{rs}S_{\widetilde{rs}}S_{ab}$

(f)

$S_{ab}S_{\widetilde{ab}}S_{rs}$
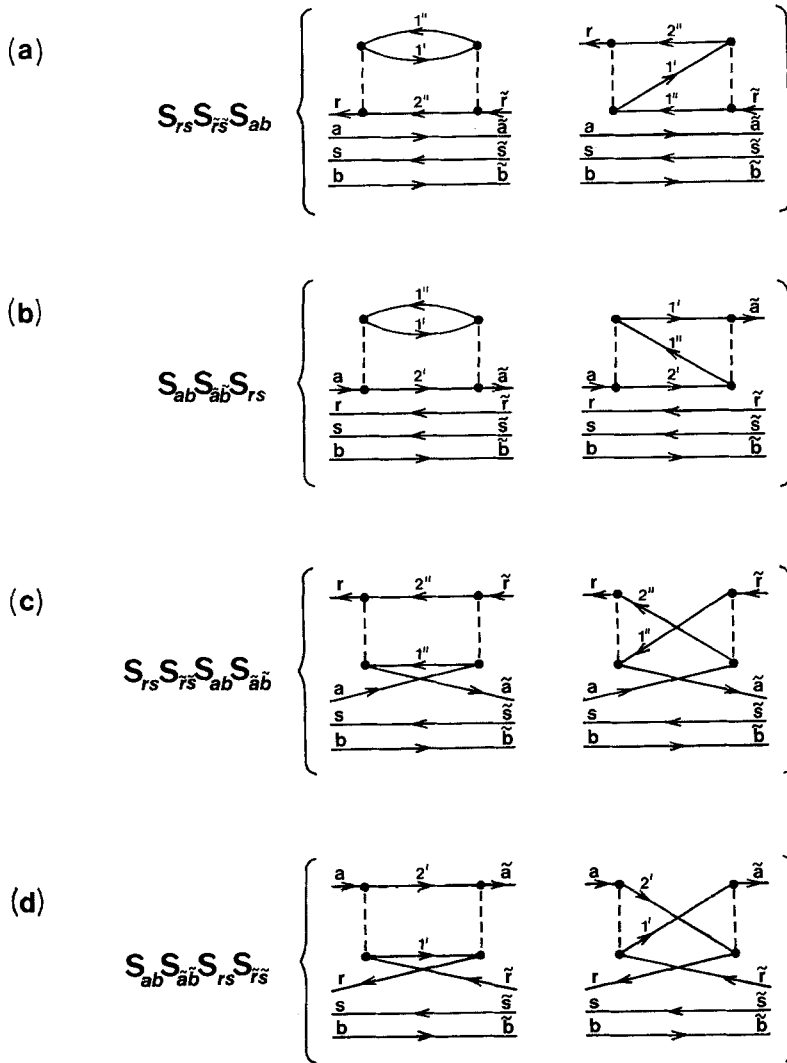
Fig. 8e, f

Fig. 8a–h. Goldstone–Brandow orbital diagrams contributing to the effective interaction matrix elements $W_{ij}^{(3)X}(\varepsilon)$. They correspond to the oriented unlabeled Hugenholtz diagrams of Fig. 4 in [34] (see text for details)

Since Goldstone–Brandow diagrams of Figs. 7–9 and their counterparts in [34] are ordered in the same way, one can easily identify contributions $R^{(4)}_{ij}(x)$, $R^{(3)'}_{ij}(x)$ and $R^{(3)''}_{ij}(x)$, Eqs. (127) and (129), with the corresponding terms defined in [34]. According to the labeling convention introduced in Sect. 2, sums in Eqs. (127) and (129) extend over an appropriate set of hole (l') and/or particle (l'') labels. The numerators $v_4(x)$ and $v_3^{'(")}(x)$ are given by products of two-electron integrals $\langle mn \| pq \rangle$, Eq. (36), $\langle mn \| pq \rangle_S$, Eq. (37), or $\langle mn \| pq \rangle_a$, where

$$\langle mn \| pq \rangle_a = 2\langle mn \| pq \rangle - \langle mn \| qp \rangle, \qquad (130)$$

Kronecker delta symbols $\langle m | n \rangle$ and/or quantities $A^{\bar{m}\bar{n}}_{mn}(S)$, Eq. (111), and spin coupling coefficients. The denominators $\Delta_k(x) \equiv \Delta^X(1'', 2'', \ldots, r, s; 1', 2', \ldots, a, b)$, $k = 3, 4$, $X = \text{RHF, HMO}$, are given by the RHF ($X = \text{RHF}$) or Hückel ($X = \text{HMO}$) orbital energy differences,

$$\Delta^X(1'', 2'', \ldots, r, s; 1', 2', \ldots, a, b) = \varepsilon^X_{1''} + \varepsilon^X_{2''} + \cdots + \varepsilon^X_r$$
$$+ \varepsilon^X_s - \varepsilon^X_{1'} - \varepsilon^X_{2'} - \cdots - \varepsilon^X_a - \varepsilon^X_b, \quad (131)$$

and the "symmetry forcing" projection operators $\mathscr{P}_4(x)$, $\mathscr{P}'_3(x)$ and $\mathscr{P}''_3(x)$ are the appropriate products of the (anti)symmetrizers $\mathscr{S}_{ab}(S_i)$, $\mathscr{S}_{rs}(S_i)$, $\mathscr{S}_{\bar{a}\bar{b}}(\tilde{S}_i)$ and $\mathscr{S}_{\bar{r}\bar{s}}(\tilde{S}_i)$.

For the numerators $v_4(x)$ associated with diagrams in Fig. 7a–i we get the following expressions:

$$v_4(a) = \delta_{S_i \tilde{S}_i} A^{\bar{r}\bar{s}}_{rs}(S_i) A^{\bar{a}\bar{b}}_{ab}(S_i) \langle 1'2' \| 1''2'' \rangle \langle 1''2'' \| 1'2' \rangle_a, \qquad (132a)$$

$$v_4(b) = -\delta_{S_i \tilde{S}_i} A^{\bar{r}\bar{s}}_{rs}(S_i) \langle b | \tilde{b} \rangle \langle 1'\tilde{a} \| 1''2'' \rangle \langle 1''2'' \| 1'a \rangle_a, \qquad (132b)$$

$$v_4(c) = -\delta_{S_i \tilde{S}_i} A^{\bar{a}\bar{b}}_{ab}(S_i) \langle s | \tilde{s} \rangle \langle 1'2' \| 1''\tilde{r} \rangle \langle 1''r \| 1'2' \rangle_a, \qquad (132c)$$

$$v_4(d) = \delta_{S_i \tilde{S}_i} A^{\bar{r}\bar{s}}_{rs}(S_i) \langle \tilde{a}\tilde{b} \| 1''2'' \rangle \langle 1''2'' \| ab \rangle_{S_i}, \qquad (132d)$$

$$v_4(e) = \delta_{S_i \tilde{S}_i} A^{\bar{a}\bar{b}}_{ab}(S_i) \langle 1'2' \| \tilde{r}\tilde{s} \rangle \langle rs \| 1'2' \rangle_{S_i}, \qquad (132e)$$

$$v_4(f) = \langle s | \tilde{s} \rangle \langle b | \tilde{b} \rangle \{ \tfrac{1}{2}[S_i, \tilde{S}_i]^{1/2} (\langle 1'\tilde{a} \| 1''\tilde{r} \rangle \langle 1''r \| 1'a \rangle_a$$
$$- \langle 1'\tilde{a} \| \tilde{r}1'' \rangle \langle 1''r \| 1'a \rangle) + \delta_{S_i \tilde{S}_i} \langle 1'\tilde{a} \| \tilde{r}1'' \rangle \langle 1''r \| a1' \rangle \}, \qquad (132f)$$

$$v_4(g) = -\tfrac{1}{2}[S_i, \tilde{S}_i]^{1/2} \langle s | \tilde{s} \rangle \langle \tilde{a}\tilde{b} \| \tilde{r}1'' \rangle_{\tilde{S}_i} \langle r1'' \| ab \rangle_{S_i}, \qquad (132g)$$

$$v_4(h) = -\tfrac{1}{2}[S_i, \tilde{S}_i]^{1/2} \langle b | \tilde{b} \rangle \langle \tilde{a}1' \| \tilde{r}\tilde{s} \rangle_{\tilde{S}_i} \langle rs \| a1' \rangle_{S_i}, \qquad (132h)$$

$$v_4(i) = [S_i, \tilde{S}_i]^{1/2} \langle \tilde{a}\tilde{b} \| \tilde{r}\tilde{s} \rangle_{\tilde{S}_i} \langle rs \| ab \rangle_{S_i}. \qquad (132i)$$

The corresponding denominators $\Delta_4(x)$ are given by

$$\Delta_4(x) = \Delta^X(u^x_1, u^x_2, r, s; c^x_1, c^x_2, a, b) \quad (x = a\text{–}i), \qquad (133x)$$

with the orbital labels listed in Table 1. The projection operators $\mathscr{P}_4(x)$ have the form

$$\mathscr{P}_4(x) = \mathscr{S}_{ab}(S_i)^{k^x_1} \mathscr{S}_{\bar{a}\bar{b}}(\tilde{S}_i)^{k^x_2} \mathscr{S}_{rs}(S_i)^{k^x_3} \mathscr{S}_{\bar{r}\bar{s}}(\tilde{S}_i)^{k^x_4} \quad (x = a\text{–}i), \qquad (134x)$$

with k^x_i ($i = 1\text{–}4$), that are either 0 or 1, also listed in Table 1. Note that $\mathscr{P}_4(a) = \mathscr{P}_4(d) = \mathscr{P}_4(e) = \mathscr{P}_4(i) = 1$. We recall a simple relationship between the diagrams of Fig. 7 due to p–h symmetry, namely between 7b and 7c, 7d and 7e, 7g and 7h, that is reflected in the corresponding algebraic expressions: particle (hole) lines and the corresponding orbital labels are replaced by hole (particle)
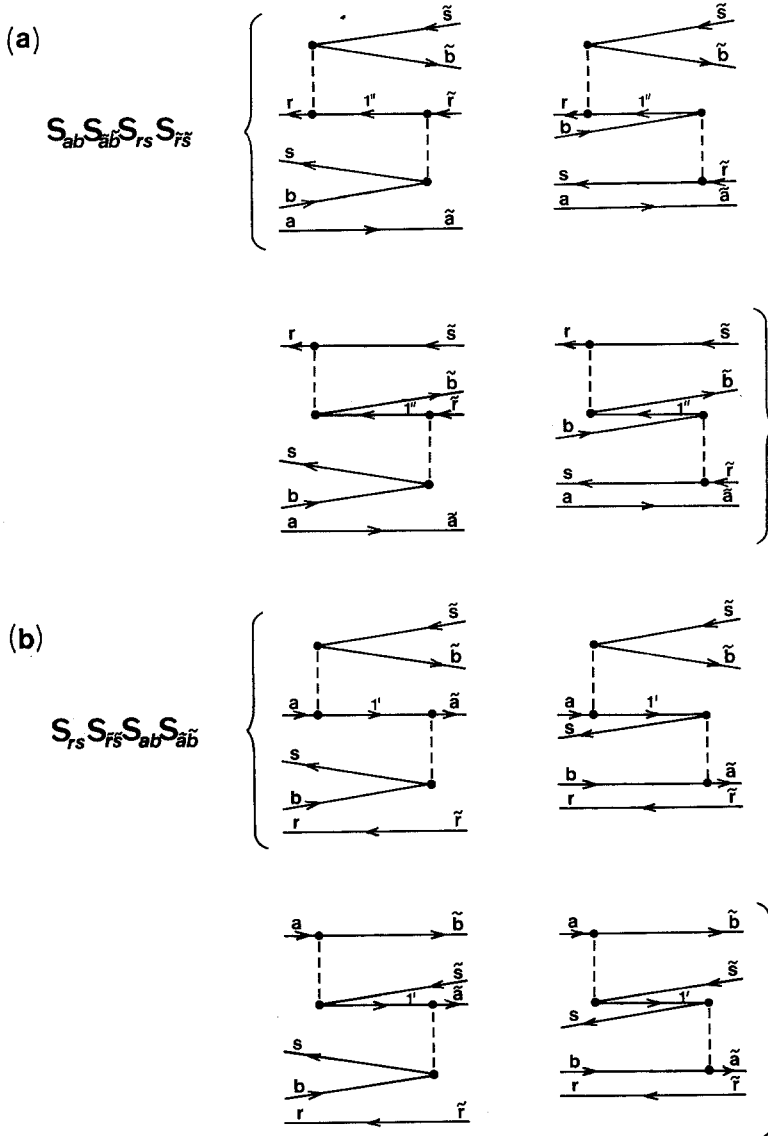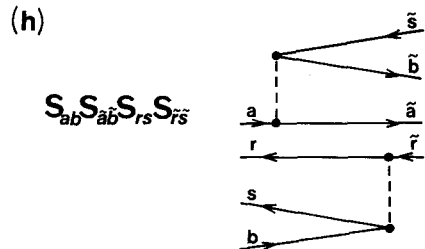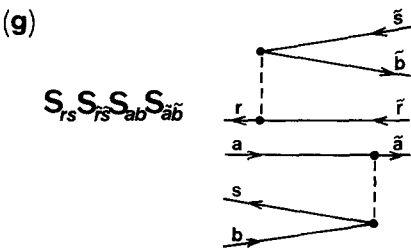
(a)

$$S_{ab}S_{\tilde{a}\tilde{b}}S_{rs}S_{\tilde{r}\tilde{s}}$$
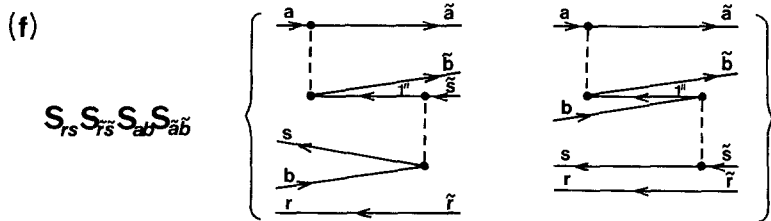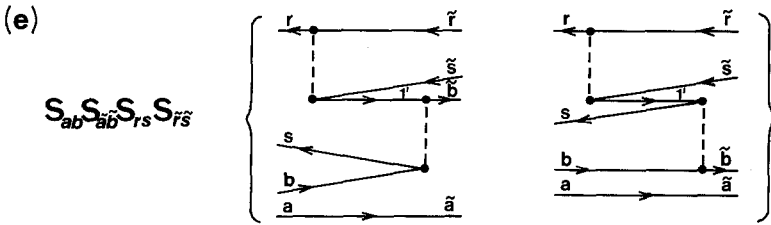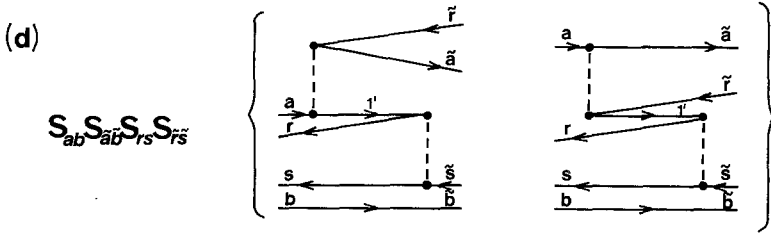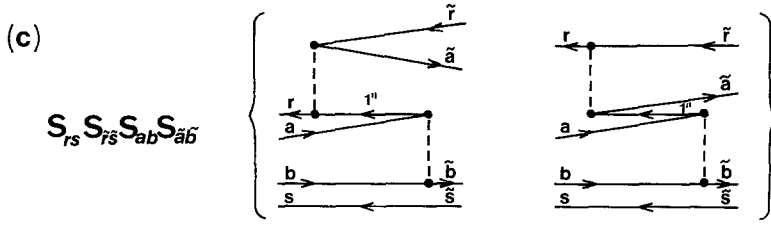
Fig. 9a, b

Fig. 9a–h. Remaining Goldstone–Brandow orbital diagrams contributing to $W_{ij}^{(3)X}(\varepsilon)$. Their oriented unlabeled Hugenholtz counterparts are shown in Fig. 5 of [34] (see text for details)

Table 1. Orbital labels and parameter values that determine $\Delta_4(x)$ and the projectors $\mathscr{P}_4(x)$, $x = a-i$, Eqs. (133x) and (134x), respectively

x	u_1^x	u_2^x	c_1^x	c_2^x	k_1^x	k_2^x	k_3^x	k_4^x
a	$1''$	$2''$	$1'$	$2'$	0	0	0	0
b	$1''$	$2''$	$1'$	$\tilde{a}$	1	1	0	0
c	$1''$	$\tilde{r}$	$1'$	$2'$	0	0	1	1
d	$1''$	$2''$	$\tilde{a}$	$\tilde{b}$	0	0	0	0
e	$\tilde{r}$	$\tilde{s}$	$1'$	$2'$	0	0	0	0
f	$1''$	$\tilde{r}$	$1'$	$\tilde{a}$	1	1	1	1
g	$1''$	$\tilde{r}$	$\tilde{a}$	$\tilde{b}$	0	0	1	1
h	$\tilde{r}$	$\tilde{s}$	$1'$	$\tilde{a}$	1	1	0	0
i	$\tilde{r}$	$\tilde{s}$	$\tilde{a}$	$\tilde{b}$	0	0	0	0

lines and labels, respectively, according to the following scheme

$$r(a) \to a(r), \; s(b) \to b(s), \; \tilde{r}(\tilde{a}) \to \tilde{a}(\tilde{r}), \; \tilde{s}(\tilde{b}) \to \tilde{b}(\tilde{s}), \; 1''(1') \to 1'(1''), \; 2''(2') \to 2'(2'').$$

In the formulas for the numerators $v_4(x)$, two-electron integrals must be also replaced by their complex conjugates. Clearly, diagrams a, f and i of Fig. 7, and the associated algebraic expressions for $R_{ij}^{(4)}(a)$, $R_{ij}^{(4)}(f)$ and $R_{ij}^{(4)}(i)$, respectively, are $p-h$ selfconjugate.

For the triexcited case, $W_{ij}^{(3)X}(\varepsilon)$, the numerators $v_3'(x)$ and $v_3''(x)$, $x = a-h$, corresponding to diagrams of Figs. 8a–h and 9a–h, respectively, can be written as follows

$$v_3'(a) = \delta_{S_i \tilde{S}_i} A_{ab}^{\tilde{a}\tilde{b}}(S_i) \langle s|\tilde{s} \rangle \langle 1'r \| 1''2'' \rangle \langle 1''2'' \| 1'\tilde{r} \rangle_a, \tag{135a}$$

$$v_3'(b) = \delta_{S_i \tilde{S}_i} A_{rs}^{\tilde{r}\tilde{s}}(S_i) \langle b|\tilde{b} \rangle \langle 1'2' \| 1''a \rangle \langle 1''\tilde{a} \| 1'2' \rangle_a, \tag{135b}$$

$$v_3'(c) = \langle s|\tilde{s} \rangle \langle b|\tilde{b} \rangle \langle \tilde{a}r \| 1''2'' \rangle \{ \tfrac{1}{2}[S_i, \tilde{S}_i]^{1/2} \langle 1''2'' \| \tilde{r}a \rangle - \delta_{S_i \tilde{S}_i} \langle 1''2'' \| a\tilde{r} \rangle \}, \tag{135c}$$

$$v_3'(d) = \langle b|\tilde{b} \rangle \langle s|\tilde{s} \rangle \langle 1'2' \| \tilde{r}a \rangle \{ \tfrac{1}{2}[S_i, \tilde{S}_i]^{1/2} \langle \tilde{a}r \| 1'2' \rangle - \delta_{S_i \tilde{S}_i} \langle \tilde{a}r \| 2'1' \rangle \}, \tag{135d}$$

$$v_3'(e) = \delta_{S_i \tilde{S}_i} A_{ab}^{\tilde{a}\tilde{b}}(S_i) (\langle 1'r \| 1''\tilde{r} \rangle \langle 1''s \| 1'\tilde{s} \rangle_a - \langle 1'r \| \tilde{r}1'' \rangle \langle 1''s \| 1'\tilde{s} \rangle_{S_i}), \tag{135e}$$

$$v_3'(f) = \delta_{S_i \tilde{S}_i} A_{rs}^{\tilde{r}\tilde{s}}(S_i) (\langle 1'\tilde{a} \| 1''a \rangle \langle 1''\tilde{b} \| 1'b \rangle_a - \langle 1'\tilde{a} \| a1'' \rangle \langle 1''\tilde{b} \| 1'b \rangle_{S_i}), \tag{135f}$$

$$v_3'(g) = -\langle s|\tilde{s} \rangle \langle b|\tilde{b} \rangle \{ \delta_{S_i \tilde{S}_i} (\langle 1'r \| 1''\tilde{r} \rangle \langle 1''\tilde{a} \| 1'a \rangle_a$$
$$- \langle 1'r \| \tilde{r}1'' \rangle \langle 1''\tilde{a} \| 1'a \rangle) + \tfrac{1}{2}[S_i, \tilde{S}_i]^{1/2} \langle 1'r \| \tilde{r}1'' \rangle \langle 1''\tilde{a} \| a1' \rangle \}, \tag{135g}$$

$$v_3'(h) = -\langle b|\tilde{b} \rangle \langle s|\tilde{s} \rangle \{ \delta_{S_i \tilde{S}_i} (\langle 1'\tilde{a} \| 1''a \rangle \langle 1''r \| 1'\tilde{r} \rangle_a$$
$$- \langle 1'\tilde{a} \| a1'' \rangle \langle 1''r \| 1'\tilde{r} \rangle) + \tfrac{1}{2}[S_i, \tilde{S}_i]^{1/2} \langle 1'\tilde{a} \| a1'' \rangle \langle 1''r \| \tilde{r}1' \rangle \}, \tag{135h}$$

$$v_3''(a) = \langle a|\tilde{a} \rangle \{ \tfrac{1}{2}[S_i, \tilde{S}_i]^{1/2} (\langle \tilde{b}r \| \tilde{s}1'' \rangle \langle 1''s \| \tilde{r}b \rangle_{S_i}$$
$$+ (-1)^{\tilde{S}_i} \langle \tilde{b}r \| 1''\tilde{s} \rangle \langle 1''s \| \tilde{r}b \rangle) - (-1)^{S_i} \delta_{S_i \tilde{S}_i} \langle \tilde{b}r \| 1''\tilde{s} \rangle \langle 1''s \| b\tilde{r} \rangle \}, \tag{136a}$$

$$v_3''(b) = \langle r|\tilde{r} \rangle \{ \tfrac{1}{2}[S_i, \tilde{S}_i]^{1/2} (\langle 1'\tilde{b} \| a\tilde{s} \rangle \langle \tilde{a}s \| 1'b \rangle_{S_i}$$
$$+ (-1)^{\tilde{S}_i} \langle 1'\tilde{b} \| \tilde{s}a \rangle \langle \tilde{a}s \| 1'b \rangle) - (-1)^{S_i} \delta_{S_i \tilde{S}_i} \langle 1'\tilde{b} \| \tilde{s}a \rangle \langle \tilde{a}s \| b1' \rangle \}, \tag{136b}$$

$$v_3''(c) = \langle s|\tilde{s} \rangle \langle 1'\tilde{b} \| ab \rangle_{S_i} (\delta_{S_i \tilde{S}_i} \langle \tilde{a}r \| 1''\tilde{r} \rangle - \tfrac{1}{2}[S_i, \tilde{S}_i]^{1/2} \langle \tilde{a}r \| \tilde{r}1'' \rangle), \tag{136c}$$

$$v_3''(d) = \langle b|\tilde{b} \rangle \langle rs \| 1'\tilde{s} \rangle_{S_i} (\delta_{S_i \tilde{S}_i} \langle 1'\tilde{a} \| \tilde{r}a \rangle - \tfrac{1}{2}[S_i, \tilde{S}_i]^{1/2} \langle 1'\tilde{a} \| a\tilde{r} \rangle), \tag{136d}$$

$$v_3''(e) = \langle a|\tilde{a} \rangle \langle 1'r \| \tilde{s}\tilde{r} \rangle_{S_i} (\delta_{S_i \tilde{S}_i} \langle \tilde{b}s \| b1' \rangle - \tfrac{1}{2}[S_i, \tilde{S}_i]^{1/2} \langle \tilde{b}s \| 1'b \rangle), \tag{136e}$$

$$v_3''(f) = \langle r|\tilde{r}\rangle\langle\tilde{a}\tilde{b}\|a1''\rangle_{S_i}(\delta_{S_i,\bar{S}_i}\langle 1''s\|b\tilde{s}\rangle - \tfrac{1}{2}[S_i,\tilde{S}_i]^{1/2}\langle 1''s\|\tilde{s}b\rangle), \tag{136f}$$

$$v_3''(g) = -\tfrac{1}{2}[S_i,\tilde{S}_i]^{1/2}\langle\tilde{a}s\|ab\rangle_{S_i}\langle r\tilde{b}\|\tilde{r}\tilde{s}\rangle_{S_i}, \tag{136g}$$

$$v_3''(h) = -\tfrac{1}{2}[S_i,\tilde{S}_i]^{1/2}\langle rs\|\tilde{r}b\rangle_{S_i}\langle\tilde{a}\tilde{b}\|a\tilde{s}\rangle_{S_i}. \tag{136h}$$

The corresponding denominators are defined as

$$\Delta_3'(x) = \Delta^X(u_1'^x, u_2'^x, s; c_1'^x, c_2'^x, b) \quad (x = a-h), \tag{137x}$$

$$\Delta_3''(x) = \Delta^X(u_1''^x, u_2''^x, s; c_1''^x, c_2''^x, b) \quad (x = a-h), \tag{138x}$$

and the projectors as

$$\mathcal{P}_3'(x) = \mathcal{S}_{ab}(S_i)^{k_1'^x}\mathcal{S}_{\tilde{a}\tilde{b}}(\tilde{S}_i)^{k_2'^x}\mathcal{S}_{rs}(S_i)^{k_3'^x}\mathcal{S}_{\tilde{r}\tilde{s}}(\tilde{S}_i)^{k_4'^x} \quad (x = a-h), \tag{139x}$$

$$\mathcal{P}_3''(x) = \mathcal{S}_{ab}(S_i)^{k_1''^x}\mathcal{S}_{\tilde{a}\tilde{b}}(\tilde{S}_i)^{k_2''^x}\mathcal{S}_{rs}(S_i)^{k_3''^x}\mathcal{S}_{\tilde{r}\tilde{s}}(\tilde{S}_i)^{k_4''^x} \quad (x = a-h), \tag{140x}$$

with the orbital labels $u_1'^x$, etc., and the parameters $k_1'^x$, etc., listed in Table 2. Again, simple relationship between the $p-h$ conjugate diagrams of Figs. 8 and 9, namely a and b, c and d, e and f, g and h is reflected in the corresponding algebraic expressions, Eqs. (135)–(140).

Equations (126)–(129) together with Eqs. (132)–(140) represent the complete set of formulas for the matrix elements $W_{ij}^{(k)X}(\varepsilon)$ of the effective interaction operator

$$W^{(k)X}(\varepsilon) = V_N \frac{Q^{(k)}}{\varepsilon - \Omega_N^X} V_N. \tag{141}$$

Since the operator $W^{(k)X}(\varepsilon)$ is Hermitian (as long as ε is real), the corresponding $M \times M$ matrix $W^{(k)X}(\varepsilon) \equiv \|W_{ij}^{(k)X}(\varepsilon)\|_{1 \leqslant i,j \leqslant M}$ between orthogonally spin-adapted

Table 2. Orbital labels and parameters defining the denominators $\Delta_3'(x)$, $\Delta_3''(x)$ and projectors $\mathcal{P}_3'(x)$, $\mathcal{P}_3''(x)$, $x = a-h$, given by Eqs. (137x), (138x) and (139x), (140x), respectively

x	$u_1'^x$	$u_2'^x$	$c_1'^x$	$c_2'^x$	$k_1'^x$	$k_2'^x$	$k_3'^x$	$k_4'^x$
a	$1''$	$2''$	$1'$	a	0	0	1	1
b	$1''$	r	$1'$	$2'$	1	1	0	0
c	$1''$	$2''$	a	$\tilde{a}$	1	1	1	1
d	r	$\tilde{r}$	$1'$	$2'$	1	1	1	1
e	$1''$	$\tilde{r}$	$1'$	a	0	0	1	1
f	$1''$	r	$1'$	$\tilde{a}$	1	1	0	0
g	$1''$	$\tilde{r}$	$1'$	a	1	1	1	1
h	$1''$	r	$1'$	$\tilde{a}$	1	1	1	1

x	$u_1''^x$	$u_2''^x$	$c_1''^x$	$c_2''^x$	$k_1''^x$	$k_2''^x$	$k_3''^x$	$k_4''^x$
a	$1''$	$\tilde{s}$	a	$\tilde{b}$	1	1	1	1
b	r	$\tilde{s}$	$1'$	$\tilde{b}$	1	1	1	1
c	$1''$	$\tilde{r}$	a	$\tilde{a}$	0	1	1	1
d	r	$\tilde{r}$	$1'$	$\tilde{a}$	1	1	0	1
e	$\tilde{r}$	$\tilde{s}$	$1'$	a	1	1	1	0
f	$1''$	r	$\tilde{a}$	$\tilde{b}$	1	0	1	1
g	$\tilde{r}$	$\tilde{s}$	a	$\tilde{b}$	0	1	1	0
h	r	$\tilde{s}$	$\tilde{a}$	$\tilde{b}$	1	0	0	1

doubly excited configurations must be Hermitian,

$$W^{(k)X}(\varepsilon)^\dagger = W^{(k)X}(\varepsilon). \tag{142}$$

From explicit expressions for the numerators $v_k(x)$, denominators $\Delta_k(x)$ and projection operators $\mathscr{P}_k(x)$, Eqs. (132)–(140), it follows that most of the individual contributions $R_{ij}^{(k)}(x)$ to $W_{ij}^{(k)X}(\varepsilon)$ satisfy the Hermitian property

$$R_{ji}^{(k)}(x)^* = R_{ij}^{(k)}(x). \tag{143}$$

One can easily check that Eq. (143) holds for all the contributions except for $R_{ij}^{(3)\prime}(g)$, $R_{ij}^{(3)\prime}(h)$ and $R_{ij}^{(3)\prime\prime}(x)$, $x = c-h$. The fact that Eq. (143) is not satisfied by all the components $R_{ij}^{(k)}(x)$ does not, however, affect the Hermiticity of the matrix $W^{(k)X}(\varepsilon)$, Eq. (142). Careful inspection of Eqs. (135g), (135h), (136c)–(136h), (137g), (137h), (138c)–(138h), (139g), (139h) and (140c)–(140h) shows that expressions corresponding to diagrams in Fig. 8g and h, Fig. 9c and f, d and e, and g and h form Hermitian-conjugate pairs, i.e.,

$$R_{ij}^{(3)\prime}(g) = R_{ji}^{(3)\prime}(h)^*, \tag{144}$$

$$R_{ij}^{(3)\prime\prime}(c) = R_{ji}^{(3)\prime\prime}(f)^*, \tag{145}$$

$$R_{ij}^{(3)\prime\prime}(d) = R_{ji}^{(3)\prime\prime}(e)^*, \tag{146}$$

$$R_{ij}^{(3)\prime\prime}(g) = R_{ji}^{(3)\prime\prime}(h)^*. \tag{147}$$

Consequently, when all the individual contributions $R_{ij}^{(k)}(x)$ to $W_{ij}^{(k)X}(\varepsilon)$ are summed up, the Hermiticity of the resulting matrix $W^{(k)X}(\varepsilon)$ will be automatically assured.

From Eqs. (127), (132a), (133a), (134a) and (113), it follows that $R_{ij}^{(4)}(a)$ vanish for $i \neq j$. In other words, matrix $\mathbf{R}^{(4)}(a) = \|R_{ij}^{(4)}(a)\|_{1 \leqslant i,j \leqslant M}$ is diagonal. Similarly, several other matrix elements $R_{ij}^{(k)}(x)$ vanish when certain relations between the biexcited configurations $\Phi_i = \left|\begin{matrix} r & s \\ a & b \end{matrix}\right\rangle_{S_i}$ and $\Phi_j = \left|\begin{matrix} \tilde{r} & \tilde{s} \\ \tilde{a} & \tilde{b} \end{matrix}\right\rangle_{S_i}$ are not satisfied. Additional simplifications in general spin symmetry adapted expressions for $W_{ij}^{(k)X}(\varepsilon)$, Eqs. (126)–(129) and (132)–(140), are possible when other symmetries available for a given molecular system are exploited. We shall not, however, discuss the problem of symmetry adaptation of Eqs. (126)–(129) and (132)–(140) here. Instead, in the last section of the present paper we concentrate on another important aspect of the spin-adaptation formalism, namely, comparison of different procedures for spin-adaptation. The problem of exploitation of other than spin symmetries will be discussed in greater detail in Parts II and III of this series, where general expressions (126)–(129) and (132)–(140) are used to compute the effective interaction matrix elements $W_{ij}^{(3)}$, $W_{ij}^{(3)}(\varepsilon)$ and $W_{ij}^{(4)}(\varepsilon)$, Eqs. (57), (115) and (116), respectively, for the highly symmetric PPP model of cyclic polyenes.

6. Comparison of different diagrammatic procedures for spin-adaptation

In the preceding section, we have applied the spin-adaptation procedure of [38] to derive explicit expressions for the matrix elements $W_{ij}^{(k)X}(\varepsilon)$, Eq. (122). This procedure relies on a spin independent form of the Hamiltonian, Eqs. (1)–(4), and the respresentation of the two-electron interaction operator V_N by bare vertices shown in Fig. 1b. Since these vertices do not enter the resulting spin

diagrams, spin graphs appearing in the applications of the bare-interaction approach [38] usually contain a small number of nodes and thus are easy to evaluate. This main advantage of the method of [38] is, to some extent, lost when, like in the case of the matrix elements $W_{ij}^{(k)X}(\varepsilon)$, it is necessary to consider a relatively large number of orbital diagrams due to the fact that the two-body part of the Hamiltonian is represented by Goldstone-type vertices.

The bare-interaction technique [38] was formulated in the context of CC theory. Since the CC equations are linear in V_N (cf. Eqs. (14) and (15)), the number of the resulting Goldstone–Brandow orbital diagrams is not much larger than the number of Hugenholtz diagrams [40] (at most two distinct Goldstone–Brandow representatives may be associated with each Hugenholtz diagram). However, in the present article we are dealing with the perturbation theory-like expression (122), which is quadratic in V_N. Consequently, up to four distinct Goldstone–Brandow representatives may be associated with each Hugenholtz diagram of [34] (cf. Figs. 7f, 8e–h, 9a,b). To reduce the number of diagrams, which have to be explicitly considered to evaluate the right-hand side of Eq. (122), we may apply an alternative diagrammatic spin-adaptation procedure proposed by Mukherjee and Bhattacharya [106] and Mukhopadhyay [107]. This technique was specially designed to evaluate highly nonlinear expressions in the two-electron interaction operator appearing in higher orders of the MBPT. An essential feature of this approach is an intermediate spin-adaptation (or pre-adaptation) of the two-body component V_N of the Hamiltonian H_N, Eq. (2), so that Eq. (4) now becomes

$$V_N = \tfrac{1}{4}\sum_S \langle mn\|pq\rangle_S \sum_{\substack{\sigma_m\sigma_n \\ \sigma_p\sigma_q}} \sum_\sigma \langle \tfrac{1}{2}\sigma_m, \tfrac{1}{2}\sigma_n | S\sigma \rangle \langle \tfrac{1}{2}\sigma_p, \tfrac{1}{2}\sigma_q | S\sigma \rangle N[e_{m\sigma_m,p\sigma_p}\, e_{n\sigma_n,q\sigma_q}],$$
(148)

where the unitary group generators $e_{m\sigma_m,n\sigma_n}$ are defined as [53]

$$e_{m\sigma_m,n\sigma_n} = X_{m\sigma_m}^\dagger X_{n\sigma_n}.$$
(149)

Consequently, operator V_N can be represented by a Hugenholtz-type orbital diagram shown in Fig. 10a, or by its Brandow version given in Fig. 10b. However, in contrast with the Goldstone representation (bare-interaction vertices), the spin-adapted orbital vertices (Fig. 10a,b) are accompanied by a nontrivial spin diagram shown in Fig. 10c; this spin diagram is a graphical representation of the product of Clebsch–Gordan coefficients together with the summation over σ appearing in Eq. (148). On the other hand, when constructing the resulting orbital diagrams, we can now employ Hugenholtz-type representation for both F_N (G_N) and V_N vertices, as well as for vertices representing excitations and (in the case of the CC theory) cluster operators T_j. This feature of the spin-adaptation technique of [106] and [107] is very desirable, especially for the MBPT-type expressions, since Hugenholtz diagrams are fewer in number. The latter must be represented in Brandow form so that we can determine the orbital phase factors. In either approach, Brandow representation is also required for the construction of pertinent spin graphs, which are then evaluated using the graphical methods of spin algebras (cf. Sect. 2).

Now, while the use of spin-adapted interaction vertices [106, 107] reduces the number of diagrams that must be considered, it simultaneously yields more complicated spin diagrams than the bare-interaction technique [38]. Mukherjee and Bhattacharya [106] and Mukhopadhyay [107] applied their method to the MBPT equations, obtaining very compact and formally appealing results
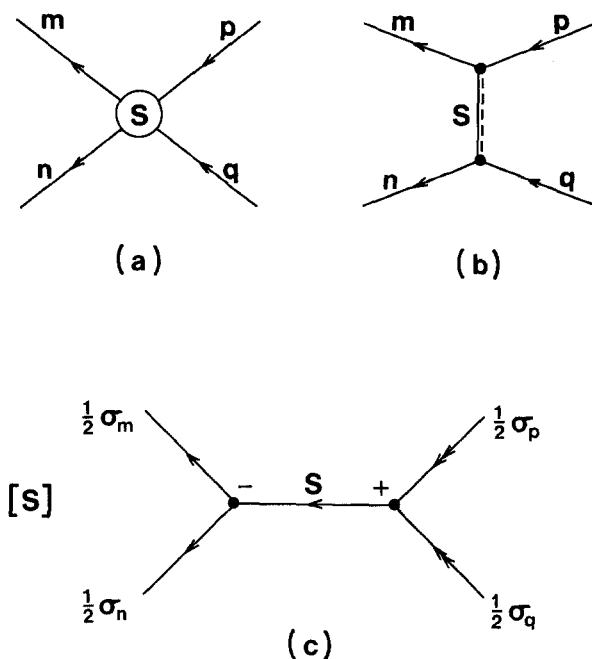
Fig. 10a–c. Diagrams representing the spin-reduced form of the operator V_N, Eq. (148): **a** represents spin-adapted Hugenholtz-type orbital vertex, **b** its Brandow version, and **c** the corresponding 3-*jm*-type spin diagram

[106, 107]. Since the right-hand side of Eq. (122) is reminiscent of the standard MBPT expressions, it is of interest to try out this approach for the matrix elements $\bar{W}_{ij}^{(k)X}(\varepsilon)$ ($k = 3, 4$) and compare the results with those in Sect. 5. So far, a relationship between the two different versions of diagrammatic spin-adaptation employing either bare or spin-adapted interaction vertices was only examined in the context of the CC theory [40]. In this section, we wish to obtain a more complete picture of this relationship by comparing both spin-adaptation techniques for the perturbation theory-like expression (122).

In Figs. 7–9 distinct Goldstone–Brandow orbital diagrams that are associated with a given Hugenholtz diagram are grouped together. Thus, the decomposition of $W_{ij}^{(k)X}(\varepsilon)$ into individual terms $R_{ij}^{(k)}(x)$, Eq. (126), as well as general expressions for $R_{ij}^{(k)}(x)$, Eqs. (127)–(129), will remain unchanged when the spin-adaptation procedure [106] and [107] is applied. Likewise, explicit expressions for the denominators $\Delta_k(x)$, Eqs. (133), (137) and (138), and projection operators $\mathcal{P}_k(x)$, Eqs. (134), (139) and (140), will remain unchanged. Only expressions for the numerators $v_k(x)$ will differ from those given in Sect. 5, since both spin-adaptation procedures yield different spin factors. Thus, only numerators need to be considered. For the sake of brevity, we restrict ourselves to a few representative cases.

It is easily seen that spin-adaptation techniques of [38] and [106, 107] yield identical or almost identical expressions for the contributions $R_{ij}^{(4)}(x)$, $x = d, e, g-i$, $R_{ij}^{(3)\prime\prime}(g)$ and $R_{ij}^{(3)\prime\prime}(h)$. This is immediately obvious in view of the discussion given in [40], since the Goldstone–Brandow diagrams of Figs.

7d,e,g–i, 9g,h have no distinct exchange versions so that in each case the corresponding Hugenholtz diagram is uniquely represented by only one Goldstone–Brandow diagram. Thus, to appreciate the difference between the two versions of diagrammatic spin-adaptation we consider those contributions $R_{ij}^{(k)}(x)$, which correspond to several Goldstone–Brandow diagrams, namely $R_{ij}^{(4)}(f)$, $R_{ij}^{(3)'}(a)$, $R_{ij}^{(3)'}(c)$, $R_{ij}^{(3)'}(e)$, $R_{ij}^{(3)'}(g)$, and $R_{ij}^{(3)''}(a)$. Figure 8a and c corresponds to the components $R_{ij}^{(3)'}(a)$ and $R_{ij}^{(3)'}(c)$, respectively, and contain two Goldstone–Brandow diagrams each, while each of Figs. 7f, 8e,g and 9a contains four distinct Goldstone–Brandow diagrams. Using spin-adapted interaction vertices [106, 107] we can replace all these diagrams by Hugenholtz-like orbital diagrams shown (in Brandow representation) in Figs. 11, 12a,c,e,g and 13. Combining orbital and spin factors associated with Brandow diagrams of Figs. 11–13, we then obtain the following new expressions for the numerators $v_4(f)$, $v_3'(x)$, $x = a, c, e$ and g, and $v_3''(a)$,

$$v_4(f) = [S_i, \tilde{S}_i]^{1/2} \langle s|\tilde{s}\rangle \langle b|\tilde{b}\rangle \sum_{S^1 S^2} [S^1, S^2] R(S_i, \tilde{S}_i, S^1, S^2)$$

$$\times \langle 1''r\|1'a\rangle_{S^1} \langle 1'\tilde{a}\|1''\tilde{r}\rangle_{S^2}, \tag{150}$$

$$v_3'(a) = \tfrac{1}{4}\delta_{S_i \tilde{S}_i} A_{ab}^{\tilde{a}\tilde{b}}(S_i) \langle s|\tilde{s}\rangle \sum_{S} [S] \langle 1'r\|1''2''\rangle_S \langle 1''2''\|1'\tilde{r}\rangle_S, \tag{151a}$$

$$v_3'(c) = \tfrac{1}{2}[S_i, \tilde{S}_i]^{1/2} \langle s|\tilde{s}\rangle \langle b|\tilde{b}\rangle \sum_{S} [S] C(S_i, \tilde{S}_i, S) \langle \tilde{a}r\|1''2''\rangle_S \langle 1''2''\|\tilde{r}a\rangle_S, \tag{151c}$$

$$v_3'(e) = \delta_{S_i \tilde{S}_i} A_{ab}^{\tilde{a}\tilde{b}}(S_i) \sum_{S^1 S^2} [S^1, S^2] C(S_i, S^1, S^2) \langle 1'r\|1''\tilde{r}\rangle_{S^1} \langle 1''s\|1'\tilde{s}\rangle_{S^2}, \tag{151e}$$

$$v_3'(g) = -[S_i, \tilde{S}_i]^{1/2} \langle s|\tilde{s}\rangle \langle b|\tilde{b}\rangle \sum_{S^1 S^2} [S^1, S^2] W(S_i, \tilde{S}_i, S^1, S^2)$$

$$\times \langle 1'r\|1''\tilde{r}\rangle_{S^1} \langle 1''\tilde{a}\|1'a\rangle_{S^2}, \tag{151g}$$

$$v_3''(a) = [S_i, \tilde{S}_i]^{1/2} \langle a|\tilde{a}\rangle \sum_{S^1 S^2} [S^1, S^2] W(S^2, S_i, \tilde{S}_i, S^1) \langle \tilde{b}r\|\tilde{s}1''\rangle_{S^1} \langle 1''s\|\tilde{r}b\rangle_{S^2}, \tag{152}$$

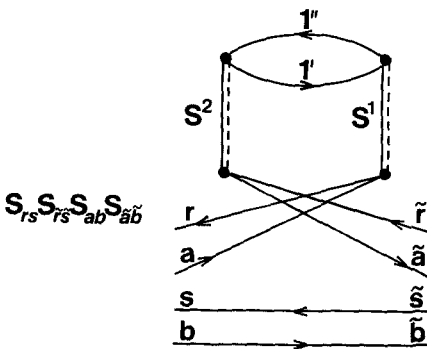where C is a 9-j symbol defined by Eq. (32), while the coefficients R and W are

Fig. 11. The Brandow form of the Hugenholtz-like orbital diagram corresponding to the four Goldstone–Brandow diagrams of Fig. 7f
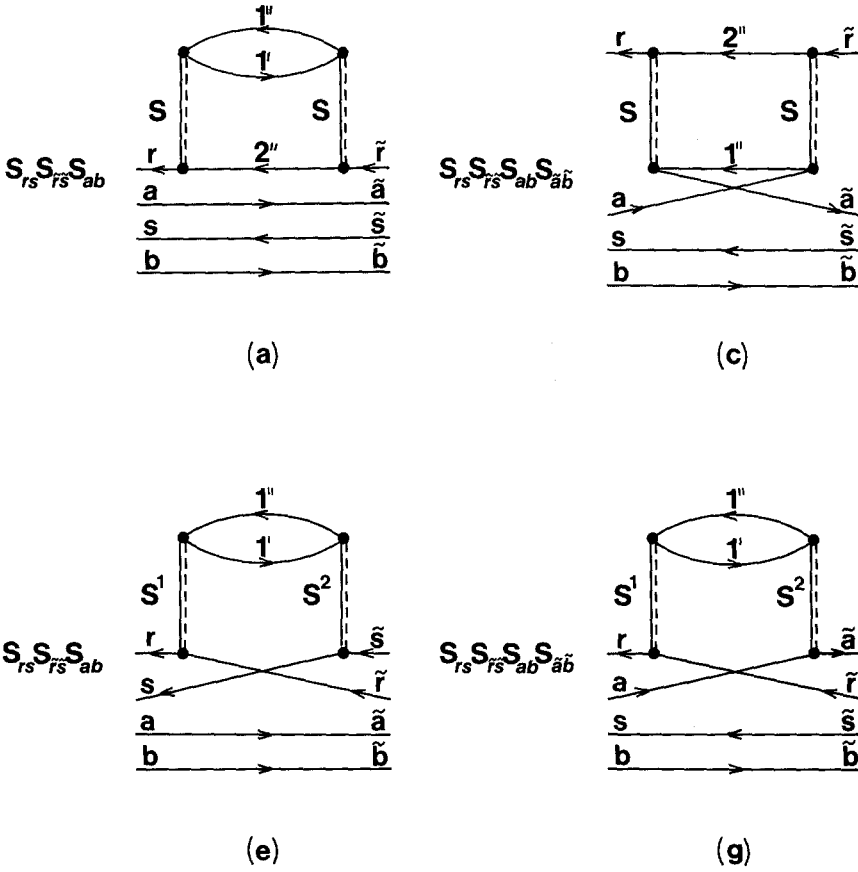
Fig. 12. Brandow orbital diagrams of [106] and [107] corresponding to Goldstone–Brandow diagrams given in Fig. 8a,c,e,g
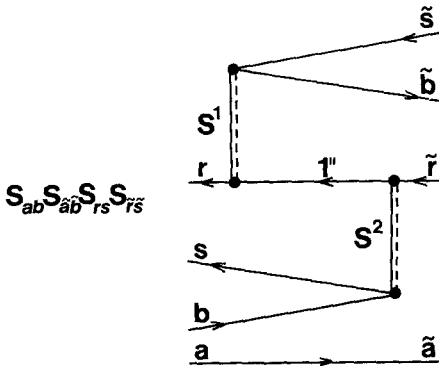

Fig. 13. Brandow-type orbital diagram of [106] and [107] representing four Goldstone–Brandow diagrams shown in Fig. 9a

two different types of 12-j symbol of the second kind [80, 81], namely

$$R(X_1, X_2, X_3, X_4) = \begin{bmatrix} \frac{1}{2} & \frac{1}{2} & \frac{1}{2} & \frac{1}{2} \\ X_1 & X_2 & X_3 & X_4 \\ \frac{1}{2} & \frac{1}{2} & \frac{1}{2} & \frac{1}{2} \end{bmatrix}, \tag{153}$$

and

$$W(X_1, X_2, X_3, X_4) = \begin{bmatrix} X_1 & X_2 & \frac{1}{2} & \frac{1}{2} \\ \frac{1}{2} & \frac{1}{2} & \frac{1}{2} & \frac{1}{2} \\ \frac{1}{2} & X_3 & \frac{1}{2} & X_4 \end{bmatrix}. \tag{154}$$

The 12-j symbol R, Eq. (153), was introduced in [40] and can be regarded as a higher-order analogue of the 9-j symbol C. For example, both C and R are highly symmetric in their indices [39, 40]. The coefficient W has lower symmetry than the coefficient R. Symmetry properties for both R and W can be easily deduced from the general symmetry properties of the 12-j symbol of the second kind [80, 81].

Expressions (150)–(152), except for Eq. (151a), involve genuine 9-j and 12-j coefficients that cannot be expressed as products of simpler $3n$-j symbols, since each pair of spin-adapted two-electron interaction vertices enters a spin diagram adding four nodes to it. Consequently, each of the spin graphs that is associated with diagrams in Figs. 11–13 (as well as with remaining contributions $R_{ij}^{(k)}(x)$) contains 8 nodes and 12 lines. As follows from Eqs. (150)–(152), only some of these spin graphs are separable over $n \leqslant 3$ lines [22, 80, 81] and factorize into products of simpler $3n$-j coefficients. Let us recall that each of the spin diagrams corresponding to Figs. 7–9 contains only 4 nodes and 6 lines. It must be remembered that each of Eqs. (150)–(152) is a single algebraic expression representing several (two or four) distinct Goldstone–Brandow diagrams. As may be seen from Eqs. (132), (135) and (136), expressions that are associated with Goldstone–Brandow orbital diagrams, which are exchange versions of one another, usually differ by spin coupling coefficients. Thus, to combine them together and represent them by a single formula, we must introduce appropriate angular momentum recoupling coefficients. This gives another explanation of the presence of 9-j and 12-j symbols in Eqs. (150)–(152) (cf., Sect. 4 in [40]).

Let us now compare explicit expressions for $R_{ij}^{(4)}(f)$, $R_{ij}^{(3)\prime}(x)$, $x = a, c, e, g$, and $R_{ij}^{(3)\prime\prime}(a)$, as derived in this section, with the corresponding results obtained in Sect. 5. First, we must expand Eqs. (150)–(152) in terms of non-symmetric v-matrix elements $\langle mn \| pq \rangle$ [40]. This gives

$$v_4(f) = [S_i, \tilde{S}_i]^{1/2} \langle s | \tilde{s} \rangle \langle b | \tilde{b} \rangle \Bigg\{ \langle 1''r \| 1'a \rangle \langle 1'\tilde{a} \| 1''\tilde{r} \rangle \sum_{S^1 S^2} [S^1, S^2] R(S_i, \tilde{S}_i, S^1, S^2)$$

$$+ \langle 1''r \| a1' \rangle \langle 1'\tilde{a} \| 1''\tilde{r} \rangle \sum_{S^1 S^2} (-1)^{S^1} [S^1, S^2] R(S_i, \tilde{S}_i, S^1, S^2)$$

$$+ \langle 1''r \| 1'a \rangle \langle 1'\tilde{a} \| \tilde{r}1'' \rangle \sum_{S^1 S^2} (-1)^{S^2} [S^1, S^2] R(S_i, \tilde{S}_i, S^1, S^2)$$

$$+ \langle 1''r \| a1' \rangle \langle 1'\tilde{a} \| \tilde{r}1'' \rangle \sum_{S^1 S^2} (-1)^{S^1 + S^2} [S^1, S^2] R(S_i, \tilde{S}_i, S^1, S^2) \Bigg\}, \tag{155}$$

$$v_3'(a) = \tfrac{1}{2}\delta_{S_i\tilde{S}_i}A_{ab}^{\tilde{a}\tilde{b}}(S_i)\langle s|\tilde{s}\rangle\Big\{\langle 1'r\|1''2''\rangle\langle 1''2''\|1'\tilde{r}\rangle\sum_S[S]$$

$$+\langle 1'r\|1''2''\rangle\langle 1''2''\|\tilde{r}1'\rangle\sum_S(-1)^S[S]\Big\}, \tag{156a}$$

$$v_3'(c) = [S_i,\tilde{S}_i]^{1/2}\langle s|\tilde{s}\rangle\langle b|\tilde{b}\rangle\Big\{\langle\tilde{a}r\|1''2''\rangle\langle 1''2''\|\tilde{r}a\rangle\sum_S[S]C(S_i,\tilde{S}_i,S)$$

$$+\langle\tilde{a}r\|1''2''\rangle\langle 1''2''\|a\tilde{r}\rangle\sum_S(-1)^S[S]C(S_i,\tilde{S}_i,S)\Big\}, \tag{156c}$$

$$v_3'(e) = \delta_{S_i\tilde{S}_i}A_{ab}^{\tilde{a}\tilde{b}}(S_i)\Big\{\langle 1'r\|1''\tilde{r}\rangle\langle 1''s\|1'\tilde{s}\rangle\sum_{S^1S^2}[S^1,S^2]C(S_i,S^1,S^2)$$

$$+\langle 1'r\|\tilde{r}1''\rangle\langle 1''s\|1'\tilde{s}\rangle\sum_{S^1S^2}(-1)^{S^1}[S^1,S^2]C(S_i,S^1,S^2)$$

$$+\langle 1'r\|1''\tilde{r}\rangle\langle 1''s\|\tilde{s}1'\rangle\sum_{S^1S^2}(-1)^{S^2}[S^1,S^2]C(S_i,S^1,S^2)$$

$$+\langle 1'r\|\tilde{r}1''\rangle\langle 1''s\|\tilde{s}1'\rangle\sum_{S^1S^2}(-1)^{S^1+S^2}[S^1,S^2]C(S_i,S^1,S^2)\Big\}, \tag{156e}$$

$$v_3'(g) = -[S_i,\tilde{S}_i]^{1/2}\langle s|\tilde{s}\rangle\langle b|\tilde{b}\rangle$$

$$\times\Big\{\langle 1'r\|1''\tilde{r}\rangle\langle 1''\tilde{a}\|1'a\rangle\sum_{S^1S^2}[S^1,S^2]W(S_i,\tilde{S}_i,S^1,S^2)$$

$$+\langle 1'r\|\tilde{r}1''\rangle\langle 1''\tilde{a}\|1'a\rangle\sum_{S^1S^2}(-1)^{S^1}[S^1,S^2]W(S_i,\tilde{S}_i,S^1,S^2)$$

$$+\langle 1'r\|1''\tilde{r}\rangle\langle 1''\tilde{a}\|a1'\rangle\sum_{S^1S^2}(-1)^{S^2}[S^1,S^2]W(S_i,\tilde{S}_i,S^1,S^2)$$

$$+\langle 1'r\|\tilde{r}1''\rangle\langle 1''\tilde{a}\|a1'\rangle\sum_{S^1S^2}(-1)^{S^1+S^2}[S^1,S^2]W(S_i,\tilde{S}_i,S^1,S^2)\Big\}, \tag{156g}$$

$$v_3''(a) = [S_i,\tilde{S}_i]^{1/2}\langle a|\tilde{a}\rangle\Big\{\langle\tilde{b}r\|\tilde{s}1''\rangle\langle 1''s\|\tilde{r}b\rangle\sum_{S^1S^2}[S^1,S^2]W(S^2,S_i,\tilde{S}_i,S^1)$$

$$+\langle\tilde{b}r\|1''\tilde{s}\rangle\langle 1''s\|\tilde{r}b\rangle\sum_{S^1S^2}(-1)^{S^1}[S^1,S^2]W(S^2,S_i,\tilde{S}_i,S^1)$$

$$+\langle\tilde{b}r\|\tilde{s}1''\rangle\langle 1''s\|b\tilde{r}\rangle\sum_{S^1S^2}(-1)^{S^2}[S^1,S^2]W(S^2,S_i,\tilde{S}_i,S^1)$$

$$+\langle\tilde{b}r\|1''\tilde{s}\rangle\langle 1''s\|b\tilde{r}\rangle\sum_{S^1S^2}(-1)^{S^1+S^2}[S^1,S^2]W(S^2,S_i,\tilde{S}_i,S^1)\Big\}. \tag{157}$$

To get Eqs. (156a) and (156c) we have also exploited the fact that the denominators $\varDelta_3'(a)$ and $\varDelta_3'(c)$, Eqs. (137a) and (137c), respectively, are symmetric in the summation indices $1''$ and $2''$.

Now, the right-hand sides of Eqs. (135a) and (156a) are identical, since $\sum_S[S] = 4$ and $\sum_S(-1)^S[S] = -2$ (recall that S assumes only two values: $S = 0$ and $S = 1$). Thus, for $R_{ij}^{(3)\nu}(a)$, the results of two different spin-adaptation procedures are easily transformed one into the other. To show that the remaining expressions (155), (156c), (156e), (156g) and (157) are identical with their

counterparts given in Sect. 5, we have to apply slightly more complicated sum rules for 9-j and 12-j coefficients.

We can easily verify that the 9-j symbol C, Eq. (32), satisfies the following relations [80, 81] (see also [40]),

$$\sum_{S} [S]C(S_i, \tilde{S}_i, S) = \tfrac{1}{2}, \tag{158}$$

$$\sum_{S} (-1)^S[S]C(S_i, \tilde{S}_i, S) = -\delta_{S_i\tilde{S}_i}[S_i]^{-1}, \tag{159}$$

$$\sum_{S^1S^2} [S^1, S^2]C(S_i, S^1, S^2) = 2, \tag{160}$$

$$\sum_{S^1S^2} (-1)^{S^1}[S^1, S^2]C(S_i, S^1, S^2) = \sum_{S^1S^2} (-1)^{S^2}[S^1, S^2]C(S_i, S^1, S^2) = -1, \tag{161}$$

$$\sum_{S^1S^2} (-1)^{S^1 + S^2}[S^1, S^2]C(S_i, S^1, S^2) = (-1)^{1 + S_i}. \tag{162}$$

In a similar way, we can show that the 12-j coefficient R, Eq. (153), satisfies [80, 81]

$$\sum_{S^1S^2} [S^1, S^2]R(S_i, \tilde{S}_i, S^1, S^2) = 1, \tag{163}$$

$$\sum_{S^1S^2} (-1)^{S^1}[S^1, S^2]R(S_i, \tilde{S}_i, S^1, S^2) = \sum_{S^1S^2} (-1)^{S^2}[S^1, S^2]R(S_i, \tilde{S}_i, S^1, S^2) = -\tfrac{1}{2}, \tag{164}$$

$$\sum_{S^1S^2} (-1)^{S^1 + S^2}[S^1, S^2]R(S_i, \tilde{S}_i, S^1, S^2) = \delta_{S_i\tilde{S}_i}[S_i]^{-1}. \tag{165}$$

For the 12-j symbol W, Eq. (154), two different categories of sum rules can be written. The following relations [80, 81] belong to the first category,

$$\sum_{S^1S^2} [S^1, S^2]W(S_i, \tilde{S}_i, S^1, S^2) = 2\delta_{S_i\tilde{S}_i}[S_i]^{-1}, \tag{166}$$

$$\sum_{S^1S^2} (-1)^{S^1}[S^1, S^2]W(S_i, \tilde{S}_i, S^1, S^2) = \sum_{S^1S^2} (-1)^{S^2}[S^1, S^2]W(S_i, \tilde{S}_i, S^1, S^2)$$
$$= -\delta_{S_i\tilde{S}_i}[S_i]^{-1}, \tag{167}$$

$$\sum_{S^1S^2} (-1)^{S^1 + S^2}[S^1, S^2]W(S_i, \tilde{S}_i, S^1, S^2) = \tfrac{1}{2}, \tag{168}$$

while the sum rules given below, namely [80, 81],

$$\sum_{S^1S^2} [S^1, S^2]W(S^2, S_i, \tilde{S}_i, S^1) = \tfrac{1}{2}, \tag{169}$$

$$\sum_{S^1S^2} (-1)^{S^1}[S^1, S^2]W(S^2, S_i, \tilde{S}_i, S^1) = \tfrac{1}{2}(-1)^{\tilde{S}_i}, \tag{170}$$

$$\sum_{S^1S^2} (-1)^{S^2}[S^1, S^2]W[S^2, S_i, \tilde{S}_i, S^1) = \tfrac{1}{2}(-1)^{S_i}, \tag{171}$$

$$\sum_{S^1S^2} (-1)^{S^1 + S^2}[S^1, S^2]W(S^2, S_i, \tilde{S}_i, S^1) = (-1)^{1 + S_i}\delta_{S_i\tilde{S}_i}[S_i]^{-1}, \tag{172}$$

belong to the second category. As a matter of fact, Eqs. (170) and (171) represent the same sum rule since [80, 81]

$$W(S^2, S_i, \tilde{S}_i, S^1) = W(S^1, \tilde{S}_i, S_i, S^2). \qquad (173)$$

In further considerations, however, both relations (170) and (171) are useful.

Equations (158)–(172) allow us to eliminate the 9-j and 12-j symbols from expressions (155), (156c), (156e), (156g) and (157) and to replace them by the same simple spin factors that result from the application of the bare-interaction technique [38]. Thus, inserting Eqs. (163)–(165) into Eq. (155), we immediately obtain expression (132f). Quite similarly, inserting Eqs. (158) and (159) into Eq. (156c) and Eqs. (160)–(162) into Eq. (156e), we get formulas (135c) and (135e), respectively. Finally, sum rules (166)–(172) allow us to convert Eqs. (156g) and (157) into Eqs. (135g) and (136a), respectively.

It can be easily verified that Eqs. (150)–(152) represent all possible types of expressions for $R_{ij}^{(k)}(x)$, that result from the use of the spin-adaptation procedure [106, 107], except for the formulas for $R_{ij}^{(4)}(x)$, $x = d, e, g-i$, $R_{ij}^{(3)''}(g)$ and $R_{ij}^{(3)''}(h)$, which are identical with the expressions obtained through the exploitation of bare-interaction approach [38]. We can thus conclude that the relationship between both spin-adaptation approaches employing either bare or spin-adapted interaction vertices is very simple for the problem considered in this paper. As in the case of CC equations, we must only expand the (anti)symmetrized two-electron interaction integrals [106, 107] in terms of non-symmetric v-matrix elements and apply the sum rules of the type given by Eqs. (158)–(172), whenever necessary. This brings about a considerable simplification, as a comparison of Eqs. (150)–(152) with their counterparts given in Sect. 5 reveals. Although the procedure employing spin-adapted two-electron interaction vertices [106, 107] yields formally more compact formulas than the bare-interaction technique [38], they become much more complicated when written in an explicit form. For example, summations over S in Eqs. (151a) and (151c) involving 9-j symbols C factorize into much simpler products

$$4\langle 1'r \| 1''2'' \rangle \langle 1''2'' \| 1'\tilde{r} \rangle_a$$

and

$$\langle \tilde{a}r \| 1''2'' \rangle \{ \langle 1''2'' \| \tilde{r}a \rangle - 2\delta_{S_i \tilde{S}_i}[S_i]^{-1} \langle 1''2'' \| a\tilde{r} \rangle \},$$

respectively, when a Goldstone–Brandow representation is used or, equivalently, when they are rewritten in terms of non-symmetric v-matrix elements. Since the spin-adapted two-electron interaction vertices enter the resulting spin diagrams, double summations over S^1 and S^2 appearing in Eqs. (150), (151e), (151g) and (152) involve the 9-j symbols C, Eq. (32), and the 12-j coefficients R and W, Eqs. (153) and (154), respectively. When bare-interaction vertices are used, these summations reduce to very simple bilinear forms in the non-symmetric v-matrix elements with the coefficients proportional to spin factors $\delta_{S_i \tilde{S}_i}$ or $\frac{1}{2}[S_i, \tilde{S}_i]^{1/2}$. Some of these bilinear forms are extremely compact when expressed in terms of the matrix elements $\langle mn \| pq \rangle_a$ and $\langle mn \| pq \rangle_S$ [cf., for example, Eq. (135e)].

To summarize, the diagrammatic spin-adaptation procedure employing Goldstone representation for two-electron interaction vertices [38] leads to simpler expressions for the components $R_{ij}^{(k)}(x)$ than the method using spin-adapted interaction vertices [106, 107]. On the other hand, the latter technique is more economical than the bare-interaction approach [38]. In order to evaluate matrix elements $W_{ij}^{(k)X}(\varepsilon)$ ($k = 3, 4$), we have to draw 57 Goldstone–Brandow

orbital diagrams (cf. Figs. 7–9), while using spin-adapted interaction vertices and Hugenholtz representation, only 25 diagrams must be considered. Unfortunately, this advantage of the method of [106, 107] is partially lost since we have to construct and evaluate a relatively large number of quite complicated spin diagrams. Moreover, once all the Hugenholtz diagrams are drawn, it is not difficult to construct their pertinent Goldstone–Brandow versions. This is why the final expressions for $W_{ij}^{(k)X}(\varepsilon)$ given in Sect. 5 were derived using the bare-interaction procedure [38] rather than the other method [106, 107], although the latter one was specially designed to evaluate expressions of the type (122).

There is yet another, entirely different, diagrammatic spin-adaptation procedure, which yields expressions related to non-symmetric v-matrix elements and which was employed in [34] to evaluate the OIP effective interaction matrix elements $W_{ij}^{(3)}(\varepsilon)$ and $W_{ij}^{(4)}(\varepsilon)$, Eqs. (115) and (116), respectively, in a straightforward way. It employs bare-interaction vertices but does not construct spin diagrams to evaluate the relevant spin factors. Instead, it introduces [34] appropriate orbital coupling coefficients that yield the required orthogonally spin-adapted doubly excited configurations by defining the spin independent operators $R_{ab}^{rs}(S_i)$,

$$R_{ab}^{rs}(S_i) = \tfrac{1}{2} \sum_{mnpq} \langle mn|r(S_i)|pq \rangle N[E_{mp}E_{nq}], \qquad (174)$$

and their Hermitian conjugates $L_{ab}^{rs}(S_i)$. Here, the matrix elements $\langle mn|r(S_i)|pq \rangle$ have the same symmetry properties as the orthogonally spin-adapted biexcited configurations $\left| \begin{matrix} r & s \\ a & b \end{matrix} \right\rangle_{S_i}$, namely,

$$\langle mn|r(S_i)|pq \rangle = (-1)^{S_i} \langle mn|r(S_i)|qp \rangle = (-1)^{S_i}\langle nm|r(S_i)|pq \rangle = \langle nm|r(S_i)|qp \rangle, \qquad (175)$$

and all of them vanish except for those involving the labels r, s and a, b. For the matrix elements $\langle rs|r(S_i)|ab \rangle$ we then have [34]

$$\langle rs|r(S_i)|ab \rangle = \tfrac{1}{2}[S_i]^{-1/2}(N_{ab}^{rs})^{-1}, \qquad (176)$$

where N_{ab}^{rs} is· the normalization factor given by Eq. (20). Of course,

$$L_{ab}^{rs}(S_i) \equiv R_{ab}^{rs}(S_i)^{\dagger} = \tfrac{1}{2} \sum_{mnpq} \langle pq|l(S_i)|mn \rangle N[E_{pm}E_{qn}], \qquad (177)$$

where

$$\langle pq|l(S_i)|mn \rangle = \langle mn|r(S_i)|pq \rangle. \qquad (178)$$

One can easily verify that [34]

$$R_{ab}^{rs}(S_i) = {}^{2S_i+1}G_{ab}^{rs}, \qquad (179)$$

where

$${}^{2S_i+1}G_{ab}^{rs} = {}^{2S_i+1}N_{ab}^{rs}\mathscr{S}_{rs}(S_i)E_{ra}E_{sb}, \qquad (180)$$

is the spin-adapted excitation operator of [75, 76] which generates a normalized pp-hh coupled biexcited singlet configuration $\left| \begin{matrix} r & s \\ a & b \end{matrix} \right\rangle_{S_i}$, Eq. (18), from Φ_0. The normalization factor ${}^{2S_i+1}N_{ab}^{rs}$ [75, 76] is related to the normalization factor N_{ab}^{rs},

Eq. (20), as follows [40]:

$$^{2S_i+1}N_{ab}^{rs} = \tfrac{1}{2}[S_i]^{-1/2}N_{ab}^{rs},\tag{181}$$

so that Eq. (176) can also be written as [34]

$$\langle rs|r(S_i)|ab\rangle = \langle ab|l(S_i)|rs\rangle = {}^{2S_i+1}N_{ab}^{rs}(1+\delta_{ab})(1+\delta_{rs}).\tag{182}$$

Equations (179) and (180) then give

$$R_{ab}^{rs}(S_i)\Phi_0 = \left|\begin{matrix} r & s \\ a & b \end{matrix}\right\rangle_{S_i},\tag{183}$$

and $W_{ij}^{(k)X}(\varepsilon)$, Eq. (122), can be expressed as a Fermi vacuum [8, 51, 52] mean value

$$W_{ij}^{(k)X}(\varepsilon) = \langle\Phi_0|L_{ab}^{rs}(S_i)V_N\frac{Q^{(k)}}{\varepsilon-\Omega_N^X}V_N R_{ab}^{\tilde{r}\tilde{s}}(\tilde{S}_i)|\Phi_0\rangle.\tag{184}$$

Since the excitation operators $R_{ab}^{\tilde{r}\tilde{s}}(\tilde{S}_i)$ and $L_{ab}^{rs}(S_i)$, Eqs. (174) and (177), respectively, can be regarded as general two-body operators, we can now easily evaluate the right-hand side of Eq. (184) by applying standard time-independent diagrammatic techniques [8, 51, 52]. Moreover, all the operators involved are spin independent, so that we can use the rules for spin-free formalism [8, 51, 52]. As in Sect. 5, we first construct all nonequivalent, nonoriented vacuum Hugenholtz skeletons involving two nonoriented Hugenholtz V_N vertices and two similar vertices representing excitation operators $L_{ab}^{rs}(S_i)$ and $R_{ab}^{\tilde{r}\tilde{s}}(\tilde{S}_i)$ (cf. Fig. 18). Orienting the lines we then obtain all the resulting Hugenholtz diagrams (see Figs. 3–5 in [34]). In contrast with the diagrams used in spin-adaptation approaches [38, 44, 106, 107], all the internal lines in Hugenholtz diagrams in [34] carry free (i.e., summation) labels. According to the rules of spin-free formalism [8, 51, 52], it remains to draw all the distinct Goldstone diagrams by replacing the interaction and excitation Hugenholtz vertices in each diagram by the corresponding Goldstone ones (cf., e.g., Fig. 1b) and by performing an "exchange" operation on each vertex starting, for example, with the Goldstone diagram having a maximal number of loops (cf., e.g. [51]). Examples of Goldstone diagrams with a maximal number of closed loops that correspond to Hugenholtz diagrams, Figs. 3f and 4g of [34] (or Figs. 7f and 8g of this paper) are shown in Figs. 14 and 15, respectively. To evaluate these diagrams and all their exchange versions (as well as the remaining Goldstone diagrams associated with Figs. 3–5 in [34] or Figs. 7–9 of this article), we have to label the fermion lines by the appropriate particle or hole orbital indices, and find the corresponding weights and sign and scalar factors. We recall that each scalar factor, which is the product of v-, l-, and r-matrix elements divided by the MBPT denominator and summed over all orbital labels, must be finally multiplied by the numerical factor 2^l, where l is the number of closed loops (cf. Sect. 5).

Grouping together expressions corresponding to all the Goldstone versions of a given Hugenholtz diagram, we obtain formulas for the contributions $R_{ij}^{(4)}(x)$ $(x=a-i)$, $R_{ij}^{(3)'}(x)$ $(x=a-h)$ and $R_{ij}^{(3)''}(x)$ $(x=a-h)$ associated with Figs. 7x $(x=a-i)$, 8x $(x=a-h)$, and 9x $(x=a-h)$, respectively. As was shown in [34], all these formulas have the following general form

$$R_{ij}^{(k)}(x) = \sum_{\{cduw;\tilde{c}\tilde{d}\tilde{u}\tilde{w}\}}\sum_{\{\bar{r}\bar{r}'\}} n_k(x)[\varepsilon-D_k(x)]^{-1}\quad(k=3,4),\tag{185}$$
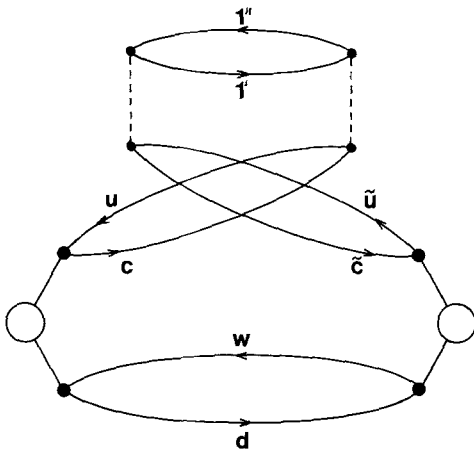
Fig. 14. Goldstone representative of the Hugenholtz diagram 3f of [34] having a maximal number of closed loops; for the labeling convention, see Sects. 2 and 6. This is one of 16 distinct Goldstone diagrams that can be associated with four Goldstone–Brandow orbital diagrams of Fig. 7f
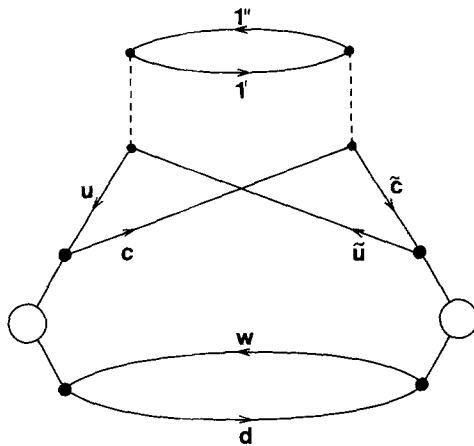
Fig. 15. Goldstone version of the Hugenholtz diagram 4g of [34] having a maximal number of closed loops (see text for labeling convention). The above diagram and its 15 exchange versions correspond to the four Goldstone–Brandow orbital diagrams given in Fig. 8g

where the numerator $n_k(x)$ is given by the products of two v-matrix elements and two orbital coupling coefficients, $\langle cd|l(S_i)|uw\rangle$ and $\langle \tilde{u}\tilde{w}|r(\tilde{S}_i)|\tilde{c}\tilde{d}\rangle$, whereas the denominators $D_k(x)$ are given by the appropriate RHF or Hückel orbital energy differences (cf., Eq. (131)). Both in Figs. 14, 15 and in Eq. (185), summations over hole and particle labels carried by the lines interconnecting interaction vertices l' and l'', respectively, are distinguished from the summations over hole and particle labels carried by the lines leaving or entering excitation vertices $L_{ab}^{rs}(S_i)$ and $R_{ab}^{\tilde{r}\tilde{s}}(\tilde{S}_i)$. The latter summations are symbolically denoted as $\sum_{\{cduw;\tilde{c}\tilde{d}\tilde{u}\tilde{w}\}}$. For example, in the case of the expression for $R_{ij}^{(4)}(f)$, corresponding to the Goldstone diagram of Fig. 14 and all its exchange versions,

$$\sum_{\{cduw;\tilde{c}\tilde{d}\tilde{u}\tilde{w}\}} = \sum_{cduw,\tilde{c}\tilde{u}}.$$

Let us now concentrate on an explicit form of Eq. (185) for the contributions $R_{ij}^{(4)}(f)$ and $R_{ij}^{(3)'}(g)$. By evaluating Goldstone diagram of Fig. 14 and all its 15 distinct exchange versions and grouping together the resulting expressions, we

obtain the following formulas for the numerator $n_4(f)$ and the denominator $D_4(f)$ [34]:

$$n_4(f) = \langle 1'\tilde{c} \| 1''\tilde{u} \rangle_a \langle 1''u \| 1'c \rangle_a \langle cd|l(S_i)|uw \rangle_a \langle \tilde{u}w|r(\tilde{S}_i)|\tilde{c}d \rangle_a$$

$$+ 3 \langle 1'\tilde{c} \| \tilde{u}1'' \rangle \langle 1''u \| c1' \rangle \langle cd|l(S_i)|wu \rangle \langle \tilde{u}w|r(\tilde{S}_i)|d\tilde{c} \rangle, \qquad (186)$$

$$D_4(f) = \Delta^X(1'', u, \tilde{u}, w; 1', c, \tilde{c}, d), \qquad (187)$$

where (cf., Eq. (130))

$$\langle pq|l(S_i)|mn \rangle_a = 2\langle pq|l(S_i)|mn \rangle - \langle pq|l(S_i)|nm \rangle, \qquad (188)$$

$$\langle \tilde{m}\tilde{n}|r(\tilde{S}_i)|\tilde{p}\tilde{q} \rangle_a = 2\langle \tilde{m}\tilde{n}|r(\tilde{S}_i)|\tilde{p}\tilde{q} \rangle - \langle \tilde{m}\tilde{n}|r(\tilde{S}_i)|\tilde{q}\tilde{p} \rangle. \qquad (189)$$

Similarly, by considering all 16 Goldstone diagrams that result from performing an "exchange" operation on each vertex of the diagram of Fig. 15, we find that [34]

$$n_3'(g) = -2[(\langle 1'u \| 1''\tilde{u} \rangle \langle 1''\tilde{c} \| 1'c \rangle_a + \langle 1'u \| \tilde{u}1'' \rangle \langle 1''\tilde{c} \| c1' \rangle_a)$$

$$\times (\langle cd|l(S_i)|uw \rangle \langle \tilde{u}w|r(\tilde{S}_i)|\tilde{c}d \rangle_a + \langle cd|l(S_i)|wu \rangle \langle \tilde{u}w|r(\tilde{S}_i)|d\tilde{c} \rangle_a)$$

$$- 3\langle 1'u \| \tilde{u}1'' \rangle \langle 1''\tilde{c} \| c1' \rangle \langle cd|l(S_i)|wu \rangle \langle \tilde{u}w|r(\tilde{S}_i)|d\tilde{c} \rangle], \qquad (190)$$

$$D_3'(g) = \Delta^X(1'', \tilde{u}, w; 1', c, d). \qquad (191)$$

Clearly, the main difference between $n_4(f)$ and $n_3'(g)$ and their analogues $v_4(f)$ and $v_3'(g)$, Eqs. (132f) and (135g), respectively, lies in an appearance of the orbital coupling coefficients $\langle cd|l(S_i)|uw \rangle$ and $\langle \tilde{u}\tilde{w}|r(\tilde{S}_i)|\tilde{c}\tilde{d} \rangle$ in the former. Thus, to compare the above given formulas for $R_{ij}^{(4)}(f)$ and $R_{ij}^{(3)\prime}(g)$ with those derived earlier using the diagrammatic spin-adaptation procedure of [38], we must perform the summations over the indices c, d, u, w and $\tilde{c}, \tilde{u}$ and remove the non-zero l- and r-matrix elements by applying Eqs. (176) and (178) or Eq. (182) and the symmetry properties (175).

Let us first rewrite expressions for the numerators $n_4(f)$ and $n_3'(g)$, Eqs. (186) and (190), respectively, as follows:

$$n_4(f) = \langle cd|l(S_i)|uw \rangle \langle \tilde{u}w|r(\tilde{S}_i)|\tilde{c}d \rangle$$

$$\times \{[2 - (-1)^{S_i}][2 - (-1)^{\tilde{S}_i}] \langle 1'\tilde{c} \| 1''\tilde{u} \rangle_a \langle 1''u \| 1'c \rangle_a$$

$$+ 3(-1)^{S_i + \tilde{S}_i} \langle 1'\tilde{c} \| \tilde{u}1'' \rangle \langle 1''u \| c1' \rangle \}, \qquad (192)$$

$$n_3'(g) = -2\langle cd|l(S_i)|uw \rangle \langle \tilde{u}w|r(\tilde{S}_i)|\tilde{c}d \rangle$$

$$\times \{[1 + (-1)^{S_i + \tilde{S}_i}][2 - (-1)^{\tilde{S}_i}](\langle 1'u \| 1''\tilde{u} \rangle \langle 1''\tilde{c} \| 1'c \rangle_a$$

$$+ \langle 1'u \| \tilde{u}1'' \rangle \langle 1''\tilde{c} \| c1' \rangle_a) - 3(-1)^{S_i + \tilde{S}_i} \langle 1'u \| \tilde{u}1'' \rangle \langle 1''\tilde{c} \| c1' \rangle \}. \qquad (193)$$

Here we applied the symmetry properties of the l- and r-matrix elements, Eq. (175), and definitions of $\langle pq|l(S_i)|mn \rangle_a$ and $\langle \tilde{m}\tilde{n}|r(\tilde{S}_i)|\tilde{p}\tilde{q} \rangle_a$, Eqs. (188) and (189), respectively. Since the intermediate spin quantum numbers, S_i and $\tilde{S}_i$, assume only two values, 0 or 1, we can write the following relations

$$2 - (-1)^{S_i} = [S_i], \qquad (194)$$

$$2 - (-1)^{\tilde{S}_i} = [\tilde{S}_i], \qquad (195)$$

$$1 + (-1)^{S_i + \tilde{S}_i} = 2\delta_{S_i \tilde{S}_i}. \qquad (196)$$

Consequently, formulas for the numerators $n_4(f)$ and $n'_3(g)$ become

$$n_4(f) = 4[S_i, \tilde{S}_i]^{1/2}\langle cd|l(S_i)|uw\rangle\langle \tilde{u}w|r(\tilde{S}_i)|\tilde{c}d\rangle$$
$$\times \{\tfrac{1}{2}[S_i, \tilde{S}_i]^{1/2}(\langle 1'\tilde{c}\|1''\tilde{u}\rangle\langle 1''u\|1'c\rangle_a - \langle 1'\tilde{c}\|\tilde{u}1''\rangle\langle 1''u\|1'c\rangle)$$
$$+ A(S_i, \tilde{S}_i)\langle 1'\tilde{c}\|\tilde{u}1''\rangle\langle 1''u\|c1'\rangle\}, \tag{197}$$

$$n'_3(g) = -4[S_i, \tilde{S}_i]^{1/2}\langle cd|l(S_i)|uw\rangle\langle \tilde{u}w|r(\tilde{S}_i)|\tilde{c}d\rangle$$
$$\times \{\delta_{S_i \tilde{S}_i}(\langle 1'u\|1''\tilde{u}\rangle\langle 1''\tilde{c}\|1'c\rangle_a - \langle 1'u\|\tilde{u}1''\rangle\langle 1''\tilde{c}\|1'c\rangle)$$
$$+ B(S_i, \tilde{S}_i)\langle 1'u\|\tilde{u}1''\rangle\langle 1''\tilde{c}\|c1'\rangle\}, \tag{198}$$

where

$$A(S_i, \tilde{S}_i) = \tfrac{1}{4}([S_i, \tilde{S}_i]^{1/2} + 3(-1)^{S_i + \tilde{S}_i}[S_i, \tilde{S}_i]^{-1/2}), \tag{199}$$

and

$$B(S_i, \tilde{S}_i) = 2\delta_{S_i \tilde{S}_i} - \tfrac{3}{2}(-1)^{S_i + \tilde{S}_i}[S_i, \tilde{S}_i]^{-1/2}. \tag{200}$$

Now, to get the explicit expressions for $R_{ij}^{(4)}(f)$ and $R_{ij}^{(3)\prime}(g)$ we have to insert Eqs. (197) and (198), respectively, into the right-hand side of Eq. (185) and perform the summations over the orbital indices c, d, u, w, $\tilde{c}$, $\tilde{u}$ and $1'$, $1''$. Since, however, we wish to compare the results of these summations with the formulas given in Sect. 5, we introduce Kronecker delta symbols $\langle w|\tilde{w}\rangle$ and $\langle d|\tilde{d}\rangle$ into Eqs. (197) and (198) and replace the summations over c, d, u, w, $\tilde{c}$ and $\tilde{u}$ by the summations over c, d, u, w and $\tilde{c}$, $\tilde{d}$, $\tilde{u}$, $\tilde{w}$. In this way, we obtain

$$R_{ij}^{(4)}(f) = \sum_{\substack{cduw \\ \tilde{c}\tilde{d}\tilde{u}\tilde{w}}} \sum_{1'1''} N_4(f)[\varepsilon - D_4(f)]^{-1}, \tag{201}$$

$$R_{ij}^{(3)\prime}(g) = \sum_{\substack{cduw \\ \tilde{c}\tilde{d}\tilde{u}\tilde{w}}} \sum_{1'1''} N'_3(g)[\varepsilon - D'_3(g)]^{-1}, \tag{202}$$

where

$$N_4(f) = \langle w|\tilde{w}\rangle\langle d|\tilde{d}\rangle n_4(f), \tag{203}$$

$$N'_3(g) = \langle w|\tilde{w}\rangle\langle d|\tilde{d}\rangle n'_3(g). \tag{204}$$

We can also easily verify that

$$A(S_i, \tilde{S}_i) = \delta_{S_i \tilde{S}_i}, \tag{205}$$

whereas

$$B(S_i, \tilde{S}_i) = \tfrac{1}{2}[S_i, \tilde{S}_i]^{1/2}, \tag{206}$$

for S_i and $\tilde{S}_i$ equal to 0 or 1. Consequently, expressions for the numerators $N_4(f)$ and $N'_3(g)$, Eqs. (203) and (204), respectively, can be given the following form:

$$N_4(f) = 4[S_i, \tilde{S}_i]^{1/2}\langle cd|l(S_i)|uw\rangle\langle \tilde{u}\tilde{w}|r(\tilde{S}_i)|\tilde{c}\tilde{d}\rangle\langle w|\tilde{w}\rangle\langle d|\tilde{d}\rangle$$
$$\times \{\tfrac{1}{2}[S_i, \tilde{S}_i]^{1/2}(\langle 1'\tilde{c}\|1''\tilde{u}\rangle\langle 1''u\|1'c\rangle_a$$
$$- \langle 1'\tilde{c}\|\tilde{u}1''\rangle\langle 1''u\|1'c\rangle) + \delta_{S_i \tilde{S}_i}\langle 1'\tilde{c}\|\tilde{u}1''\rangle\langle 1''u\|c1'\rangle\}, \tag{207}$$

$$N'_3(g) = -4[S_i, \tilde{S}_i]^{1/2}\langle cd|l(S_i)|uw\rangle\langle \tilde{u}\tilde{w}|r(\tilde{S}_i)|\tilde{c}\tilde{d}\rangle\langle w|\tilde{w}\rangle\langle d|\tilde{d}\rangle$$
$$\times \{\delta_{S_i \tilde{S}_i}(\langle 1'u\|1''\tilde{u}\rangle\langle 1''\tilde{c}\|1'c\rangle_a - \langle 1'u\|\tilde{u}1''\rangle\langle 1''\tilde{c}\|1'c\rangle)$$
$$+ \tfrac{1}{2}[S_i, \tilde{S}_i]^{1/2}\langle 1'u\|\tilde{u}1''\rangle\langle 1''\tilde{c}\|c1'\rangle\}. \tag{208}$$

Notice the similarity between the right-hand sides of Eqs. (207) and (208) and the formulas for the numerators $v_4(f)$ and $v'_3(g)$ given in the previous section, Eqs. (132f) and (135g), respectively.

All matrix elements $\langle \tilde{u}\tilde{w}|r(\tilde{S}_i)|\tilde{c}\tilde{d}\rangle$ ($\langle cd|l(S_i)|uw\rangle$) vanish except for those involving the labels $\tilde{r}$, $\tilde{s}$ and $\tilde{a}$, $\tilde{b}$ (a, b and r, s), so that the summation over c, d, u, w and $\tilde{c}$, $\tilde{d}$, $\tilde{u}$, $\tilde{w}$ in both Eq. (201) and Eq. (202) reduces to at most sixteen terms. It also follows from the symmetry properties of the r-matrix elements, Eq. (175), that any matrix element $\langle \tilde{u}\tilde{w}|r(\tilde{S}_i)|\tilde{c}\tilde{d}\rangle$ involving the labels $\tilde{r}$, $\tilde{s}$ and $\tilde{a}$, $\tilde{b}$ can be related to the matrix element $\langle \tilde{r}\tilde{s}|r(\tilde{S}_i)|\tilde{a}\tilde{b}\rangle$. Similarly, every matrix element $\langle cd|l(S_i)|uw\rangle$ involving the labels a, b and r, s differs from $\langle ab|l(S_i)|rs\rangle$ by at most a phase factor $(-1)^{S_i}$. Consequently, expressions for $R_{ij}^{(4)\prime}(f)$ and $R_{ij}^{(3)\prime}(g)$ take the form

$$R_{ij}^{(4)\prime}(f) = 4[S_i, \tilde{S}_i]^{1/2}\langle ab|l(S_i)|rs\rangle\langle \tilde{r}\tilde{s}|r(\tilde{S}_i)|\tilde{a}\tilde{b}\rangle(N_{ab}^{rs}N_{\tilde{a}\tilde{b}}^{\tilde{r}\tilde{s}})^2$$

$$\times \mathscr{S}_{rs}(S_i)\mathscr{S}_{\tilde{r}\tilde{s}}(\tilde{S}_i)\mathscr{S}_{ab}(S_i)\mathscr{S}_{\tilde{a}\tilde{b}}(\tilde{S}_i) \sum_{1'1''} v_4(f)[\varepsilon - \Delta_4(f)]^{-1}, \qquad (209)$$

$$R_{ij}^{(3)\prime}(g) = 4[S_i, \tilde{S}_i]^{1/2}\langle ab|l(S_i)|rs\rangle\langle \tilde{r}\tilde{s}|r(\tilde{S}_i)|\tilde{a}\tilde{b}\rangle(N_{ab}^{rs}N_{\tilde{a}\tilde{b}}^{\tilde{r}\tilde{s}})^2$$

$$\times \mathscr{S}_{rs}(S_i)\mathscr{S}_{\tilde{r}\tilde{s}}(\tilde{S}_i)\mathscr{S}_{ab}(S_i)\mathscr{S}_{\tilde{a}\tilde{b}}(\tilde{S}_i) \sum_{1'1''} v'_3(g)[\varepsilon - \Delta'_3(g)]^{-1}, \qquad (210)$$

where the numerators $v_4(f)$ and $v'_3(g)$ are given by Eqs. (132f) and (135g), respectively, and the denominators $\Delta_4(f)$ and $\Delta'_3(f)$ by Eqs. (133f) and (137g), respectively. The product of the (anti)symmetrizers, $\mathscr{S}_{rs}(S_i)\mathscr{S}_{\tilde{r}\tilde{s}}(\tilde{S}_i) \times \mathscr{S}_{ab}(S_i)\mathscr{S}_{\tilde{a}\tilde{b}}(\tilde{S}_i)$, produces 16 terms, when acting on $\sum_{1'1''} v_4(f)[\varepsilon - \Delta_4(f)]^{-1}$ or $\sum_{1'1''} v'_3(g)[\varepsilon - \Delta'_3(g)]^{-1}$. To eliminate repetitions of identical terms in case the hole (a and b or $\tilde{a}$ and $\tilde{b}$) and/or particle (r and s or $\tilde{r}$ and $\tilde{s}$) labels are equal, we have introduced the factor $(N_{ab}^{rs}N_{\tilde{a}\tilde{b}}^{\tilde{r}\tilde{s}})^2 = [(1 + \delta_{ab})(1 + \delta_{rs})(1 + \delta_{\tilde{a}\tilde{b}})(1 + \delta_{\tilde{r}\tilde{s}})]^{-1}$. One can easily verify that (see Eq. (176))

$$4[S_i, \tilde{S}_i]^{1/2}\langle ab|l(S_i)|rs\rangle\langle \tilde{r}\tilde{s}|r(\tilde{S}_i)|\tilde{a}\tilde{b}\rangle(N_{ab}^{rs}N_{\tilde{a}\tilde{b}}^{\tilde{r}\tilde{s}})^2 = N_{ab}^{rs}N_{\tilde{a}\tilde{b}}^{\tilde{r}\tilde{s}}. \qquad (211)$$

Thus, Eqs. (209) and (210) are identical with the expressions for $R_{ij}^{(4)\prime}(f)$ and $R_{ij}^{(3)\prime}(g)$ given in Sect. 5.

In a similar way, we can transform the remaining expressions for $R_{ij}^{(k)\prime}(x)$ given in [34] into the formulas derived in the previous section. We thus see that the relationship between the results of both spin-adaptation approaches ([34] and [38]) is rather simple, particularly in view of their different nature. Let us summarize the transformation procedure that we have just performed. First, we carry out the summations over all the orbital labels that appear in l- and r-matrix elements. Then, the remaining non-vanishing l- and r-matrix elements have to be removed by applying Eqs. (176) and (178) as well as the symmetry properties (175). In order to introduce the spin factors, which result from angular momentum theory, we must additionally apply relations of type (194) – (196) and (205) and (206). We see (cf. Eqs. (185) – (187), (190), (191) and their counterparts in Sect. 5) that the above operations introduce essential simplifications into the resulting expressions for $R_{ij}^{(k)\prime}(x)$. Indeed, summations over the labels carried by the lines leaving and entering Goldstone interaction vertices $L_{ab}^{rs}(S_i)$ and $R_{\tilde{a}\tilde{b}}^{\tilde{r}\tilde{s}}(\tilde{S}_i)$ disappear, the orbital coupling coefficients $\langle cd|l(S_i)|uw\rangle$ and $\langle \tilde{u}\tilde{w}|r(\tilde{S}_i)|\tilde{c}\tilde{d}\rangle$ are replaced by very simple normalization and spin factors, and expressions, which are formally quartic in different types of orbital matrix elements, become simple bilinear forms in v-matrix elements. The price that we

have to pay for these simplifications is very small, namely the introduction of the "symmetry forcing" projectors $\mathscr{P}_k(x)$.

The spin-adaptation procedure that was exploited in [34] is undoubtedly much simpler than the method of [38]. Spin diagrams are not constructed, so that the graphical techniques of spin algebras can be replaced by much simpler and standard diagrammatic spin-free formalism. However, the normalization and spin coupling coefficients do not appear in an explicit form but rather in an implicit way as the l- and r-matrix elements. Consequently, approach [34] yields more complicated expressions. Moreover, the number of orbital diagrams, which have to be explicitly considered, is much larger when using the technique of [34]. For example, in the case of the contributions $R_{ij}^{(4)}(f)$ or $R_{ij}^{(3)'}(g)$, we have to draw and evaluate 16 distinct Goldstone diagrams instead of 4 Goldstone–Brandow diagrams shown in Figs. 7f and 8g, respectively. This drawback of the approach [34] is of course connected with the fact that both interaction and excitation vertices are represented in Goldstone form. Finally, an incorporation of higher than double excitations into the spin-adaptation formalism [34] would be rather complicated. Spin-adaptation procedures based on the graphical techniques of spin algebras employing either bare [38] or spin-adapted [106, 107] interaction vertices are free from the above shortcomings. For example, higher excitations can be incorporated into these formalisms at the same level of complexity as double excitations [39].

The above discussion implies that an application of the diagrammatic spin-adaptation approach of [38], which was originally elaborated in the context of the CC theory, yields the simplest structure of explicit expressions for the effective interaction matrix elements $W_{ij}^{(k)X}(\varepsilon)$. The use of spin-adapted interaction vertices in diagrams and the (anti)symmetrized v-matrix elements in formulas or orbital normalization and coupling l- and r-coefficients and spin-free formalism make the expressions for $W_{ij}^{(k)X}(\varepsilon)$ unnecessarily complicated. The orthogonally spin-adapted equations given in Sect. 5 are extremely compact, particularly when we realize that the effective interaction matrix elements are not trivial quantities and that their evaluation is rather demanding. Most importantly, expressions derived in Sect. 5 are not only formally appealing but also computationally advantageous. For these reasons, they were used in actual calculations reported in Parts II and III of this series, where the orthogonally spin-adapted formulations of the CC methods, CCDT-1, CCD + T(CCD) and ACPTQ, as well as the OIP technique are implemented and applied to the PPP π-electron model of cyclic polyenes.

Appendix: Diagrammatic derivation of the explicit expressions for the matrix elements $_{S_i}\left\langle \begin{matrix} r & s \\ a & b \end{matrix} \middle| G_N \middle| \begin{matrix} \tilde{r} & \tilde{s} \\ \tilde{a} & \tilde{b} \end{matrix} \right\rangle_{S_i}$, $\left\langle \Phi_0 \middle| V_N \middle| \begin{matrix} \tilde{r} & \tilde{s} \\ \tilde{a} & \tilde{b} \end{matrix} \right\rangle_{S_i}$ and $_{S_i}\left\langle \begin{matrix} r & s \\ a & b \end{matrix} \middle| V_N \middle| \begin{matrix} \tilde{r} & \tilde{s} \\ \tilde{a} & \tilde{b} \end{matrix} \right\rangle_{S_i}$

General formulas for matrix elements of arbitrary one- and two-electron operators in the normal product form between the ground state and orthogonally spin-adapted pp-hh coupled biexcited singlet states as well as between the orthogonally spin-adapted doubly excited configurations themselves were, in fact, already given as early as in 1966 by Čížek [43]. Although the derivation of these expressions was to a large extent accomplished by exploiting the time

independent diagrammatic techniques based on the second quantization formalism and Wick's theorem [8, 51, 52], the spin-adaptation and the subsequent derivation of matrix elements between spin symmetry adapted configurations was carried out algebraically. The same matrix elements were considered once more by Paldus et al. [44]. It was shown that the time independent diagrammatic techniques [8, 51, 52] may be conveniently combined with the graphical methods of spin algebras [22, 80, 81], so that both the orbital factors and the associated spin coupling coefficients can be found in a straightforward, purely graphical, manner. However, in order to get the pertinent orbital factors, a Goldstone representation was assumed for both one- and two-electron vertices and biexcited configurations. Consequently, a considerable number of resulting orbital diagrams (4, 2 and 12 for the matrix elements considered [44]) had to be explicitly drawn giving, after their evaluation, numerous terms having common spin coefficient. Additional algebraic manipulations had to be carried out in order to write the final formulas in a concise form. We shall now show that the desired

expressions   for $\displaystyle {}_{S_i}\!\left\langle \begin{matrix} r & s \\ a & b \end{matrix} \middle| G_N \middle| \begin{matrix} \tilde{r} & \tilde{s} \\ \tilde{a} & \tilde{b} \end{matrix} \right\rangle_{\!S_i}$, $\displaystyle \left\langle \Phi_0 \middle| V_N \middle| \begin{matrix} \tilde{r} & \tilde{s} \\ \tilde{a} & \tilde{b} \end{matrix} \right\rangle_{\!S_i}$,   and

$\displaystyle {}_{S_i}\!\left\langle \begin{matrix} r & s \\ a & b \end{matrix} \middle| V_N \middle| \begin{matrix} \tilde{r} & \tilde{s} \\ \tilde{a} & \tilde{b} \end{matrix} \right\rangle_{\!S_i}$ can be obtained in a much simpler manner using the

diagrammatic spin-adaptation procedure of [38]. Although this procedure, as briefly outlined in Sect. 2, still employs the Goldstone form for one-electron (G_N) and two-electron (V_N) vertices, Fig. 1a and b, respectively, it uses the Hugenholtz (Brandow) form to represent bra and ket orthogonally spin-adapted doubly excited states (see Fig. 1e and c, respectively). Consequently, the number of the resulting orbital diagrams is considerably smaller.

   Let us start, for example, with the matrix element $\displaystyle {}_{S_i}\!\left\langle \begin{matrix} r & s \\ a & b \end{matrix} \middle| G_N \middle| \begin{matrix} \tilde{r} & \tilde{s} \\ \tilde{a} & \tilde{b} \end{matrix} \right\rangle_{\!S_i}$,

where G_N is a one-body operator. Applying a concise notation for the distinct labeling schemes carried by external lines, which employs symmetrizers $\mathcal{S}_{ab}(\mathcal{S}_{\tilde{a}\tilde{b}})$ and $\mathcal{S}_{rs}(\mathcal{S}_{\tilde{r}\tilde{s}})$ [40] (cf., Sect. 2), we must explicitly draw only two Goldstone–Brandow diagrams shown in Fig. 16 (as in Sects. 5 and 6, Brandow vertices representing both bra and ket configurations given in Fig. 1e and c, respectively, are not explicitly drawn). Evaluating orbital and spin factors corresponding to diagrams in Fig. 16a,b, in which symmetrizers $\mathcal{S}_{ab}$, $\mathcal{S}_{\tilde{a}\tilde{b}}$, $\mathcal{S}_{rs}$ and $\mathcal{S}_{\tilde{r}\tilde{s}}$ are ignored, and making use of the fact that there is a one-to-one correspondence between the operators $\mathcal{S}_{ab}$, $\mathcal{S}_{\tilde{a}\tilde{b}}$, $\mathcal{S}_{rs}$ and $\mathcal{S}_{\tilde{r}\tilde{s}}$ in diagrams and (anti)symmetrizers
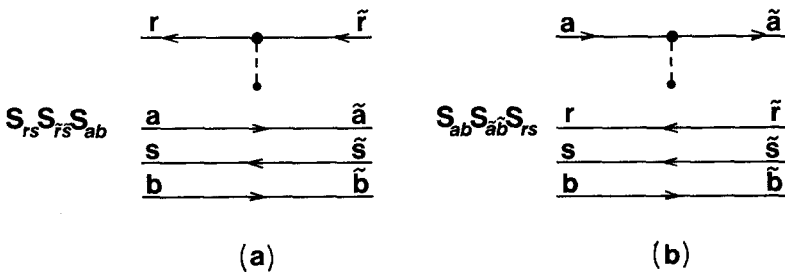

Fig. 16. Goldstone–Brandow orbital diagrams associated with successive terms on the right-hand side of Eq. (A2)

$\mathscr{S}_{ab}(S_i)$, $\mathscr{S}_{\tilde{a}\tilde{b}}(\tilde{S}_i)$, $\mathscr{S}_{rs}(S_i)$ and $\mathscr{S}_{\tilde{r}\tilde{s}}(\tilde{S}_i)$ in associated algebraic expressions, we find that

$$G_{ij} \equiv \langle \Phi_i | G_N | \Phi_j \rangle = \left\langle \begin{matrix} r & s \\ a & b \end{matrix} \middle| G_N \middle| \begin{matrix} \tilde{r} & \tilde{s} \\ \tilde{a} & \tilde{b} \end{matrix} \right\rangle_{S_i}, \tag{A1}$$

can be written as

$$G_{ij} = G_{ij}(a) + G_{ij}(b), \tag{A2}$$

where

$$G_{ij}(a) = N_{ab}^{rs} N_{\tilde{a}\tilde{b}}^{\tilde{r}\tilde{s}} \delta_{S_i \tilde{S}_i} \mathscr{S}_{ab}(S_i) \langle a|\tilde{a} \rangle \langle b|\tilde{b} \rangle \mathscr{S}_{rs}(S_i) \mathscr{S}_{\tilde{r}\tilde{s}}(S_i) \langle r|g|\tilde{r} \rangle \langle s|\tilde{s} \rangle, \tag{A3}$$

$$G_{ij}(b) = - N_{ab}^{rs} N_{\tilde{a}\tilde{b}}^{\tilde{r}\tilde{s}} \delta_{S_i \tilde{S}_i} \mathscr{S}_{rs}(S_i) \langle r|\tilde{r} \rangle \langle s|\tilde{s} \rangle \mathscr{S}_{ab}(S_i) \mathscr{S}_{\tilde{a}\tilde{b}}(S_i) \langle \tilde{a}|g|a \rangle \langle b|\tilde{b} \rangle, \tag{A4}$$

are the expressions corresponding to Fig. 16a and b, respectively. This is the desired result [43, 44], which we used in Sect. 4 (see Eq. (110)). Instead of 4 Goldstone diagrams given in [44], only 2 diagrams are needed when Goldstone–Brandow representation is employed.

The advantages of the latter representation are even bigger when considering matrix elements

$$V_{ij} = \langle \Phi_i | V_N | \Phi_j \rangle. \tag{A5}$$

In this case, instead of 12 Goldstone orbital diagrams [44], only 4 Goldstone–Brandow diagrams, shown in Fig. 17, are needed. All of them result from one nonoriented Hugenholtz skeleton, which is schematically illustrated in Fig. 18.
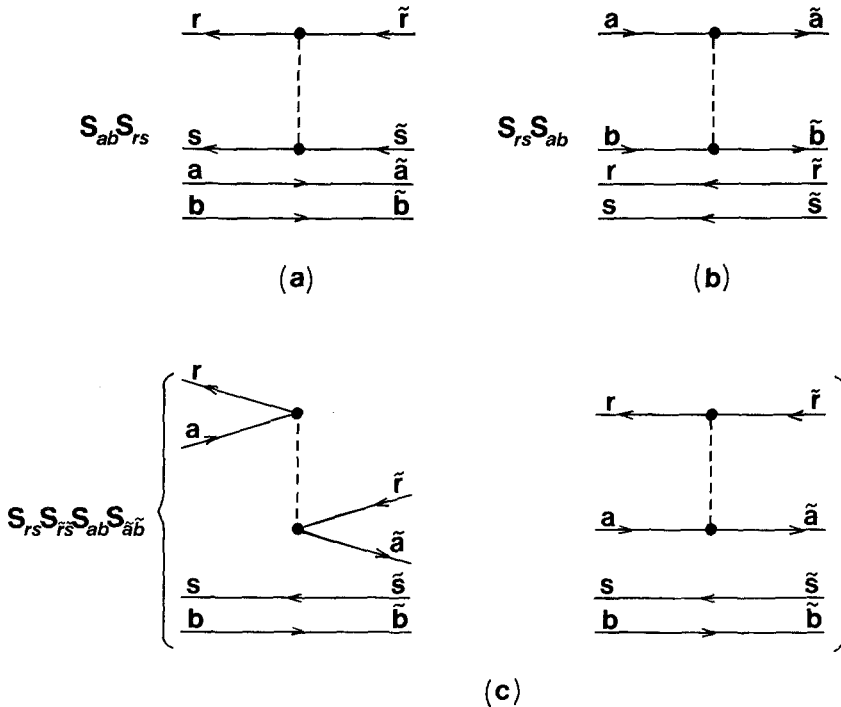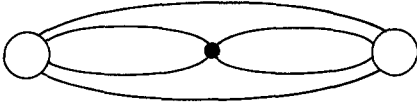

Fig. 17. Goldstone–Brandow orbital diagrams corresponding to successive terms on the right-hand side of Eq. (A6)

Fig. 18. The only arrowless Hugenholtz skeleton corresponding to Eq. (A5). As usual, the *small solid circle* represents the nonoriented Hugenholtz V_N vertex. Both bra and ket biexcited configurations are represented by *large open circles*. All Goldstone–Brandow diagrams of Fig. 17 can be obtained from the above skeleton in the usual way by introducing the orientation of lines, replacing Hugenholtz V_N vertex by the Goldstone one and by labeling the excitation vertices and oriented fermion lines with appropriate indices specifying configurations ${}_{S_i}\!\left\langle\begin{array}{cc} r & s \\ a & b \end{array}\right|$ and $\left.\left|\begin{array}{cc} \tilde{r} & \tilde{s} \\ \tilde{a} & \tilde{b} \end{array}\right\rangle_{S_i}$

The third and fourth diagrams in Fig. 17 are grouped together, since they are two distinct Goldstone–Brandow representatives associated with one oriented (particle-hole type) Hugenholtz skeleton. Applying the general rules of the diagrammatic approach of [38], we obtain

$$V_{ij} = V_{ij}(a) + V_{ij}(b) + V_{ij}(c), \tag{A6}$$

where

$$V_{ij}(a) = N_{ab}^{rs} N_{\tilde{a}\tilde{b}}^{\tilde{r}\tilde{s}} \delta_{S_i \tilde{S}_i} A_{ab}^{\tilde{a}\tilde{b}}(S_i) \langle rs \| \tilde{r}\tilde{s} \rangle_{S_i}, \tag{A7}$$

$$V_{ij}(b) = N_{ab}^{rs} N_{\tilde{a}\tilde{b}}^{\tilde{r}\tilde{s}} \delta_{S_i \tilde{S}_i} A_{rs}^{\tilde{r}\tilde{s}}(S_i) \langle \tilde{a}\tilde{b} \| ab \rangle_{S_i}, \tag{A8}$$

$$V_{ij}(c) = N_{ab}^{rs} N_{\tilde{a}\tilde{b}}^{\tilde{r}\tilde{s}} \mathscr{S}_{rs}(S_i) \mathscr{S}_{\tilde{r}\tilde{s}}(\tilde{S}_i) \mathscr{S}_{ab}(S_i) \mathscr{S}_{\tilde{a}\tilde{b}}(\tilde{S}_i) \langle s|\tilde{s} \rangle \langle b|\tilde{b} \rangle$$
$$\times \{\tfrac{1}{2}[S_i, \tilde{S}_i]^{1/2} \langle r\tilde{a} \| a\tilde{r} \rangle - \delta_{S_i \tilde{S}_i} \langle r\tilde{a} \| \tilde{r}a \rangle\}, \tag{A9}$$

are the algebraic expressions corresponding to Fig. 17a, b and c, respectively, and the quantities $A_{ab}^{\tilde{a}\tilde{b}}(S_i)$ and $A_{rs}^{\tilde{r}\tilde{s}}(S_i)$ are defined by Eq. (111). An identical result is given in [43, 44] (except for a different phase convention used in [43, 44] which gives an additional phase factor $(-1)^{S_i + \tilde{S}_i}$; cf., Sect. 2).

Equation (A6) together with Eqs. (A7)–(A9) are needed to calculate matrix elements $\mathscr{V}_{ij}$ and $W_{ij}^{(2)}(\varepsilon)$ appearing in the OIP formalism, when the PPP model is examined (see Sect. 4). Matrix elements $\left\langle \Phi_0 \left| V_N \right| \begin{array}{cc} \tilde{r} & \tilde{s} \\ \tilde{a} & \tilde{b} \end{array}\right\rangle_{S_i}$ are also required (cf., Eq. (108)). However, these already appear in the orthogonally spin-adapted form of the CCD equations, Sect. 2, as the quantities (cf., Eq. (27))

$$A^{(0)}(rs, ab; S_i) = (N_{ab}^{rs})^{-1} {}_{S_i}\!\left\langle \begin{array}{cc} r & s \\ a & b \end{array} \right| H_N \left| \Phi_0 \right\rangle = (N_{ab}^{rs})^{-1} {}_{S_i}\!\left\langle \begin{array}{cc} r & s \\ a & b \end{array} \right| V_N \left| \Phi_0 \right\rangle. \tag{A10}$$

Therefore (see Eq. (28)),

$$\left\langle \Phi_0 \left| V_N \right| \begin{array}{cc} \tilde{r} & \tilde{s} \\ \tilde{a} & \tilde{b} \end{array}\right\rangle_{S_i} = N_{\tilde{a}\tilde{b}}^{\tilde{r}\tilde{s}} A^{(0)}(\tilde{r}\tilde{s}, \tilde{a}\tilde{b}; \tilde{S}_i)^* = N_{\tilde{a}\tilde{b}}^{\tilde{r}\tilde{s}}[\tilde{S}_i]^{1/2} \langle \tilde{a}\tilde{b} \| \tilde{r}\tilde{s} \rangle_{S_i}, \tag{A11}$$

which is the desired result [43, 44]. Goldstone–Brandow orbital diagram corresponding to Eq. (A10) is shown in Fig. 2. Obviously, the diagram associated with expression (A11) is conjugate to diagram 2 and carries labels $\tilde{r}$, $\tilde{s}$, $\tilde{a}$ and $\tilde{b}$.

The main aim of this Appendix was to show that the results of [43] and [44] are easily reproduced by constructing the pertinent Goldstone–Brandow diagrams, which are fewer in number than the corresponding Goldstone diagrams, and evaluating them using the procedure of [38]. Further reduction in the

number of resulting diagrams is achieved when a Hugenholtz representation is employed for all vertices and the spin adaptation procedure of [106] and [107] is applied. In the cases examined here, this reduction (from four to three diagrams) occurs only for $\langle \Phi_i | V_N | \Phi_j \rangle$ elements (two diagrams of Fig. 17c are replaced by one). However, the price we have to pay for this minor reduction is the appearance of the nontrivial 9-j symbol C, Eq. (32), in the expression for $V_{ij}(c)$, since, in contrast to bare interaction vertices, spin-adapted interaction vertices enter the resulting spin diagrams. We obtain

$$V_{ij}(c) = N_{ab}^{rs} N_{\tilde{a}\tilde{b}}^{\tilde{r}\tilde{s}} [S_i, \tilde{S}_i]^{1/2} \mathscr{S}_{rs}(S_i) \mathscr{S}_{\tilde{r}\tilde{s}}(\tilde{S}_i) \mathscr{S}_{ab}(S_i) \mathscr{S}_{\tilde{a}\tilde{b}}(\tilde{S}_i)$$

$$\times \langle s | \tilde{s} \rangle \langle b | \tilde{b} \rangle \sum_S [S] C(S_i, \tilde{S}_i, S) \langle r\tilde{a} \| a\tilde{r} \rangle_S. \qquad (A12)$$

We thus see that the result for V_{ij} becomes unnecessarily complicated (cf., Sect. 6 and discussion in [40]). We can, of course, show that Eqs. (A9) and (A12) are equivalent by applying the sum rules (158) and (159) as it was done in Sect. 6 or in [40].

References

1. Brueckner KA (1955) Phys Rev 100:36; Goldstone J (1957) Proc Roy Soc London A239:267
2. Bartlett RJ, Purvis GD (1978) Int J Quantum Chem 14:561
3. Primas H (1965) Separability in many-electron systems. In: Sinanoğlu O (ed) Modern quantum chemistry, vol. 2. Academic Press, New York, pp 45–74
4. Gell-Mann M, Brueckner K (1957) Phys Rev 106:364; Quinn JJ, Ferrell RA (1958) Phys Rev 112:812
5. de Shalit A, Feshbach H (1974) Theoretical nuclear physics, vol. 1. Nuclear structure, chap. 3. Wiley, New York; Eisenberg JM, Greiner W (1972) Nuclear theory, vol. 3. Microscopic theory of nucleus, chap 4. North-Holland, Amsterdam
6. Hubbard J (1957) Proc Roy Soc London A240:539; idem (1958) ibid A243:336, A244:199
7. Coester F (1958) Nucl Phys 7: 421; Coester F, Kümmel H (1960) ibid 17:477
8. (a) Čížek J (1966) J Chem Phys 45:4256; (b) idem (1969) Advan Chem Phys 14:35
9. Kümmel H, Lührmann KH, Zabolitzky JG (1978) Phys Rep C36:1
10. Čížek J, Paldus J (1980) Phys Scr 21:251
11. Bartlett RJ (1981) Annu Rev Phys Chem 32:359
12. Kvasnička V, Laurinc V, Biskupič S (1982) Phys Rep C90:159; Kvasnička V, Laurinc V, Biskupič S, Haring M (1983) Advan Chem Phys 52:181
13. Paldus J (1983) Coupled cluster approaches to many-electron correlation problem. In: Löwdin PO, Pullman B (eds) New horizons of quantum chemistry. Reidel, Dordrecht, pp 31–60
14. Bartlett RJ, Dykstra CE, Paldus J (1984) Coupled cluster methods for molecular calculations. In: Dykstra CE (ed) Advanced theories and computational approaches to the electronic structure of molecules. Reidel, Dordrecht, pp 127–159
15. Hoffmann MR, Schaefer III HF (1986) Advan Quantum Chem 18:207
16. Kucharski SA, Bartlett RJ (1986) Advan Quantum Chem 18:281
17. Jankowski K (1987) Electron correlation in atoms. In: Wilson S (ed) Methods in computational chemistry, vol. 1. Plenum Press, New York, pp 1–116

18. Urban M, Černušák I, Kellö V, Noga J (1987) Electron correlation in molecules. In: Wilson S (ed) Methods in computational chemistry, vol. 1. Plenum Press, New York, pp 117–250
19. Bartlett RJ (1989) J Phys Chem 93:1697
20. Hurley AC (1976) Electron correlation in small molecules. Academic Press, New York
21. Jorgensen P, Simons J (1981) Second quantization based methods in quantum chemistry. Academic Press, New York
22. Lindgren I, Morrison J (1982) Atomic many-body theory. Springer, Berlin Heidelberg New York
23. Wilson S (1984) Electron correlation in molecules. Clarendon Press, Oxford
24. Paldus J, Čížek J, Shavitt I (1972) Phys Rev A5:50
25. Noga J, Bartlett RJ (1987) J Chem Phys 86:7041; idem (1988) ibid 89:3401 (E)
26. Scuseria GE, Schaefer III HF (1988) Chem Phys Lett 152:382
27. Urban M, Noga J, Cole SJ, Bartlett RJ (1985) J Chem Phys 83:4041
28. Raghavachari K (1985) J Chem Phys 82:4607
29. Lee YS, Bartlett RJ (1984) J Chem Phys 80:4371; Lee YS, Kucharski SA, Bartlett RJ (1984) J Chem Phys 81:5906; idem (1985) ibid 82:5761 (E)
30. Čížek J, Vinette F, Paldus J (1990) Int J Quantum Chem, in press
31. Čížek J, Vrscay ER (1985) Int J Quantum Chem 28:665
32. Čížek J, Vrscay ER (1986) Int J Quantum Chem S20:65; Vinette F, Čížek J, Vrscay ER (1987) Int J Quantum Chem 32:663; idem (1988) Compt Rend Acad Sci Paris, Sér. II 306:21; Čížek J, Vinette F, Vrscay ER (1987) Int J Quantum Chem S21:757
33. Čížek J, Vinette F (1988) Coll Czech Chem Commun 53:1910; idem (1988) Chem Phys Lett 149:516
34. Čížek J, Vinette F, Paldus J (1989) Diagrammatic approach to the calculation of the lower bounds using optimized inner projection technique. Application to the cyclic polyene model. In: Kaldor U (ed) Many-body methods in quantum chemistry. (Lect Notes Chem, vol. 52) Springer, Berlin Heidelberg New York, pp 23–42
35. (a) Paldus J, Takahashi M, Cho RWH (1984) Phys Rev B30:4267; (b) Int J Quantum Chem S18:237
36. Takahashi M, Paldus J (1985) Phys Rev B31:5121
37. Paldus J, Čížek J, Takahashi M (1984) Phys Rev A30:2193
38. Paldus J (1977) J Chem Phys 67:303
39. Adams BG, Paldus J (1979) Phys Rev A20:1
40. Piecuch P, Paldus J (1989) Int J Quantum Chem 36:429
41. Geertsen J, Oddershede J (1986) J Chem Phys 85:2112
42. Geertsen J (1990) Advan Quantum Chem 20, in press
43. Čížek J (1966) Theor Chim Acta 6:292
44. Paldus J, Adams BG, Čížek J (1977) Int J Quantum Chem 11:813
45. Takahashi M, Paldus J (1986) J Chem Phys 85:1486
46. Paldus J, Wormer PES, Visser F, van der Avoird A (1982) J Chem Phys 76:2458
47. Adams BG, Jankowski K, Paldus J (1981) Phys Rev A24:2316, 2330
48. Chiles RA, Dykstra CE (1981) J Chem Phys 74:4544
49. Pauncz R, de Heer J, Löwdin P-O (1962) J Chem Phys 36:2247, 2257; de Heer J, Pauncz R (1960) J Mol Spectrosc 5:326; Pauncz R (1967) Alternant molecular orbital method. Saunders, Philadelphia
50. Parr RG (1963) The quantum theory of molecular electronic structure. Benjamin, New York
51. Paldus J, Čížek J (1975) Advan Quantum Chem 9:105
52. Paldus J (1981) Diagrammatic methods for many-fermion systems. University of Nijmegen, Holland (Lecture notes)
53. Paldus J (1976) Many electron correlation problem. A group theoretical approach. In: Eyring H, Henderson DJ (eds) Theoretical chemistry: advances and perspectives, vol. 2. Academic Press, New York, pp 131–190
54. Čížek J, Paldus J (1971) Int J Quantum Chem 5:359
55. Paldus J, Čížek J, Jeziorski B (1989) J Chem Phys 90:356
56. Purvis GD, Bartlett RJ (1982) J Chem Phys 76:1910
57. Scuseria GE, Janssen CL, Schaefer III HF (1988) J Chem Phys 89:7382

58. Laidig WD, Purvis GD, Bartlett RJ (1982) Int J Quantum Chem S16:561; idem (1983) Chem Phys Lett 97:209
59. Pople JA, Krishnan R, Schlegel HB, Binkley JS (1978) Int J Quantum Chem 14:545
60. Taylor PR, Backsay GB, Hurley AC, Hush NS (1978) J Chem Phys 69:1971
61. Paldus J, Boyle MJ (1982) Int J Quantum Chem 22:1281
62. Jankowski K, Paldus J (1980) Int J Quantum Chem 18:1243
63. Jankowski K, Meissner L, Wasilewski J (1985) Int J Quantum Chem 28:931
64. Paldus J, Wormer PES, Bénard M (1988) Coll Czech Chem Commun 53:1919
65. Bartlett RJ, Kucharski SA, Noga J, Watts JD, Trucks GW (1989) Some consideration of alternative ansätz in coupled-cluster theory. In: Kaldor U (ed) Many-body methods in quantum chemistry. (Lect Notes Chem, vol. 52) Springer, Berlin Heidelberg New York, pp 125–149; Kucharski SA, Bartlett RJ (1989) Chem Phys Lett 158:550 and references therein
66. Mukherjee D, Moitra RK, Mukhopadhyay A (1977) Mol Phys 33:955
67. Lindgren I (1978) Int J Quantum Chem S12:33
68. Mukherjee D (1979) Pramana 12:203; Haque MA, Mukherjee D (1984) J Chem Phys 80:5058
69. Jeziorski B, Monkhorst HJ (1981) Phys Rev A24:1668
70. Haque A, Kaldor U (1985) Chem Phys Lett 117:347, 120:261; idem (1986) Int J Quantum Chem 29:425; Kaldor U (1987) J Chem Phys 87:467
71. Laidig WD, Bartlett RJ (1984) Chem Phys Lett 104:424
72. Stolarczyk L, Monkhorst HJ (1985) Phys Rev A32:725,743; idem (1988) ibid 37:1908, 1926
73. Laidig WD, Saxe P, Bartlett RJ (1987) J Chem Phys 86:887
74. Lindgren I, Mukherjee D (1987) Phys Rep 151:93
75. Jeziorski B, Paldus J (1988) J Chem Phys 88:5673
76. Paldus J, Pylypow L, Jeziorski B (1989) Spin-adapted multi-reference coupled cluster formalism including non-linear terms and its application to the H_4 model system. In: Kaldor U (ed) Many-body methods in quantum chemistry. (Lect Notes Chem, vol. 52) Springer, Berlin Heidelberg New York, pp 151–170
77. Meissner L, Jankowski K, Wasilewski J (1988) Int J Quantum Chem 34:535
78. Meissner L, Kucharski SA, Bartlett RJ (1989) J Chem Phys 91:6187
79. Brandow BH (1967) Rev Mod Phys 39:771
80. Jucys AP, Levinson IB, Vanagas VV (1960) Mathematical apparatus of the theory of angular momentum. Institute of Physics and Mathematics of the Academy of Sciences of the Lithuanian S.S.R, Mintis, Vilnius (in Russian); English translations: (1962) Israel Program for Scientific Translations, Jerusalem; (1964) Gordon and Breach, New York; Jucys AP, Bandzaitis AA (1977) The theory of angular momentum in quantum mechanics, 2nd edn. Mokslas, Vilnius (in Russian); Brink DM, Satchler GR (1968) Angular momentum, 2nd edn. Clarendon Press, Oxford
81. El Baz E, Castel B (1972) Graphical methods of spin algebras in atomic, nuclear and particle physics. Marcel Dekker, New York
82. Paldus J, Wormer PES (1979) Int J Quantum Chem 16:1321
83. (a) Wilson S, Jankowski K, Paldus J (1983) Int J Quantum Chem 23:1781; (b) idem (1985) ibid 28:525
84. Chiles RA, Dykstra CE (1981) Chem Phys Lett 80:69; Bachrach SM, Chiles RA, Dykstra CE (1981) J Chem Phys 75:2270
85. Čížek J, Paldus J (1967) J Chem Phys 47: 3976; idem (1971) Phys Rev A3:525; Paldus J, Čížek J (1970) ibid A2:2268
86. Noga J, Bartlett RJ, Urban M (1987) Chem Phys Lett 134:126
87. Noga J, Kellö V, Urban M (1985) COMENIUS/2, Technical report. Comenius University, Bratislava
88. Cole SJ, Purvis III GD, Bartlett RJ (1985) Chem Phys Lett 113:271
89. Magers DH, Harrison RJ, Bartlett RJ (1986) J Chem Phys 84:3284
90. Urban M, Kellö V, Černušák I, Noga J, Diercksen GHF (1987) Chem Phys Lett 135:346
91. (a) Sosa C, Noga J, Bartlett RJ (1988) J Chem Phys 88:5974; (b) Stanton JF, Bartlett RJ, Magers DH, Lipscomb WN (1989) Chem Phys Lett 163:333; Stanton JF, Lipscomb WN, Magers DH, Bartlett RJ (1989) J Chem Phys 90:1077; Magers DH, Lipscomb WN, Bartlett RJ, Stanton JF (1989) J Chem Phys 91:1945

 92. Martin JML, François JP, Gijbels R (1989) Chem Phys Lett 157:217; 163:387
 93. Reid CE (1976) Lower bounds to energy eigenvalues. In: Calais J-L, Goscinski O, Linderberg J, Öhrn Y (eds) Quantum science, methods and structure. A tribute to Per-Olov Löwdin. Plenum Press, New York, pp 315–347
 94. Weinstein A (1937) Mém Sci Math, fasc. 88; Weinstein A, Stenger W (1972) Methods of intermediate problems for eigenvalues: theory and ramifications. Academic Press, New York
 95. Aronszajn N (1951) Approximation methods for eigenvalues of completely continuous symmetric operators. Proceedings of the Oklahoma symposium on spectral theory and differential problems. Stillwater, Oklahoma, pp 179–202
 96. Bazley NW (1959) Proc Natl Acad Sci 45:850; (1960) Phys Rev 120:144; (1961) J Math Mech 10:289
 97. Bazley NW, Fox DW (1961) J Res Natl Bur Std U.S. 65B:105; Phys Rev 124:483; (1962) J Math Phys 3:469; Arch Ratl Mech Anal 10:352; (1963) J Math Phys 4:1147; Rev Mod Phys 35:712
 98. Löwdin P-O (1962) J Math Phys 3:969; (1963) J Mol Spectr 10:12; (1965) J Math Phys 6:1341
 99. Löwdin P-O (1968) Int J Quantum Chem 2:867; (1966) The calculation of upper and lower bounds of energy eigenvalues in perturbation theory by means of partitioning techniques. In: Wilcox CH (ed) Perturbation theory and its applications in quantum mechanics. Wiley, New York, pp 255–294; Löwdin P-O, Goscinski O (1971) Int J Quantum Chem 5:685
100. Löwdin P-O (1982) Int J Quantum Chem 21:69
101. Löwdin P-O (1965) Phys Rev 139:A357; J Chem Phys 43:S175
102. Bunge CF, Bunge A (1965) J Chem Phys 43: S194; Choi JH, Smith DW (1965) ibid 43:S189; idem (1966) ibid 45:4425; Reid CE (1965) ibid 43:S186; Goscinski O (1967) Int J Quantum Chem 1:769; Choi JH (1969) J Math Phys 10:2142.
103. Micha DA, Brändas E (1971) J Chem Phys 55:4792; Brändas E, Bartlett RJ (1970) Chem Phys Lett 8:153; idem (1972) J Chem Phys 56:5467; Brändas E, Micha DA (1972) J Math Phys 13:155
104. Löwdin P-O (1956) Advan Phys 5:1
105. Löwdin P-O (1970) Advan Quantum Chem 5:185
106. Mukherjee D, Bhattacharya D (1977) Mol Phys 34:773
107. Mukhopadhyay A (1984) Int J Quantum Chem 25:965
108. Paldus J, Jeziorski B (1988) Theor Chim Acta 73:81
109. Paldus J (1988) Lie algebraic approach to the many-electron correlation problem. In: Truhlar DG (ed) Mathematical frontiers in computational chemical physics. (IMA Series, vol 15) Springer, Berlin Heidelberg New York, pp 262–299
110. Redmon LT, Bartlett RJ (1982) J Chem Phys 76:1938